

**INVESTIGATION OF ISOPRENE OH INITIATED  
PHOTO-OXIDATION MECHANISM AND  
SECONDARY ORGANIC AEROSOL FORMATION  
IN PRESENCE OF HIGH NO<sub>x</sub>**

ALTIN ELEZI

A THESIS SUBMITTED TO THE FACULTY OF  
GRADUATE STUDIES  
IN PARTIAL FULFILMENT OF THE REQUIREMENTS  
FOR THE DEGREE OF  
MASTER OF SCIENCE

GRADUATE PROGRAM IN CHEMISTRY  
YORK UNIVERSITY  
TORONTO, ONTARIO

MAY 2012

## Abstract

It is now well recognized that a wide variety of volatile organic compounds (VOCs) are emitted into the atmosphere from both biogenic and anthropogenic sources. Isoprene is the most abundant BVOCs in regional and global scale, emitted mainly from vegetation.

The purpose of this work was to investigate isoprene OH initiated photo-oxidation mechanism and Secondary Organic Aerosol (SOA) formed during Smog Chamber experiments, in presence of high NO<sub>x</sub> level. The gas phase products of isoprene oxidation are analyzed using Ion Trap –Time Of Flight Mass Spectrometer. We used “de-synthesis of spectra” approach to separate the mass spectra for individual components. This enabled us to follow all major reaction products in course of experiment, quantify yields and calculate rate constant for MVK and MACR. Our experiments showed that photo-oxidation of isoprene leads to SOA formation but over delayed timescale. The role of methacrolein as an intermediate to aerosol formation is discussed and quantified. The contribution of methacrolein to total volume of aerosol formed is estimated to be 2% to 21%, which represents a small fraction of total volume formed and suggests that other contributors and pathways should be considered and elaborated.

The role of hydroxycarbonyl compounds and their likely role in forming particulate matter is also investigated and discussed.

# Table of Contents

<b>CHAPTER 1: INTRODUCTION.....</b>	<b>1</b>
1.1    MOTIVATION.....	1
1.2    TECHNIQUES USED TO STUDY OXIDATION CHEMISTRY OF VOCs : .....	4
1.3    ISOPRENE AS THE MOST ABUNDANT BIOGENIC VOC IN THE ATMOSPHERE : GAS AND PARTICLE PHASE PRODUCTS OF ITS OXIDATION: PREVIOUS WORK .....	7
1.3.1 <i>Gas-phase products</i> .....	8
1.3.2 <i>Isoprene and SOA formation:</i> .....	14
<b>CHAPTER 2: METHODS AND INSTRUMENTATION.....</b>	<b>18</b>
2.1    EXPERIMENTAL SET UP.....	18
2.2    SMOG CHAMBER .....	20
2.3    DESCRIPTION OF IT-TOF MASS SPECTROMETER.....	21
2.4    DESCRIPTION OF DMA AND CPC.....	26
2.5    DESCRIPTION OF THE CONDITION IN WHICH THE EXPERIMENTS ARE CONDUCTED.....	29
<b>CHAPTER 3: RESULTS AND DISCUSSIONS .....</b>	<b>31</b>
3.1    GAS PHASE PRODUCTS.....	31
3.1.1 <i>Analysis of spectra (De-synthesis of spectra)</i> .....	32
3.1.2 <i>Product Yield (%) calculation</i> .....	45
3.1.3 <i>Some interesting peaks</i> .....	50
3.2    PARTICULATE PHASE PRODUCTS .....	63
3.2.1 <i>Secondary Organic Aerosol (SOA) formation and growth</i> .....	63
3.2.2 <i>Contributors to aerosol formation</i> .....	65
<b>CHAPTER 4: CONCLUSION AND FUTURE DIRECTIONS .....</b>	<b>80</b>
<b>APPENDIX .....</b>	<b>84</b>
<b>REFERENCES .....</b>	<b>90</b>

## List of Figures

Figure 1.1 Formation of $\beta$ -hydroxyperoxy radicals .....	9
Figure 1.2 Formation of $\delta$ -hydroxyperoxy radicals .....	10
Figure 1.3 Formation of $\beta$ -hydroxy alkoxy radicals .....	11
Figure 1.4 Formation of $\delta$ -hydroxy alkoxy radicals .....	11
Figure 1.5 Formation of methyl vinyl ketone (MVK) and methacrolein (MACR) .....	13
Figure 1.6 Compounds found in ambient aerosol sharing the carbon skeleton of isoprene or methacrolein. Compounds other 2-methyltetrol and 2-methylglyceric acid have multiple isomers (not shown).....	15
Figure 2.1 Experimental Setup .....	19
Figure 2.2 Schematic representation of IT-TOF MS [R.M. Jordan Co.].....	21
Figure 2.3 A schematic representation of the assembly of ionization region and Ion Trap .....	22
Figure 2.4 Three electrodes that comprise QIT [J. Throck Watson et al., 2007] .....	23
Figure 2.5 Timing and triggering diagram.....	25
Figure 2.6 A schematic presentation of DMA (Source: Prof. Mozurkewich) .....	27
Figure 2.7 A representative time profile of organic particulate volume concentration ....	28
Figure 3.1 One Mass Spectra, 10 min before UV lights irradiation .....	32
Figure 3.2 One Mass Spectra, 25 min after UV lights irradiation .....	32
Figure 3.3 Peaks vs time .....	33
Figure 3.4 Signal of $m/z=67$ (mV) vs signal of $m/z=68$ (mV) .....	35
Figure 3.5 Signal of $m/z=51$ (mV) vs signal of $m/z=68$ (mV) , (molecular ion of isoprene) .....	35
Figure 3.6 Signal of $m/z=65$ (mV) vs signal of $m/z=68$ (mV), (molecular ion of isoprene) .....	36

Figure 3.7 Signal of $m/z=39$ vs signal of $m/z=68$ (mV), (molecular ion of isoprene) .....	36
Figure 3.8 De-synthesis of peak 70 signal .....	41
Figure 3.9 De-synthesis of peak 55 signal .....	41
Figure 3.10a Time profile of signal at $m/z=65$ Figure 3.10b Time profile of signal at $m/z=67$ .....	42
Figure 3.11a De-synthesis of peak 39 signal into known contributors .....	43
Figure 3.12 Residual signal $S_{39,difference}$ versus Signal of $m/z=74$ (IPN) .....	45
Figure 3.13 Concentrations (ppm) of isoprene, MACR and MVK as function of time ...	46
Figure 3.14 “First generation product” procedure used to calculate MVK yield .....	48
Figure 3.15 “First generation product” procedure used to calculate MACR yield .....	49
Figure 3.16 Signal (mV) vs time for $m/z=82, 84, 85$ peaks .....	51
Figure 3.17 Signal of $m/z=82$ species vs signal of $m/z=68$ (isoprene) consumed .....	52
Figure 3.18 “First generation” fitting plot used to calculate relative rate constant .....	54
Figure 3.19 The proposed mechanism of formation of 3-methyl furan [Atkinson et al., 1989] .....	54
Figure 3.20 $m/z=83$ time profile      Figure 3.21 $m/z=101$ time profile .....	56
Figure 3.22 Relationship between $m/z=83$ and $m/z=101$ species .....	56
Figure 3.23 101/83,      Figure 3.24 101/73, .....	57
Figure 3.25 101/59,      Figure 3.26 101/55, .....	57
Figure 3.27 Fitting procedure used to calculate rate constant for $m/z=84$ species .....	59
Figure 3.28 De-synthesis of peak 85 signal .....	60
Figure 3.29 Mechanism of formation of C4- and C5- hydroxycarbonyls .....	62
Figure 3.30 SOA growth and isoprene concentration vs time .....	64
Figure 3.31 SOA growth and isoprene, MVK, MACR concentration profiles .....	64

Figure 3.32a SOA growth during MVK chamber experiments (March 18, 2011).....	66
Figure 3.33 SOA growth during MACR chamber experiment.....	67
Figure 3.34 Aerosol mass, expressed as a fraction of the mass when the reaction is complete, versus hydrocarbon reacted, expressed as a fraction of the initial hydrocarbon concentration, for various values of the ratio of rate constants. ....	69
Figure 3.35 Volume of particles formed, expressed as a fraction of volume when reaction is complete, versus MACR reacted, expressed as a fraction of the initial methacrolein concentration.....	70
Figure 3.36 Time profile of methacrolein concentration (as $m/z=70$ in mV).....	71
Figure 3.37 SOA growth versus methacrolein consumed in different experiments (insertion: a zoomed view close to the area where aerosol formation begins) .....	72
Figure 3.38 Volume of particles formed vs methacrolein consumed during methacrolein experiment.....	75
Figure 3.39 Linear approximation AB used to estimate the yield of MACR.....	76
Figure 3.40 Signal of $m/z=82$ species and volume of particles formed vs time.....	78
Figure 3.41 Volume of particles formed vs $m/z=82$ species consumed .....	78

# Chapter 1: Introduction

## 1.1 Motivation

Volatile organic compounds (VOCs) in the atmosphere are emitted in large quantities from a variety of different natural and anthropogenic sources. VOCs are key ingredients in the formation of ozone and aerosols and they play a significant role in regional air quality, the chemistry of the global troposphere, and possibly the global carbon cycle.

VOCs are considered to be those organic compounds having a vapour pressure greater than 10 Pa at 25°C, a boiling point of up to 260°C at atmospheric pressure, and 15 or fewer carbon atoms. The remaining compounds are designated as semivolatile organic compounds (SVOCs) or non-volatile compounds such as Polycyclic Aromatic Hydrocarbons (PAH's) found in soot. This segregation emphasises the volatile gas phase species from those that partition to the aerosol phase which is reasonable since the later undergo different transport and chemistry [Koppmann, 2007].

There are a number of source activities which lead to anthropogenic VOCs in the atmosphere: fossil fuel use and production, industrial processes, biofuel combustion, biomass burning, waste management etc. The most important source among them is estimated to be fossil fuel use and production to a global total emission of 78 Tg/year [Edgar 2005], predominately due to road transport and oil production.

On the other hand, the predominant source of biogenic VOC emissions is from the foliage of terrestrial vegetation, but other minor sources such as oceanic and soil emissions can also contribute to global totals of biogenic VOCs.

Emission inventories of biogenic volatile organic compounds (BVOCs) and of anthropogenic non-methane organic compounds (NMOCs) indicate that on regional and global scales the emissions of BVOCs exceed those of anthropogenic compounds, by a factor of  $\approx 10$  worldwide [Atkinson , Arey, 2003]. Even in regions strongly affected by anthropogenic emissions biogenic VOC emissions during the summer can be comparable in magnitude.

Of the biogenic VOCs, isoprene is by far the most important species. It has the largest flux of any single hydrocarbon, apart from methane, with global emissions estimated between 250 and 503 Tg/year [Muller, 1992; Guenther et al., 1995]. Additionally, the biogenic VOCs and especially isoprene are more reactive towards the three important atmospheric oxidants, OH radicals, NO<sub>3</sub> radicals and O<sub>3</sub>, than most of the anthropogenic VOCs [Atkinson R., 1994].

In the presence of NO emitted from combustion sources (mainly anthropogenic and exemplified by vehicle exhaust in urban areas) and, to a lesser extent , from soils,

atmospheric reactions of VOCs lead to the formation of ozone which is toxic to humans and plants becoming a major air quality problem in cities. The only significant formation route of O<sub>3</sub> in the troposphere is the photolysis of NO<sub>2</sub> [Atkinson, Arey, 2003], as it is described through Equation 1.1-1.4:

Organic peroxy (RO<sub>2</sub>) radicals and HO<sub>2</sub> radicals formed during the photo-oxidation of biogenic and anthropogenic NMOCs react with NO to form NO<sub>2</sub>:



whose photolysis then leads to net formation of ozone through equation 1.3 and 1.4:



Where: O(<sup>3</sup>P) = triplet ground state oxygen atom and M= air.

As mentioned above, aerosols, microscopically small particles suspended in air, are an important species in the Earth's atmosphere and influence both air quality and climate. Aerosols are small enough to penetrate deep into the lungs of people and have been linked to severe short- and long-term health effects such as asthma, cardio-respiratory disease, and lung cancer. Aerosols impact the Earth's climate directly through the scattering and absorption of solar radiation, and indirectly through their role as cloud-condensation nuclei. Direct emissions of organic aerosol (primary organic aerosol or POA) are distinguished from secondary organic aerosol (SOA) formed in the atmosphere by gas-to-particle conversion of the oxidation products of VOCs. [De Gouw Joost et al,

2009]. Secondary organic aerosol contributions to total organic aerosol vary with season and location but are typically substantial, 20-80% of measured mass [Yu et al., 2007, Lanz et al, 2007, 2008]. However, recently it has been noted that current atmospheric models underpredict organic aerosol mass in the lower troposphere. Without proper representation of organic aerosol in atmospheric models, development of effective air quality management plans designed to mitigate adverse health, visibility and climate effects is hindered. Model estimates rely critically on laboratory measurements of the amount of SOA produced by individual SOA precursors, typically carried out in large environmental (“smog”) chambers.

A variety of numerical models are available today to simulate chemistry and transport in the atmosphere from box models to three-dimensional chemistry and transport models. To simulate atmospheric chemistry in detail, models need to deal with VOCs which play a significant role in all reaction cycles in the atmosphere. In this regard the major input data they require are (a) the emission inventories describing the primary emission of VOCs including their specific source compositions and their spatial and temporal variations, (b) the oxidation chemistry of VOCs including kinetics as a function of temperature and pressure [Koppman, 2007].

## **1.2 Techniques used to study oxidation chemistry of VOCs :**

To investigate the atmosphere qualitatively and quantitatively, a variety of sensitive and specific sensors are employed, including mass spectrometers, flame-ionization detectors,

electron-capture detectors, optical absorption, chemiluminescence and atomic emission detectors. In many cases such detectors are coupled to pre-separation devices, for example a gas chromatograph, so that individual gases may be isolated prior to detection and a single specific compound can be measured.

In recent years introduction of online Mass Spectrometry has produced great advantages for investigation of oxidation chemistry of VOCs in terms of product identification and chemical kinetics, compared to conventional methods using adsorbent and stainless steel canister sampling followed by GC/MS analysis.

Among online Mass Spectrometric techniques used for analysis of VOCs oxidation products and mechanisms, the APCI-MS , PTR-MS and TOF-MS have shown particular interest.

Mass spectrometric instruments using atmospheric pressure ionization techniques are attractive as they can be used in an online manner and have the potential to be applied to a wide range of compounds. The most widely used atmospheric pressure ionization technique is atmospheric pressure chemical ionization (APCI). APCI is a soft ionization technique, reducing fragmentation of the target species. This results in a simpler mass spectrum, which is particularly advantageous when sampling complex matrices of compounds as is often the case in studies of VOCs oxidation.

Proton transfer reaction mass spectrometry (PTR-MS) has been used for identification and quantification of oxidation products. This is a fast-response, high sensitivity measurement technique but with limited selectivity for individual compounds. This method is now widely used for measuring oxygenated VOCs, biogenic VOC fluxes and

biogenic VOC oxidation products [Koppman, 2007]. The PTR-MS systems use chemical ionization by proton transfer from  $\text{H}_3\text{O}^+$  and a single quadrupole mass analyzer. Analysis by only a single quadrupole is considered a limitation of PTR-MS as this precludes the use of higher order MS analysis i.e. MS/MS [Auld, 2009]. The limitation of the single quadrupole in the PTR-MS systems can be overcome using an atmospheric pressure chemical ionization source with an MS/MS capable analyzer such as an ion trap or triple quadrupole.

In the past few decades, Time-of-Flight Mass Spectrometers have become widely used for analysis of air and other gas phase analytes due to a number of distinct advantages they have such as their short time analysis, potentially sub-milliseconds per spectrum acquisition, [Chambers et al., 1997] which enables them to rapidly measure an entire mass spectrum on every ionization pulse. This is particularly important in cases such as investigation of VOCs reactions where rapid monitoring of transient species may be required.

A major limitation of TOF devices is that there is no storage of ions in the acceleration region. This becomes important when chemical kinetics is involved, especially in cases of slow formation of intermediates. This limitation is overcome by interfacing it with a quadrupole Ion Trap (IT) which in itself is a powerful tool for mass analysis and storage of ions over a wide mass range with excellent sample detection limits.[Chien et al, 1994] A similar hybrid instrument, IT-TOF MS, is used in our work to sample and analyze gas phase products of isoprene photo-oxidation and it is briefly described in Chapter 2.

To study chemical composition and the mechanism of formation of Secondary Organic Aerosol formed from photo-oxidation of VOCs a suite of offline analytical techniques is used today : Liquid Chromotography/Electrospray Ionization Mass Spectrometry (LC/ESI-MS), ESI- Ion Trap Mass Spectrometry (ESI\_ITMS), Matrix-Assisted Laser Desorption Ionization – Time of Flight Mass Spectrometry (MALDI-TOFMS), High-Resolution ESI\_MS, etc. [Surrat et al, 2006], in conjunction with online instruments such as Differential Mobility Analyser and Condensation Particle Counter (DMA&CPC) and Aerodyne Time of Flight Aerosol Mass Spectrometer [Kroll et al., 2006].

In this work the DMA&CPC instruments are used to investigate mechanism of aerosol formation from the OH radical initiated photo-oxidation of isoprene.

### **1.3 Isoprene as the most abundant biogenic VOC in the atmosphere : gas and particle phase products of its oxidation: Previous work**

As it is previously mentioned, although there are large uncertainties in the magnitude of the emission rates of individual and total biogenic VOCs, it's widely accepted that isoprene is the most abundant VOC, apart from methane, emitted in the atmosphere, constituting 30% of the total biogenic VOCs, where 25% are terpenoid compounds and 40% are non-terpenoid compounds including methanol, hexene derivatives, and 2-methyl-3-buten-2-ol [Atkinson, Arey, 2003].

Because of the high reactivity of isoprene with OH radicals (lifetime 1.4 h), isoprene can significantly contribute to the formation of ozone in the troposphere (see Equation 1.1-1.4) and it potentially can lead to SOA formation.

### **1.3.1 Gas-phase products**

The photo-oxidation of isoprene initiated by OH radicals occurs by OH addition to the  $>C=C<$  bonds to form four possible hydroxyalkyl radicals, which subsequently react with oxygen molecules to form hydroxyperoxy radicals. Addition of  $O_2$  occurs only at the carbon  $\beta$  to the OH position for internal OH addition: Figure. 1.1 : isomers (II) and (IV), but takes place at two centers ( $\beta$  or  $\delta$  to the OH position) for terminal OH addition (representing the dominant process) : Figure.1.1: isomers (I) and (III) and Figure 1.2: isomers (V) and (VI).



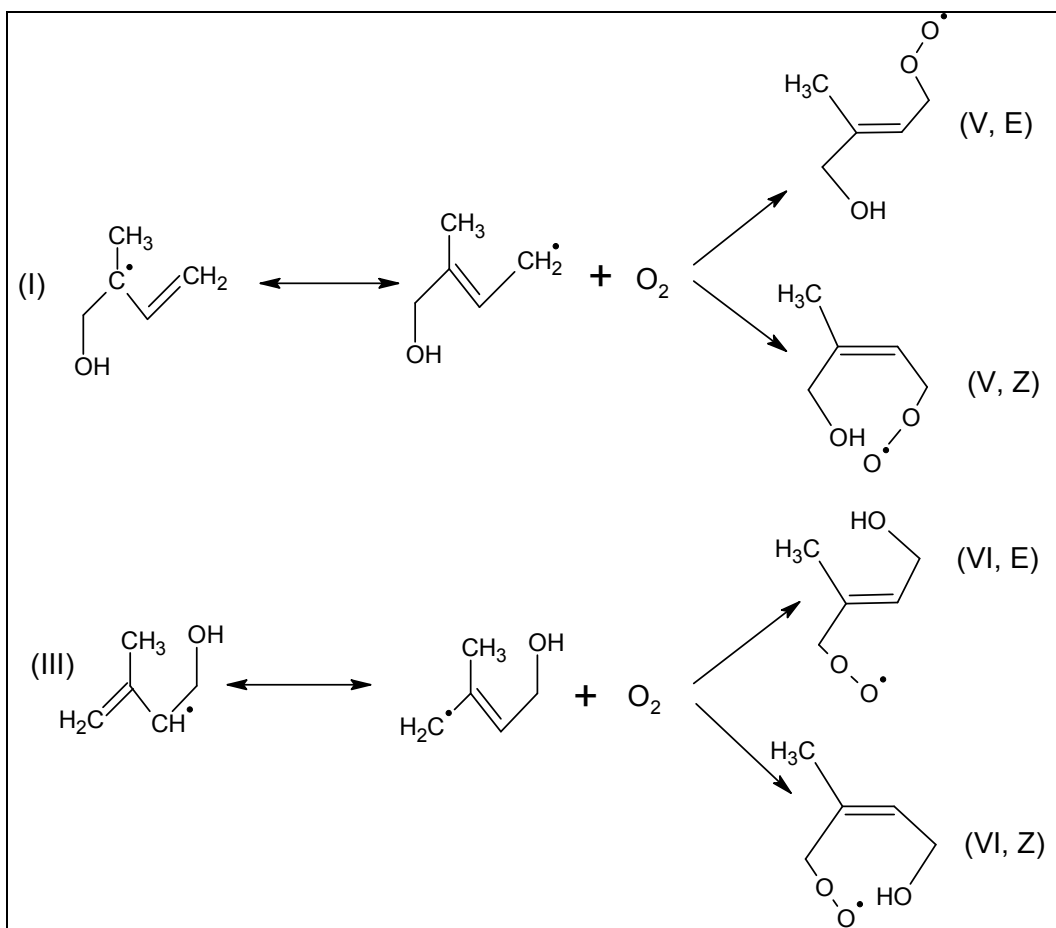


Figure 1.2 Formation of  $\delta$ -hydroperoxy radicals

In presence of large NO concentration, hydroperoxy radicals react with NO to form  $\beta$ -hydroxyalkoxy (Figure 1.3) or  $\delta$ -hydroxyalkoxy (Figure 1.4) radicals and  $\text{NO}_2$  (which leads to ozone formation, Equation 1.1-1.4) or organic nitrates (not shown here):

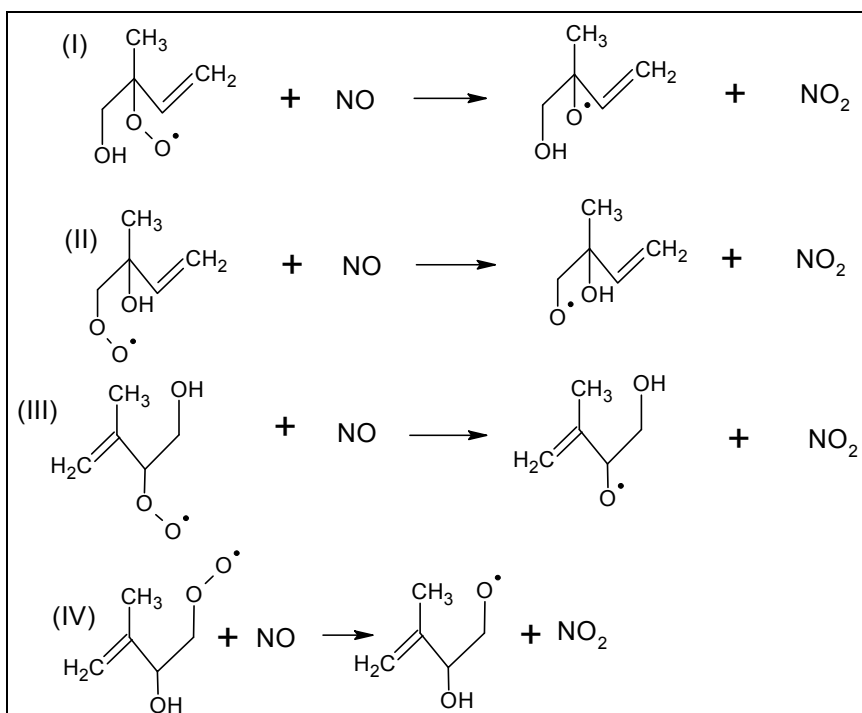


Figure 1.3 Formation of  $\beta$ -hydroxy alkoxy radicals

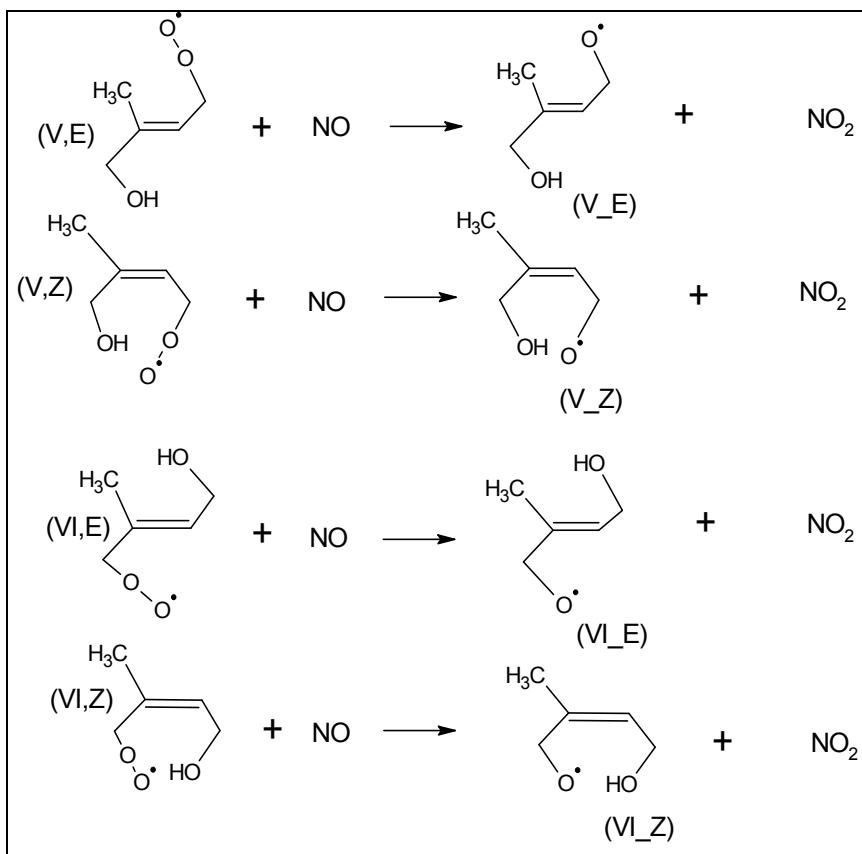


Figure 1.4 Formation of  $\delta$ -hydroxy alkoxy radicals

The hydroxy alkoxy radicals undergo decomposition, isomerisation, or hydrogen abstraction by O<sub>2</sub> to form methyl vinyl ketone (MVK), methacrolein (MACR) and other first-generation isoprene oxidation products.

Figure 1.5 gives the pathway of MVK and MACR formation from β-hydroxy alkoxy radicals.

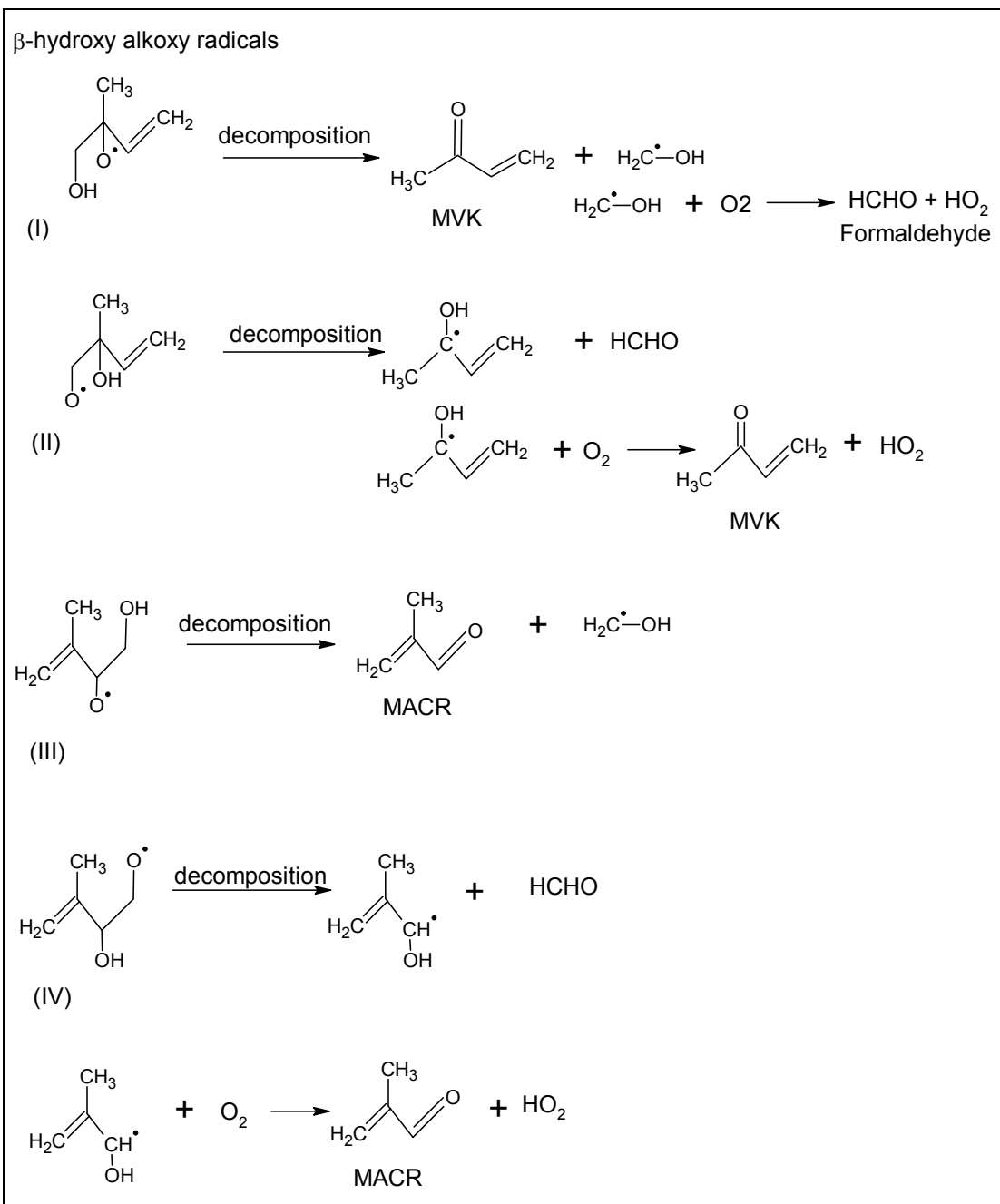


Figure 1.5 Formation of methyl vinyl ketone (MVK) and methacrolein (MACR)

Details about the fate of  $\delta$ -hydroxy alkoxy radicals will be given in Chapter 3.

### 1.3.2 Isoprene and SOA formation:

It has been generally accepted that isoprene does not contribute to atmospheric SOA [Pandis et al., 1991]. However, in recent years, the topic of SOA formation from isoprene has been re-examined and recent field [Claeys et al, 2004; Kleindienst et al, 2007] and laboratory [Kroll et al, 2005, 2006, 2007; Ng et al, 2008] studies indicate that isoprene oxidation may indeed contribute to the formation of SOA in the atmosphere. Even if the yield is small, the overall contribution of isoprene to total organic aerosol in the atmosphere could be large due to the large global source strength.

Field evidence for SOA production from isoprene oxidation are based on: 1) the similarities between carbon skeleton of compounds such as 2-methyltetrols (Figure 1.6a) [Claeys et al. 2004], C5 alkene triols (Figure 1.6b) [Wang et al. 2005], 2-methylglyceric acid (Figure 1.6c) [Ion et al. 2005], as well as accretion products such as hemiacetal dimer (Figure 1.6d) [Surratt et al. 2006], measured in ambient aerosol<sup>1</sup> and isoprene or methacrolein (a major isoprene oxidation product); 2) exhibition of strong diurnal and seasonal concentration trends of SOA similar to those of isoprene emissions, with abundances highest in the periods of highest photochemical activity: daytime [Plewka et al., 2006] and summer months [Kleindienst et al., 2007a]; 3) the observed correlation between measured concentration of organic aerosol and isoprene oxidation products [Holzinger et al., 2007]; 4) the similarity of aerosol mass spectrometer (AMS) ambient data to laboratory mass spectra from isoprene oxidation [Marcolli et al. 2006].

---

<sup>1</sup> Several laboratory studies have also found that a significant fraction of the identifiable SOA constituents are compounds with the same carbon skeleton as isoprene or methacrolein [Edney et al., 2005; Surratt et al., 2006; Szmigielski et al., 2007]. These include 2-methyltetrols and methylglyceric acid, as well as structural analogs of each.

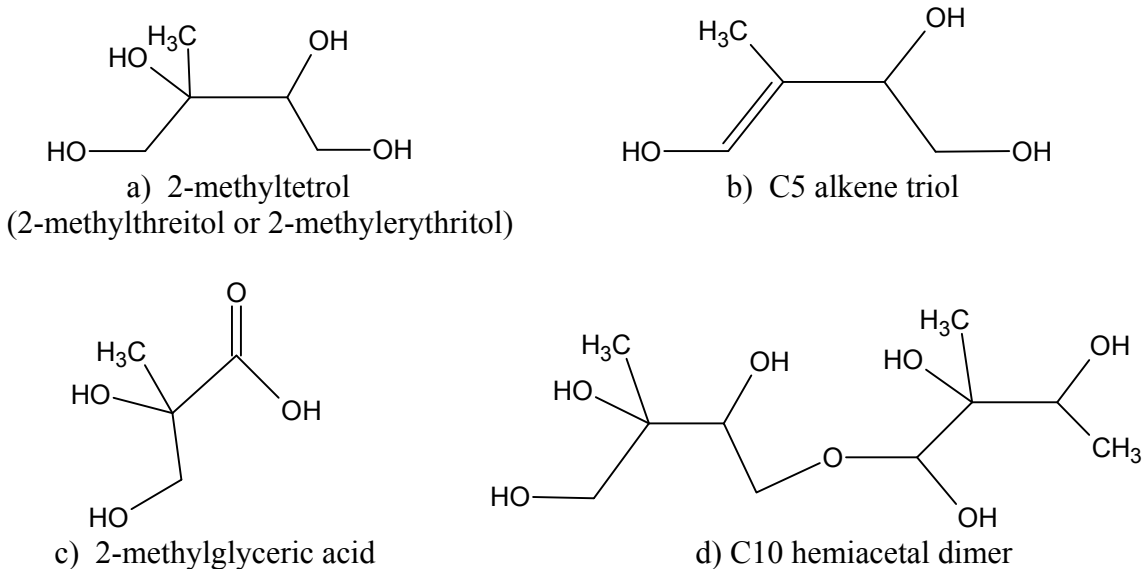


**Figure 1.6 Compounds found in ambient aerosol sharing the carbon skeleton of isoprene or methacrolein. Compounds other 2-methyltetrol and 2-methylglyceric acid have multiple isomers (not shown)**

The field evidence of isoprene SOA has been intriguing as early laboratory experiments seemed to indicate that SOA formation from isoprene was not atmospherically important. As mentioned above, recent laboratory investigations have confirmed that gas-phase isoprene oxidation products indeed forms SOA under a broad variety of experimental conditions, including wide ranges in aerosol seed acidity, NO<sub>x</sub> concentration, relative humidity and initiating oxidant [Carlton et al. 2009]. Isoprene oxidation experiments in the presence of acidic aerosol seeds [Jang et al. 2002, Edney et al. 2005, Kleindienst et al. 2007b, Surrat et al. 2007] strongly suggest the importance of particle-phase reactions that lower the volatility of organic species via accretion (oligomerization) process.

On the other hand, a number of chamber experiments [Kroll et al., 2006; Dommen et al., 2006, etc.] have shown that isoprene photo-oxidation can also form SOA in the absence of strong acidity but over delayed timescales [Ng et al., 2006]. These results indicate that

in addition to particle-phase accretion reactions, a key step in SOA formation is the further gas-phase oxidation of first-generation reaction products. However, products from the oxidation of only a few first generation compounds, including methacrolein [Tuazon and Atkinson, 1990b; Orlando et al, 1999], methyl vinyl ketone [Tuazon and Atkinson, 1989], and C5 hydroxycarbonyls [Baker et al., 2005] have been measured. Furthermore, uncertainties in detailed reaction mechanisms lead to substantial disconnect between known oxidation mechanisms and measurements of isoprene SOA composition. For example, the formation of methylglyceric acid (and other organic acids) cannot be accounted for by established reaction mechanisms suggesting an important role of as-yet unidentified chemistry (in the gas and/or particle phases) in the formation of SOA from isoprene oxidation. The same is also true for the formation of mechanism of 2-methyltetrols. A number of pathways have been put forth, including RO<sub>2</sub> chemistry [Clayes et al., 2004a], aqueous-phase oxidation by H<sub>2</sub>O<sub>2</sub> [Clayes et al., 2004b; Boge et al., 2006], reaction of epoxides [Wang et al., 2005; Boge et al., 2006], etc., but at present it is unclear which are most important under ambient conditions.

In summary we can say that understanding and describing the mechanism of SOA formation from photo-oxidation of isoprene, although the achieved progress, still constitute a challenge for numerous research groups.

As a result, work towards a detailed understanding of the oxidation mechanism of isoprene which leads to ozone formation and its potential to form condensable products and contribute to SOA is essential.

The objective of my work is to investigate the mechanism of isoprene oxidation using chemical ionization mass spectrometry and isoprene photo-oxidation contribution to Secondary Organic Aerosol formation, during chamber experiments.

## **Chapter 2: Methods and instrumentation**

### **2.1 Experimental set up**

Reactions of OH radical initiated photo-oxidation of isoprene were carried out in the York Smog Chamber.

An Ion-Trap Time of Flight Mass Spectrometer is used to investigate gas-phase products of isoprene oxidation reactions. This is a hybrid mass spectrometer composed mainly from a Source Chamber including an Ion Trap (Paul trap), where ions are produced and stored and a Time of Flight tube where ions are analyzed based on their mass to charge ratio ( $m/z$ ). Gas-phase content of the chamber is continuously withdrawn into the Mass Spectrometer.

A Differential Mobility Analyzer (DMA) and a Condensation Particle Counter (CPC) are used to measure the size distribution and hence volume concentration of particle-phase products formed from the photo-oxidation of isoprene inside the Chamber.

The basic experimental setup is shown in Figure 2.1

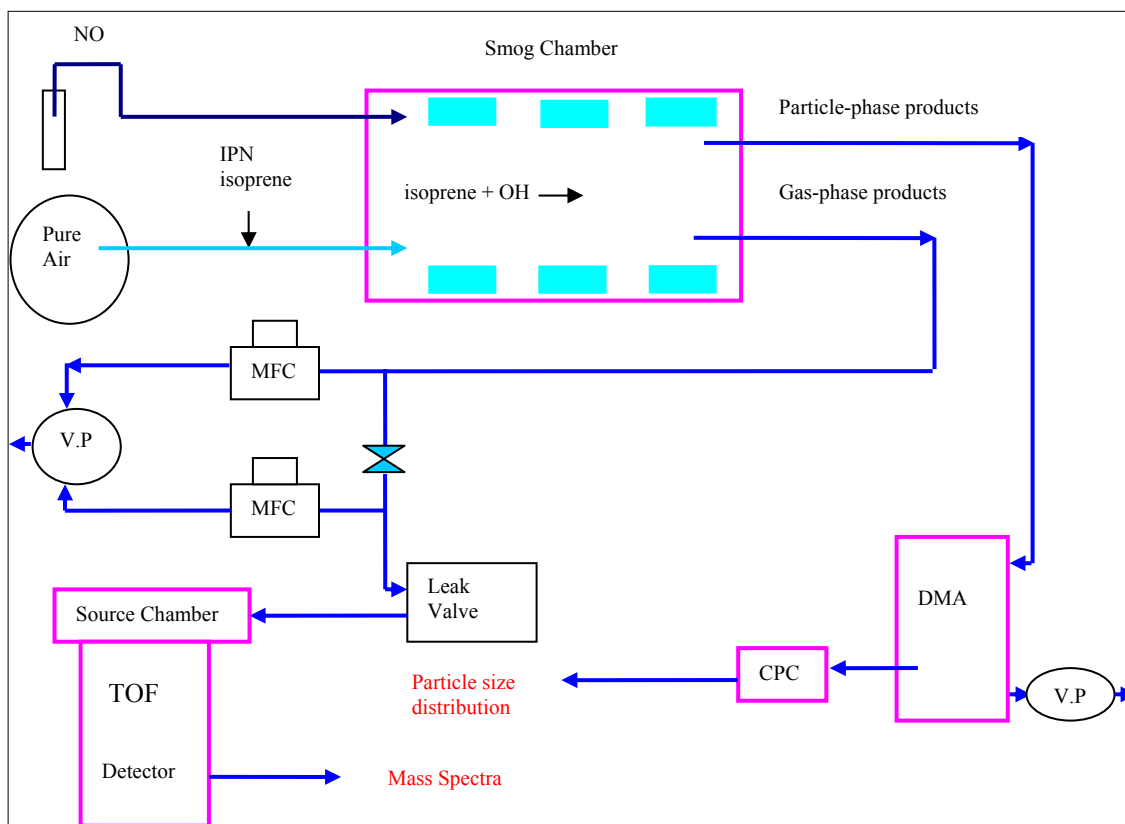


**Figure 2.1 Experimental Setup**

Teflon and stainless steel tubes are used to make the connection from the Smog Chamber to IT-ToF MS and DMA/CPC instruments. A syringe is used to inject the analyte of interest (isoprene/metacrolein/methyl vinyl ketone) into the Smog Chamber.  $\text{NO}_{(g)}$  goes to the Smog Chamber from a pressurized cylinder and the flow is controlled/calibrated by a Mass Flow Controller (not shown in the Figure 2.1).

The gas phase sample is drawn into the Mass Spectrometer by means of a vacuum pump which is connected to two Mass Flow Controllers (MFC) ( 200 scm and 2000 scm). A needle valve is used to reduce the pressure and a leak valve is used to control the gas sample going to the instrument. When the leak valve is closed no sample is allowed to go to the instrument. By opening the valve we control the pressure in Source Chamber of the instrument (the pressure should be no more than  $1 \times 10^{-5}$  torr to prevent the electron gun

from arcing). The IT-ToF MS is connected to a computer for data acquisition and processing.

A vacuum pump, attached at the excess air port of DMA, is used to sample the particulate phase products to the instrument, where aerosol particles are sorted according to their size. The monodispersed output flow is continuously passed to CPC for particle counting and calculation of particle concentration.

The most critical parts of the system which include Smog Chamber, IT-ToF MS and DMA&CPC instruments are described in more detail as follows.

## **2.2 Smog Chamber**

The York University smog chamber is cylindrical in shape with a volume of  $\sim 8 \text{ m}^3$ .

It is composed of two Teflon coated aluminum endplates, inner transparent Teflon walls and a solid mobile outer wall. The chamber can be irradiated by up to 24 ultraviolet lights, which are attached to the outer wall and have a radiation window of 350-400 nm (Philips F40BL, 40 Watt). Injections and sampling are made through the endplates; injections on one end, where an internal fan is mounted to enhance mixing, and sampling from the opposite end [Auld J., 2009].

## 2.3 Description of IT-TOF Mass spectrometer

The gas-phase products of reactions from the Smog Chamber will go to the Ion Trap – Time of Flight Mass Spectrometer.

This device combines the storage capabilities of the ion trap with relatively high resolution, speed and high mass capabilities of TOF.

Ion storage is particularly important in studying ion/molecule chemistry, very slow formation of metastables and for enhancing the detection limits by integration of the signal [Chien et al, 1994].

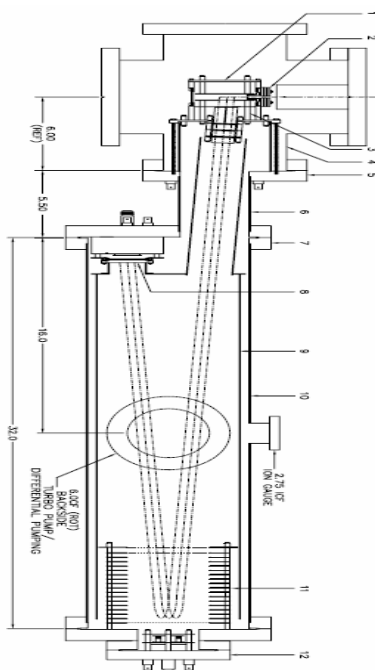
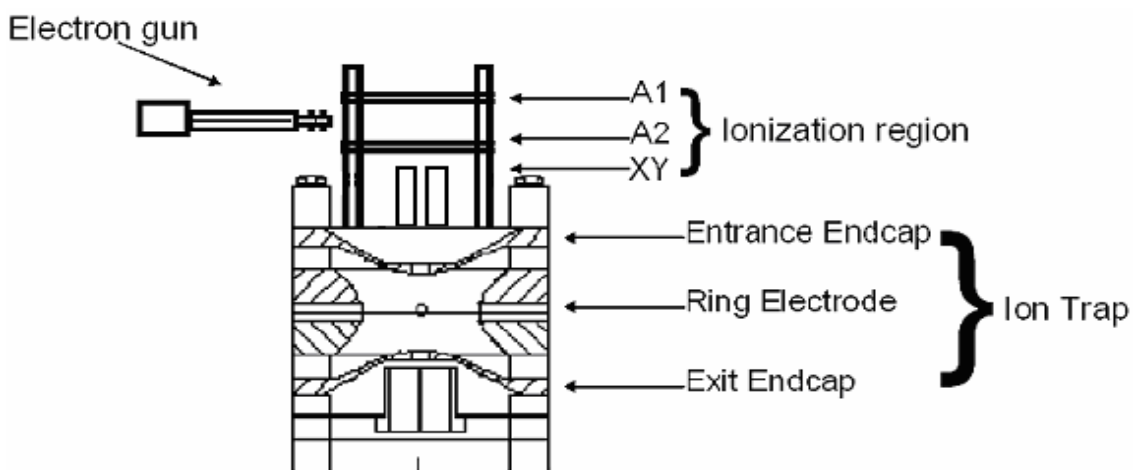


Figure 2.2 Schematic representation of IT-TOF MS [R.M. Jordan Co.]

The instrument contains two main sections: *the source chamber* and *the flight tube*. The sample air is entered at source chamber where the ions *are produced* and *stored* prior to injection into the flight tube. The source chamber is pumped by a  $550 \text{ L s}^{-1}$  turbo-

molecular pump (Turbo 550). This chamber contains an ion trap that may be used *to store* ions and *to inject a pulse of ions* into the flight tube.

The sample air after leaving the leak valve through a small diameter tube enters direct the ion trap and then it is spread out in all source chamber area. As the air sample enters the ion trap area this makes the pressure in the ion trap much higher than in the source chamber (by a factor of 45 for air). Increasing the pressure in ion trap cavity helps the *chemical ionization* to occur in this region.



**Figure 2.3** A schematic representation of the assembly of ionization region and Ion Trap

$O_2^+$  produced mainly by *Electron Impact ionization* technique in the *ionization region* (Figure 2.3) acts as chemical ionization agent inside the ion trap during the storage time , usually few milliseconds. The source chamber is equipped with an ion extraction system consisting of deflectors A1, A2 (to gate the ions into the trap) and split cylindrical lenses XY (to direct the ions into the trap). A1 and A2 are flat plates parallel to the entrance endcap of the ion trap. The electron beam passes between them. A2 is closer to the trap than A1 and has a hole covered by a grid to allow for passage of the ions.

The chemical ionization of analyte molecules (A) usually occurs by electron transfer ( $A + O_2^+ = A^+ + O_2$ ) or by hydride abstraction ( $AH + O_2^+ = A^+ + HO_2$ ). During the electron transfer reaction if the exothermicity is large enough, the analyte molecules could fragment resulting in a number of different peaks ( $A + O_2^+ = A_1^+ + O_2 + A_2$ )

*The description of Ion Trap:* The ion trap is comprised of two endcaps and a ring electrode with hyperbolic surfaces (Figure 2.4). Once the ions are generated, they are directed through the entrance endcap electrode of the ion trap. Ions present within the volume of the ion trap are trapped by the RF potential, while other ions and unionized sample are pumped away by the turbo pump located directly on the side of the source chamber. Both endcaps are held at 0 V while this process takes place (full storage mode). Varying the RF amplitude varies the range of m/z that can be stable within the trap.

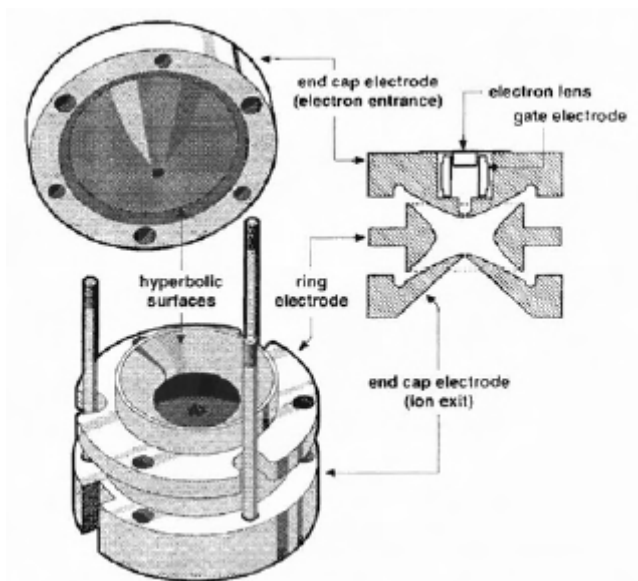


Figure 2.4 Three electrodes that comprise QIT [J. Throck Watson et al., 2007]

Ions of appropriate  $m/z$  at a particular RF amplitude have stable trajectories in the trap and can therefore be trapped. The minimum collectable  $m/z$  increases with the increase in the RF amplitude, thus small masses can be filtered out. Once a selected range of masses is trapped, a DC pulse is applied to the exit endcap to simultaneously extract all ions from the trap for ToF analysis.

This extraction pulse triggers the start for the ToF mass analysis. Once the ion packet leaves the trap, it is directed towards a flight tube (model C-855 by R.M. Jordan), in which it enters a field-free drift region. Once the ion packet arrives at the end of this region, its velocity is slowed and reversed by a reflectron (model C-852 by R.M. Jordan). The newly focused ion packet then re-traverses the drift region and is detected by dual 40 mm microchannel plate detector (model C-726 R. M. Jordan).

The mass spectrum is obtained by measuring the time required for ions to travel down the flight tube and reach the detector. The time needed to travel the flight tube and hit the detector is proportional to the square root of mass to charge ratio of ions, so low mass to charge ions will travel faster and hit the detector first and high mass to charge ions will take more time to hit the detector.

Measurements take place in a repetitive cycle, with successive measurements being averaged and stored by the computer. The entire process of *timing and triggering* (Figure 2.5) is controlled and governed by a set of electronic equipment: HP Function Generator, Digital Delay Generator (DDG), DEI Generator, Ion Trap Power Supply. Each measurement begins by admitting ions into the ion trap for a period of time (“*gate open*

time or trapping time”). The gate is then closed, and the ions are stored in the trap for some period of time, this allows the ions to thermalize and permits *chemical ionization* to occur in the trap. At the end of this *storage time*, the ion trap RF is shut off and an extraction pulse is sent to the ion trap endcap to inject the ions into the flight tube; at the same time, data acquisition is begun. When data acquisition is complete, the extraction pulse is shut off and RF potential is turned back on. The system is ready for another cycle.

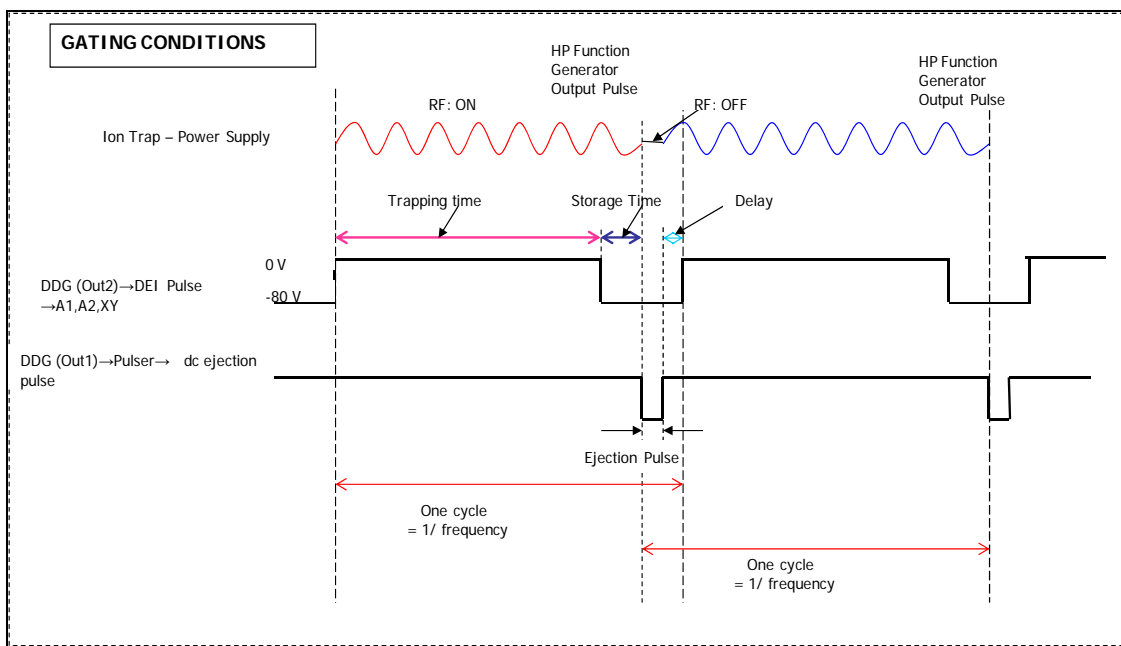


**Figure 2.5 Timing and triggering diagram**

Acquisition of the ToF mass spectrum is done via a Perkin-Elmer 9846 transient recorder which is a PC board, which comes with software that can acquire data at 500 MHz with 8 bits resolution. An external trigger signal (generated by DDG: output 1) initiates acquisition which continues until the software specified number of points is obtained. Then data are transferred to the PC, where successive spectra are averaged.

The software provides experimental error estimates of one standard deviation based on the propagation through the analysis from estimated noise levels. The magnitude of uncertainty is calculated based on the consistency of the baseline, sensitivity setting, baseline noise and the height of the peaks in the spectra.

## 2.4 Description of DMA and CPC

The Differential Mobility Analyzer (DMA) is a device (Figure 2.6) that can be used to sort submicrometer aerosol particles according to size while keeping them suspended in air.

The DMA is composed of two concentric cylinders, the inner is charged and the outer is held at ground creating an electric field in the annular space. The chamber contents are drawn into the DMA at atmospheric pressure through the polydispersed inlet ( $q_p$ ) at  $1 \text{ L min}^{-1}$  using a downstream diaphragm pump attached at the excess air port ( $q_e$ ).

The sample flow through  $q_p$  is balanced by the monodispersed outlet ( $q_m$ ). The excess air outlet is balanced by the sheath air inlet ( $q_s$ ), at  $5 \text{ L min}^{-1}$  for this work. In order to be sized by the DMA the particles must be charged, therefore the aerosol sample is passed through a Krypton-85 radioactive source, interacting with an environment of bipolar ions, before being sized. Once inside DMA the polydispersed aerosol sample and sheath air combine within the annular space between the inner and outer rod being exposed to the electric field. For a given voltage on the inner rod only particles of a certain electric mobility establish the correct flow path to exit the monodispersed flow outlet.

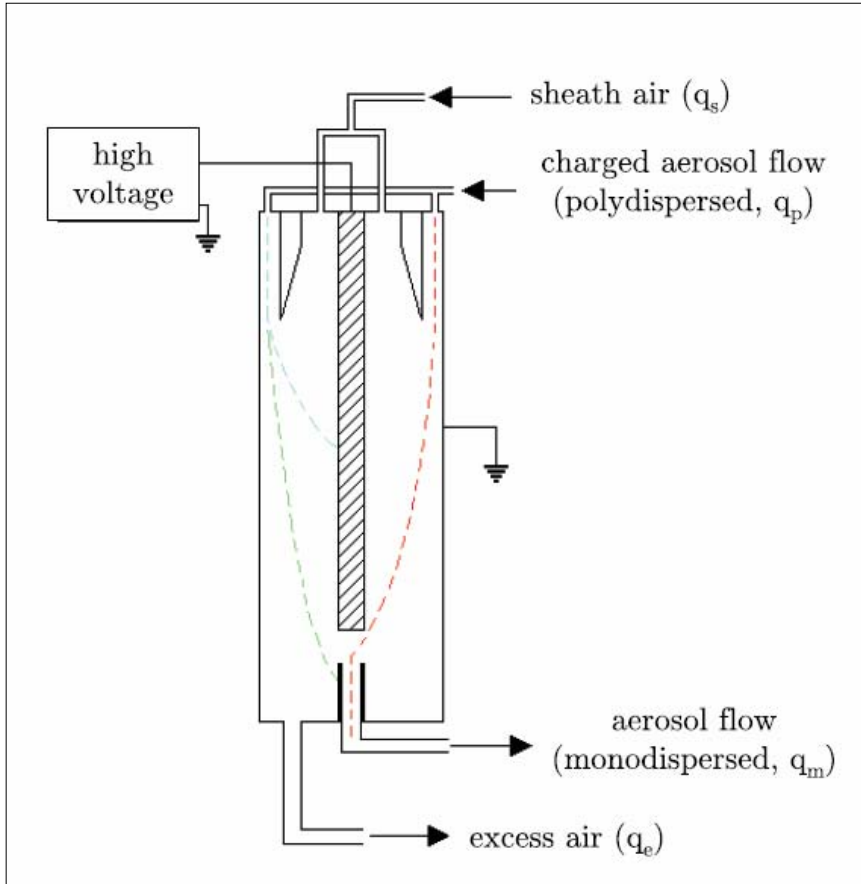


**Figure 2.6 A schematic presentation of DMA (Source: Prof. Mozurkewich)**

The monodispersed output flow is continuously passed to the CPC for particle counting.

In this device, a liquid, such as butanol, is condensed on the particles so that they grow to a diameter of about a micrometer. They are then large enough to scatter an appreciable amount of light. Then, by passing these particles through a beam of light, flashes of light are produced. These flashes can be detected and counted to determine the concentration of particles in the flow entering the CPC.

Data acquisition for this system is controlled by a program written by Prof. Mozurkewich using Igor Pro 6.0 (WaveMetrics). The program converts the frequency determined from the CPC counts to mobility distributions. The final output of data is size distributions of

the form  $dN/d\ln(D_p)$  for 32 diameter size bins ranging from 8-700 nm. The data output requires several steps of processing to convert from the number of particles in each bin to the desired organic particulate volume concentration ( $\mu\text{m}^3 \text{m}^{-3}$ ).

The number of particles per bin,  $N(D_p)$ , at a given diameter,  $D_p$  in nm, is calculated from the product of the output,  $dN/d\ln(D_p)$ , and the bin width,  $\ln(10)/16$ . From these values the particle volume per bin,  $V(D_p)$  in  $\mu\text{m}^3 \text{m}^{-3}$ , can be calculated according to Equation 2.1<sup>2</sup>:

$$V(D_p) = \frac{\pi(D_p)^3}{6} (N(D_p)) \quad \text{Equation 2.1}$$

From this calculation the volume concentration per time step can be obtained by summing (integrating) over all  $D_p$ . The volume concentration is corrected for two loss processes, the first is due to deposition of particles on the walls and the second is due to dilution of the chamber during the experiment. The Figure 2.7 gives an example of time profile of total volume concentration of organic particulate matter.

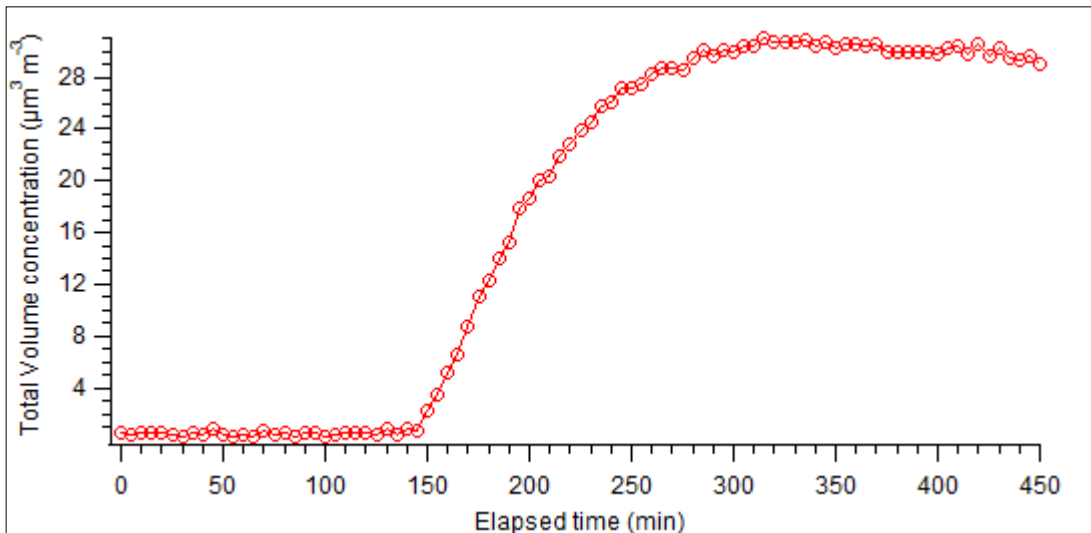


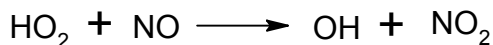
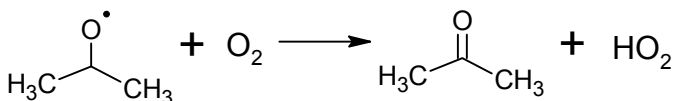
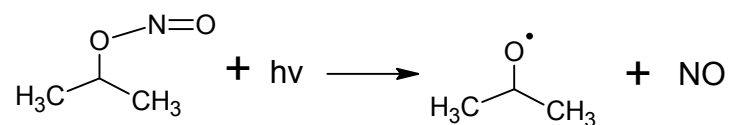
**Figure 2.7 A representative time profile of organic particulate volume concentration**

<sup>2</sup> The particles are assumed to be spherical

## 2.5 Description of the condition in which the experiments are conducted

As mentioned earlier, OH radical initiated photo-oxidation of isoprene is simulated in the Smog Chamber at atmospheric pressure. The experimental temperature range is 22-25 °C and relative humidity ~10%. The amount of isoprene injected in the Smog Chamber during experiments was 1-3 ppm.

The radical precursor used in the present experiments is Isopropyl Nitrite (IPN), synthesized in our laboratory (it is prepared by a solution of isopropanol and sulfuric acid with a solution of sodium nitrite). The following reactions describe the way the OH radicals are produced into the Chamber, starting from the moment when the lights are turned ON:



The isoprene and IPN are introduced by injecting, using a 25  $\mu\text{L}$  syringe, a known volume of each (usually  $\sim 43 \mu\text{L}$  isoprene/IPN) in a stream of pure air which carry them out to the Smog Chamber.

NO is introduced into the Chamber from a gas mixture (a Linde pressurized cylinder : Mcert NO 1.5% N<sub>2</sub> BAL 200sz) and a Mass Flow Controller is used to calibrate and control the amount of NO (as a reference : a flow rate of 1.6 L/min is used to get a concentration of  $\sim 2$  ppm of NO into the Smog Chamber).

First is introduced NO and IPN and after 10 minutes isoprene is injected. In this way it is easier to distinguish the peaks that originate from each of these compounds (see analysis of spectra). After one hour of a mixing period, the UV lights are turned ON and photolysis of IPN is initiated which means that the oxidation of isoprene has started. The lights are turned OFF after three hours and usually the sampling from the chamber continued for one hour more.

## **Chapter 3: Results and discussions**

The content of the smog chamber is continuously monitored using online IT-TOF MS for gas phase products and DMA/CPC for particulate phase products. At the end of each experiment mass spectra and particle size distributions are processed and analyzed.

### **3.1 Gas phase products**

In order to better understand the Secondary Organic Aerosol formed from photo-oxidation of isoprene it is important to understand the mechanism of formation and the fate of gas phase products of this oxidation. As mentioned above, the gas phase products of isoprene oxidation are analyzed using IT-TOF Mass Spectrometer. Since many different compounds were present, this resulted in complex mass spectra. We used “de-synthesis of spectra” procedure to separate the mass spectra for individual components. This enabled us to follow all major reaction products in course of experiment and potentially allows us for a kinetic analysis.

### 3.1.1 Analysis of spectra (De-synthesis of spectra)

The analysis of mass spectra is started by comparing mass spectra, from a time series, taken before and after the initiation of the reaction.

Below there are two mass spectra representing the peaks observed 10 min before UV lights irradiation and 25 min after the UV lights irradiation.

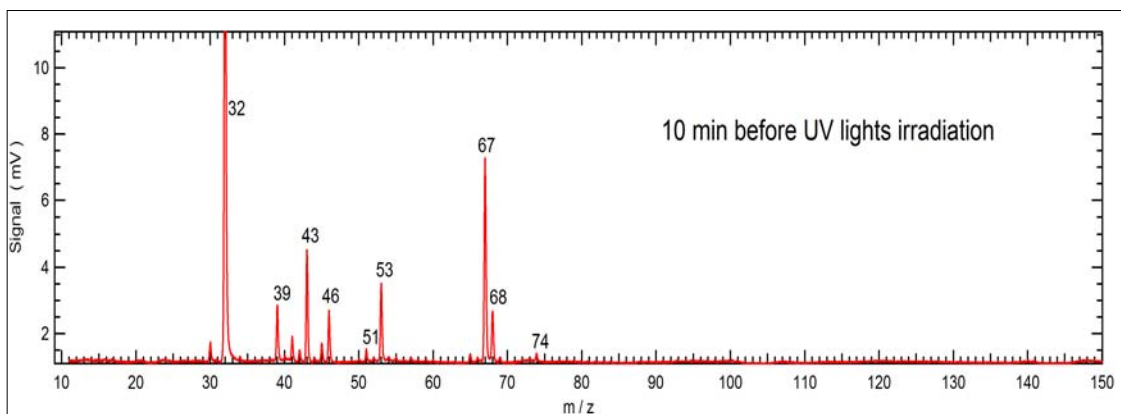


Figure 3.1 One Mass Spectrum, 10 min before UV lights irradiation

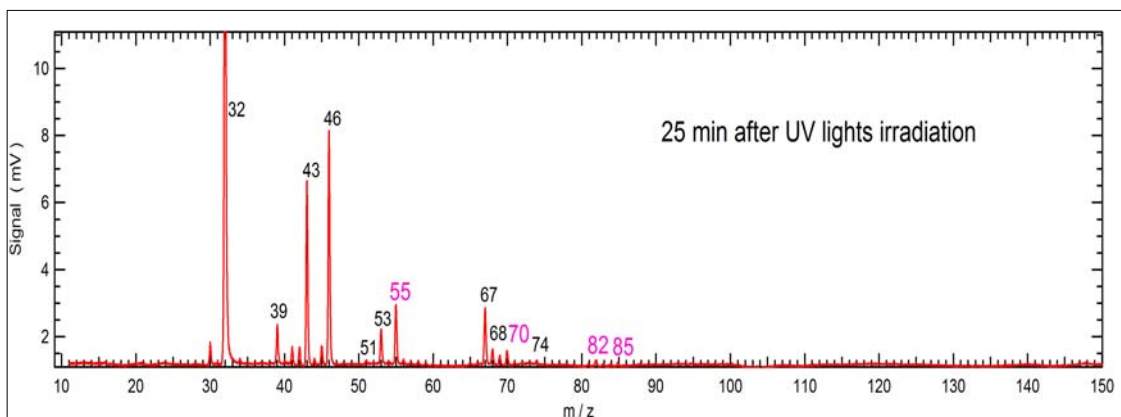


Figure 3.2 One Mass Spectrum, 25 min after UV lights irradiation

By carefully comparing these two mass spectra we are able to notice new peaks ( $m/z=55$ ,  $m/z=70$ ,  $m/z=82$ ,  $m/z=84$ ,  $m/z=85$ ) that have emerged as products of reaction after the oxidation of isoprene has started. Also, we observe increase in signal intensities for peaks 43 and 46, which suggests that there are possible contributions from products of reaction to these peaks.

The mass spectra obtained by sampling the content of Smog Chamber contain a number of peaks which need to be identified in terms of the compound that they belong to and that they represent.

By plotting the signal of each peak vs time and by assigning peak  $m/z=74$ ,  $m/z=68$  to IPN and isoprene respectively (by comparing reference spectra<sup>3</sup> of all known reactants and main products) we were able for each peak to associate with the appropriate reactant or product compound.

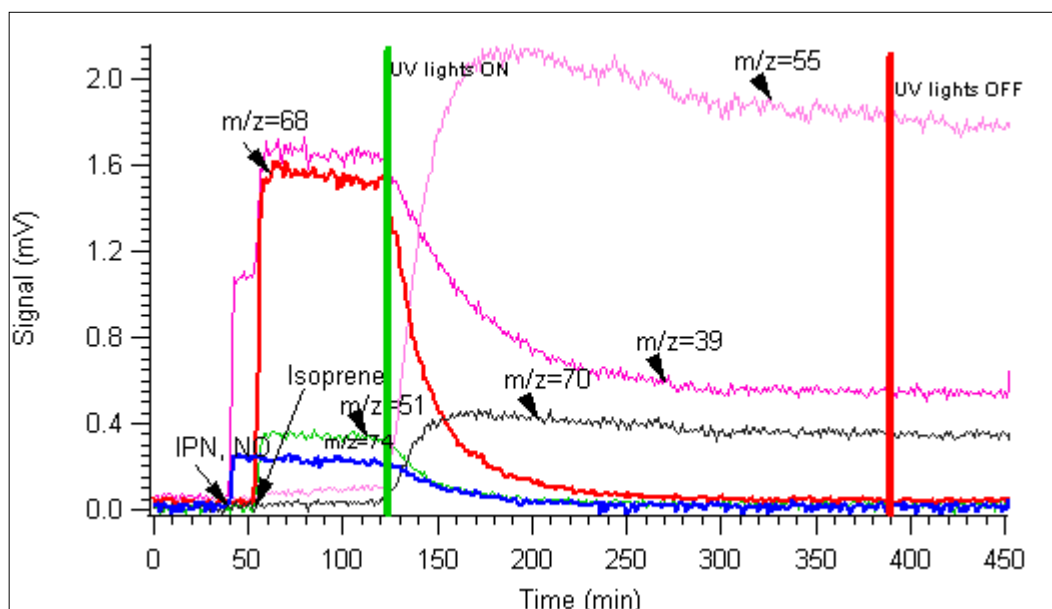


Figure 3.3 Peaks vs time

<sup>3</sup> Isopropyl Nitrite (IPN) and isoprene reference spectra were prepared by Aeysha Ahmed

For example by carefully looking at Figure 3.3, we see that  $m/z=39$  appeared at the moment when IPN is injected (moment identified by  $m/z=74$ ), and there is an increase of its signal intensity when isoprene is injected (moment identified by  $m/z=68$ ). Therefore the signal intensity of peak 39 comes from the contribution of fragments of  $m/z=39$  of IPN and isoprene. By using the same reasoning we see that peak 68 and peak 74 belong exclusively to isoprene and IPN respectively.

It's interesting to see that peak 55 and peak 70 emerge only at the moment when lights are turned ON: OH radicals start to be produced: oxidation of isoprene starts and therefore the products of this oxidation start to be present as molecular ions or as fragments.

The relationship between any peak and a given compound is further investigated by plotting the signal of the peak of interest vs the signal of the peak that represents the compound of interest. For example by plotting signal of peak 67 vs signal of peak 68 (molecular ion of isoprene) (Figure 3.4) we got a nice linear fit which is a strong indication that  $m/z=67$  species is exclusive fragment of isoprene.

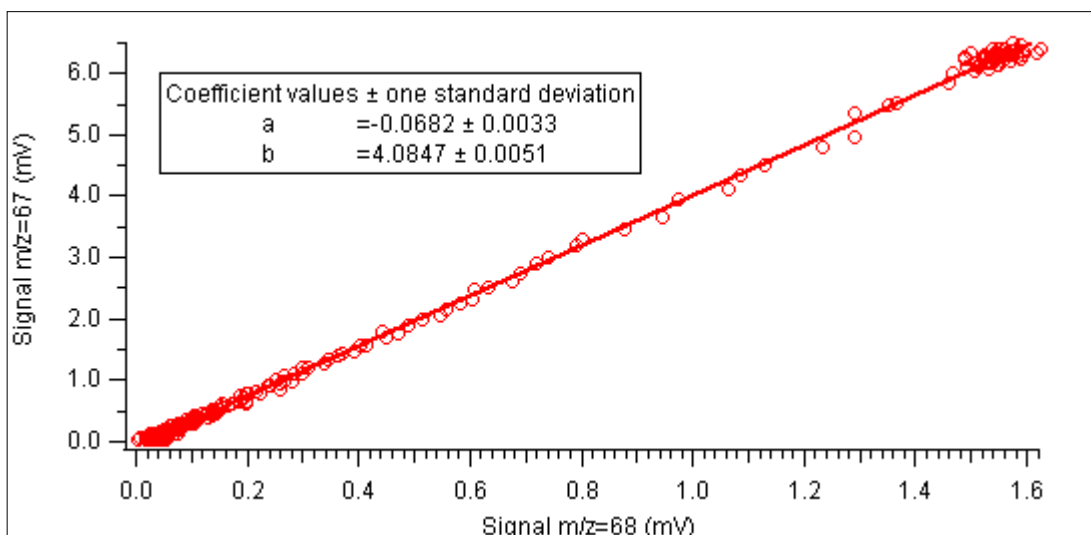


**Figure 3.4** Signal of  $m/z=67$  (mV) vs signal of  $m/z=68$  (mV)

Investigating the relationship between peak signal of  $m/z=51$  ion (Figure 3.5) and  $m/z=65$  ion (Figure 3.6) with peak signal of  $m/z=68$ , we observe that although we have a linear fit for the most of the range, the situation is different close to the origin of the system. Signal intensities are low for  $m/z=51$  and  $m/z=65$  (max 0.25-0.35 mV) and signal to noise ratio (S/N) is especially significant close to 0 values.

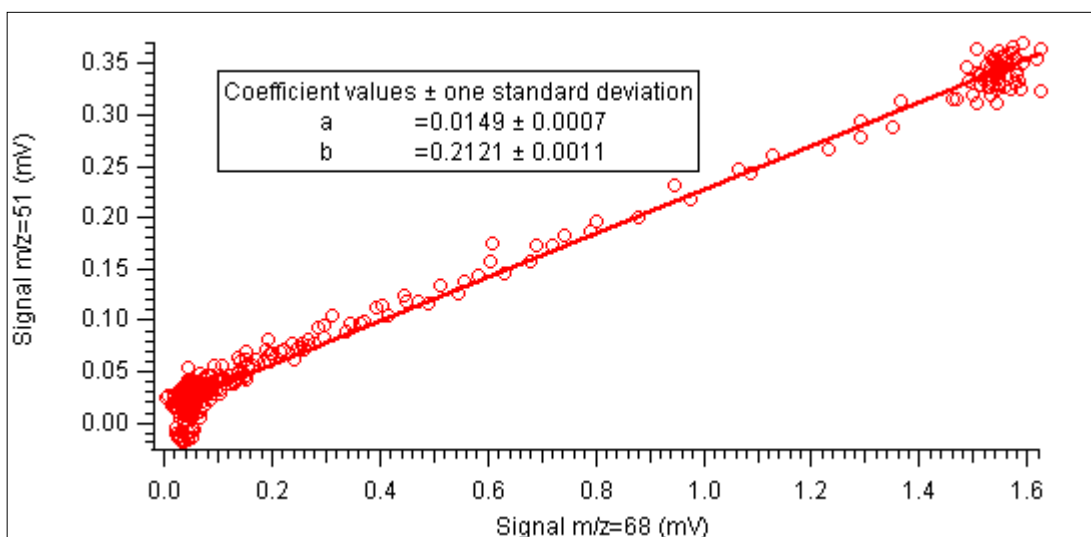


**Figure 3.5** Signal of  $m/z=51$  (mV) vs signal of  $m/z=68$  (mV) , (molecular ion of isoprene)

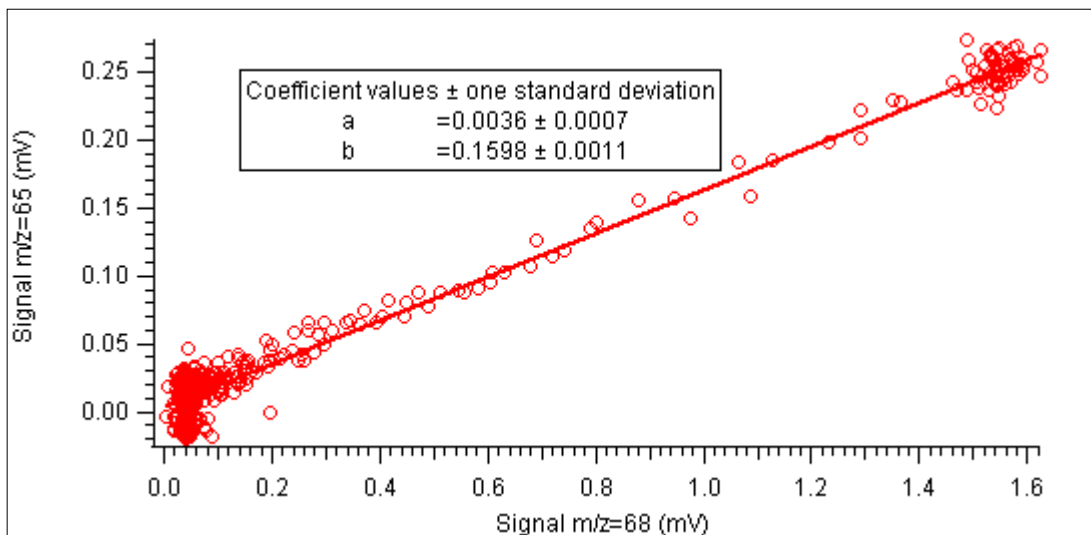


Figure 3.6 Signal of  $m/z=65$  (mV) vs signal of  $m/z=68$  (mV), (molecular ion of isoprene)

The situation could be different in terms of linearity, as it is the case for example when we investigate the relation between signal intensity of  $m/z=39$  and  $m/z=68$  (Figure 3.7) which suggest that ion  $m/z=39$  is not an exclusive fragment of isoprene and other compounds could give fragment ions with  $m/z=39$ .

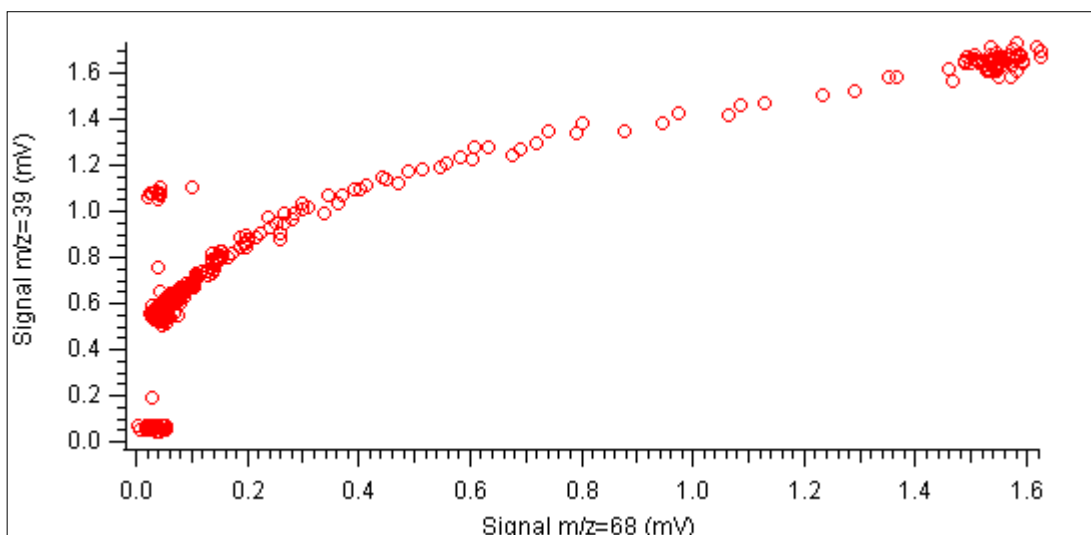


Figure 3.7 Signal of  $m/z=39$  vs signal of  $m/z=68$  (mV), (molecular ion of isoprene)

The following table (Table 3.1) is a presentation of all peaks that are observed before and after the oxidation of isoprene: we have assigned here for each peak to each compound they could be related to, in terms of Response Factors. So,  $R_{i,j}$  (mV/ppm) would be the response factor at mass to charge ratio  $i$  for the compound  $j$ . Blank cells indicate that there is no signal response of respective compound to the specific peak.

**Table 3.1. The known compounds and their response factors to the observed peaks**

Ions (m/z)	$R_{i,j}$ (mV/ppm)			
	Isoprene	MACR	MVK	Acetone
39	0.0613 ± 0.0001	1.094 ± 0.002	0.358 ± 0.001	
40	0.0052 ± 0.0001	0.062 ± 0.001		
41	0.0124 ± 0.0001	0.330 ± 0.001	0.176 ± 0.001	
42	0.0067 ± 0.001	0.254 ± 0.001	0.236 ± 0.001	0.280 ± 0.001
43			1.056 ± 0.002	5.40 ± 0.02
44				0.16 ± 0.01
50	0.0048 ± 0.0001			
51	0.0326 ± 0.0002			
53	0.1872 ± 0.0003	0.450 ± 0.001	0.138 ± 0.001	
54	0.0051 ± 0.0003			
55	0.0412 ± 0.0001		6.017 ± 0.001	
56			0.195 ± 0.001	
57	0.0062 ± 0.0001			
58				0.100 ± 0.001
65	0.0241 ± 0.0001			
66	0.0086 ± 0.0001			
67	0.6214 ± 0.0001			
68	0.154 ± 0.0003			
69	0.009 ± 0.0001	0.533 ± 0.002		
70		1.129 ± 0.003	0.349 ± 0.001	
85		0.530 ± 0.002		

The Table 3.1 was prepared by Aeysha Ahmed based on a calibration procedure developed by Prof. Mozurkewich: “Using a Continuously Stirred Tank Reactor (CSTR)

to Generate Exponential Dilution Calibration Curves". Reproducibility of these response factors should be regularly checked in order to be able to claim their validity over a long and specific period of time.

In order to quantify the contribution of each compound to every peak a de-synthesising procedure is used and described here. To de-synthesise mass spectra, or in other words, to subtract from each peak known contribution from a particular compound, we are based in general equation of signal of a particular m/z peak (noted as  $i$ ):

$$S_i(t) = S_{i,ISO}(t) + S_{i,IPN}(t) + S_{i,MVK}(t) + S_{i,MACR}(t) + \dots S_{i,j}(t) \quad (\text{Equation 3.1})$$

or 
$$S_i(t) = \sum_j S_{i,j}(t)$$

where :  $S_i(t)$  is the intensity of signal (mV) from a particular  $i$  peak at a given point in time expressed as the sum of intensity signals coming from known compounds (in general  $j =$  Isoprene, IPN, MVK, MACR and others).

Each of these signals could be given as a product of Response Factor ( $R_{i,j}$ ) with concentration ( $C_j$ ) of the compound in that time:

$$S_i(t) = \sum_j R_{i,j} C_j(t) \quad (\text{Equation 3.2})$$

where:  $j=[1 \dots M]$  in case that we have M compounds

We can build a matrix equation where the first and the last matrices are known and by solving this equation we will be able to find concentration of the compound of interest at a individual point in time :

$$\begin{bmatrix} R_{1,ISO} & R_{1,IPN} & R_{1,MVK} & R_{1,MACR} \cdots & R_{1,Cj} \\ R_{2,ISO} & R_{2,IPN} & R_{2,MVK} & R_{2,MACR} \cdots & R_{2,Cj} \\ R_{3,ISO} & R_{3,IPN} & R_{3,MVK} & R_{3,MACR} \cdots & R_{3,Cj} \\ R_{4,ISO} & R_{4,IPN} & R_{4,MVK} & R_{4,MACR} \cdots & R_{4,Cj} \\ \dots & \dots & \dots & \dots & \dots \\ R_{i,ISO} & R_{i,IPN} & R_{i,MVK} & R_{i,MACR} \cdots & R_{i,Cj} \end{bmatrix} \begin{bmatrix} C_{ISO}(t) \\ C_{IPN}(t) \\ C_{MVK}(t) \\ C_{MACR}(t) \\ \dots \\ C_{Cj}(t) \end{bmatrix} = \begin{bmatrix} S_1(t) \\ S_2(t) \\ S_3(t) \\ S_4(t) \\ \dots \\ S_i(t) \end{bmatrix} \quad (\text{Equation 3.3})$$

Hence we calculate:  $C_{ISO}(t)$  ;  $C_{IPN}(t)$ ;  $C_{MVK}(t)$ ;  $C_{MACR}(t)$ . etc., and  $S_{1,ISO}$ ;  $S_{1,IPN}$ ;  $S_{1,MVK}$ ;  $S_{1,MACR}$ ;  $S_{2,ISO}$ ; etc. By applying the Equation 3.3 at each individual point in time we are able to get time profile of concentration for each compound involved.

The de-synthesis of spectra is illustrated by first calculating the time profile of concentration of isoprene, MVK and MACR. By looking carefully at the Table 3.1 we see that these compounds give contributions to at least 6 ions, i.e  $m/z=55$ ,  $m/z=65$ ,  $m/z=67$ ,  $m/z=68$ ,  $m/z=69$ ,  $m/z=70$ . So we can build the following matrix equation:

$$\mathbf{RC} = \mathbf{S} \quad (\text{Equation 3.4})$$

or

$$\begin{bmatrix} R_{55,ISO} & R_{55,MVK} & R_{55,MACR} \\ R_{65,ISO} & R_{65,MVK} & R_{65,MACR} \\ R_{67,ISO} & R_{67,MVK} & R_{67,MACR} \\ R_{68,ISO} & R_{68,MVK} & R_{68,MACR} \\ R_{69,ISO} & R_{69,MVK} & R_{69,MACR} \\ R_{70,ISO} & R_{70,MVK} & R_{70,MACR} \end{bmatrix} \begin{bmatrix} C_{ISO}(t) \\ C_{MVK}(t) \\ C_{MACR}(t) \end{bmatrix} = \begin{bmatrix} S_{55}(t) \\ S_{65}(t) \\ S_{67}(t) \\ S_{68}(t) \\ S_{69}(t) \\ S_{70}(t) \end{bmatrix} \quad (\text{Equation 3.5})$$

where the first matrix is filled using the values extracted from Table 3.1 and the third matrix is filled by using measured signal of peak at  $m/z$  55, 65, 67, 68, 69, 70.

We have here an overdetermined system with 6 equations and 3 unknowns, the least square solution of which is given as :

$$\bar{C} = (\mathbf{R}^T \mathbf{R})^{-1} \mathbf{R}^T \mathbf{S} \quad (\text{Equation 3.6})$$

Where  $\mathbf{R}^T$  is the transpose matrix of  $\mathbf{R}$  and  $(\mathbf{R}^T \mathbf{R})^{-1}$  is matrix inverse of  $(\mathbf{R}^T \mathbf{R})$

By applying the Equation 3.6 we find the least square solution for concentration of isoprene, MVK and MACR which could be expressed as:

$$\begin{bmatrix} \bar{C}_{ISO}(t) \\ \bar{C}_{MVK}(t) \\ \bar{C}_{MACR}(t) \end{bmatrix}$$

By calculating the time profile of isoprene, MVK and MACR concentration, we are able to calculate their contribution to each of the signals included in Equation 3.5.

So in the Figure 3.8 we see de-synthesis of signal at  $m/z=70$ , where:

$$S_{70,MVK}(t) = R_{70,MVK} \bar{C}_{MVK}(t) ; \text{ and } S_{70,MACR}(t) = R_{70,MACR} \bar{C}_{MACR}(t) ;$$

$S_{70,calculated}(t) = S_{70,ISO} + S_{70,MVK}(t) + S_{70,MACR}(t)$  and  $S_{70,measured}(t)$  is the measured time profile of signal of peak at  $m/z=70$ . Note that  $S_{70,ISO} = 0$  because from Table 3.1 we have  $R_{70,ISO} = 0$ .

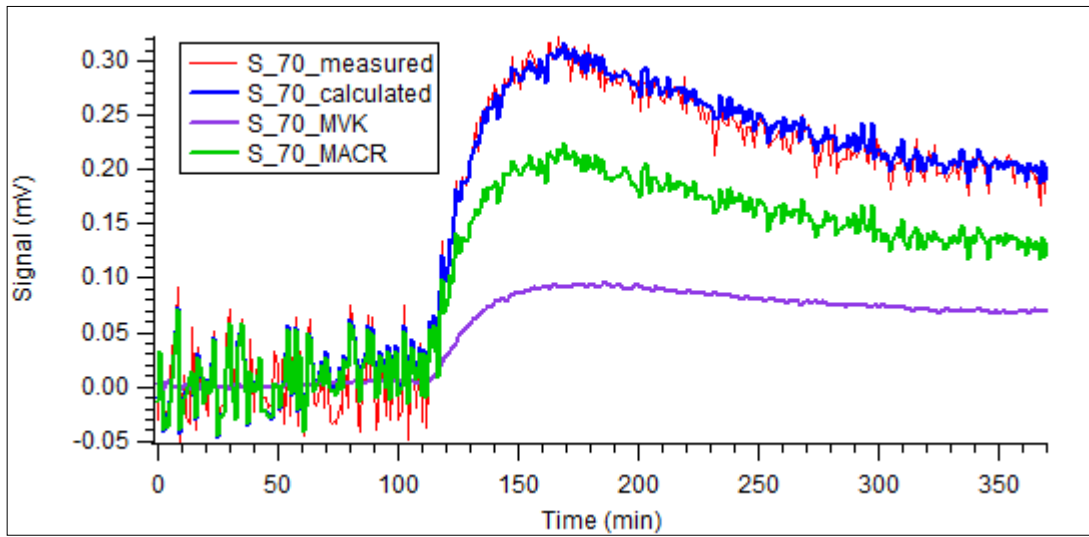


Figure 3.8 De-synthesis of peak 70 signal

The same procedure is used for Signal of  $m/z=55$  (Figure 3.9).

$$S_{55,ISO} = R_{55,ISO} \bar{C}_{ISO}(t); S_{55,MVK}(t) = R_{55,MVK} \bar{C}_{MVK}(t); S_{55,MACR}(t) = R_{55,MACR} \bar{C}_{MACR}(t)$$

$$S_{55,calculated}(t) = S_{55,ISO} + S_{55,MVK}(t) + S_{55,MACR}(t) \text{ and } S_{55,measured}(t) \text{ is the measured time}$$

profile of signal of peak  $m/z=55$ .

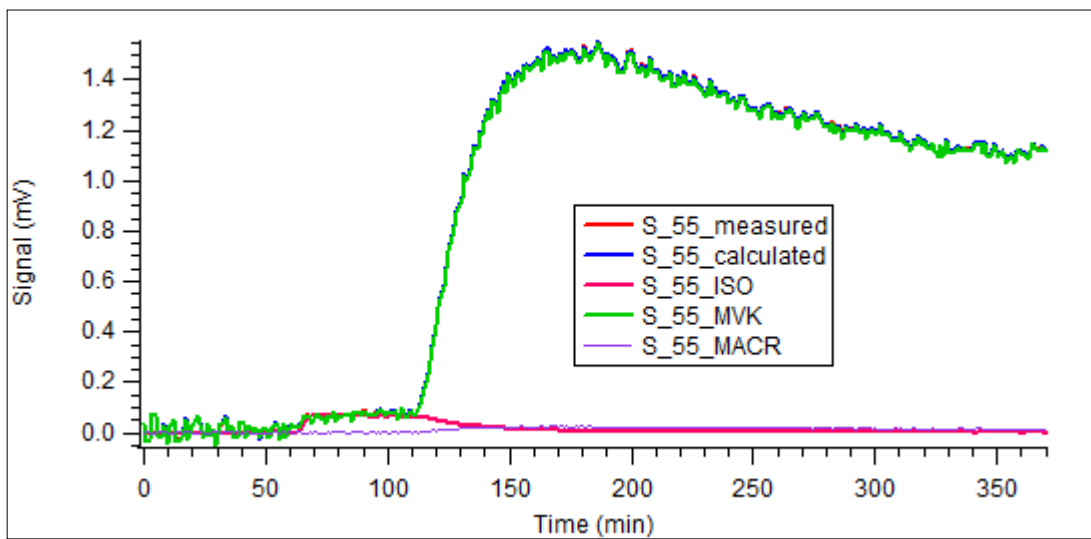


Figure 3.9 De-synthesis of peak 55 signal

For other four peaks in the Equation 3.5 we have calculated the time profile of intensity signal and compare them to respective measured signal, (Figure 3.10a,b,c,d). The calculated signal intensities are within the experimental errors, estimated as one standard deviation, based on the propagation through the analysis from estimated noise level (see Appendix). So, we have a good agreement between measured and calculated signals which indicates that using least square solution for concentration of isoprene, methacrolein and methyl vinyl ketone, give us reliable results.

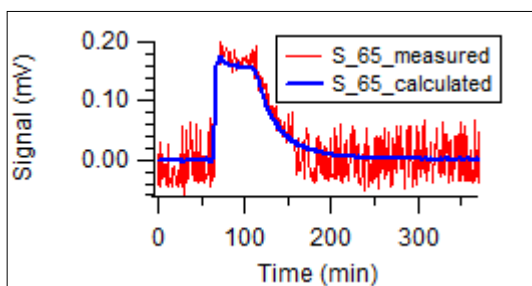


Figure 3.10a Time profile of signal at  $m/z=65$

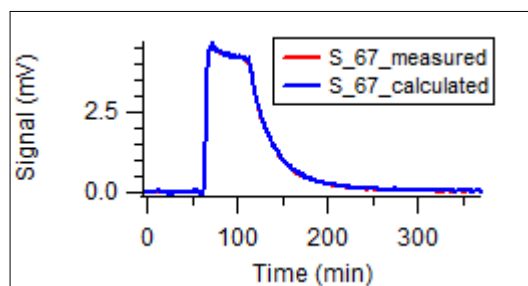


Figure 3.10b Time profile of signal at  $m/z=67$

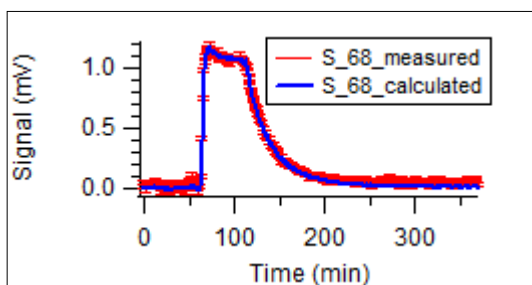


Figure 3.10c Time profile of signal at  $m/z=68$

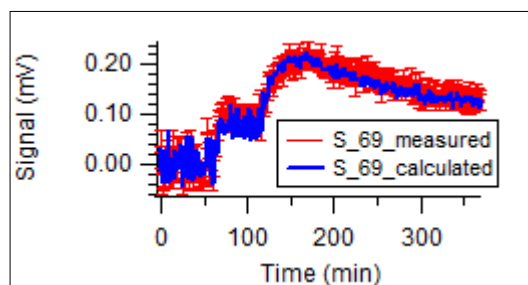


Figure 3.10d Time profile of signal at  $m/z=69$

Another example which illustrates the application of de-synthesis procedure is given for the peak at  $m/z=39$ :

From Table 3.1 we know that Signal of peak at  $m/z=39$  may be given as:

$$S_{39,calculated} = S_{39,ISO} + S_{39,MVK} + S_{39,MACR}$$

Having calculated the concentration of isoprene, methyl vinyl ketone, methacrolein ( $\bar{C}_X$ ) and knowing respective Response Factors we calculated the  $S_{39,ISO}(t)$ ,  $S_{39,MVK}(t)$  and  $S_{39,MACR}(t)$  as:

$$S_{39,X}(t) = R_{39,X} \bar{C}_X(t) \quad (\text{Equation 3.7})$$

Where X= Isoprene, MVK or MACR

Figure 3.11a represents calculated time profile of signals for ions with  $m/z=39$  coming as known fragments of isoprene, MVK and MACR ( $S_{39,ISO}(t)$ ,  $S_{39,MVK}(t)$  and  $S_{39,MACR}(t)$ )

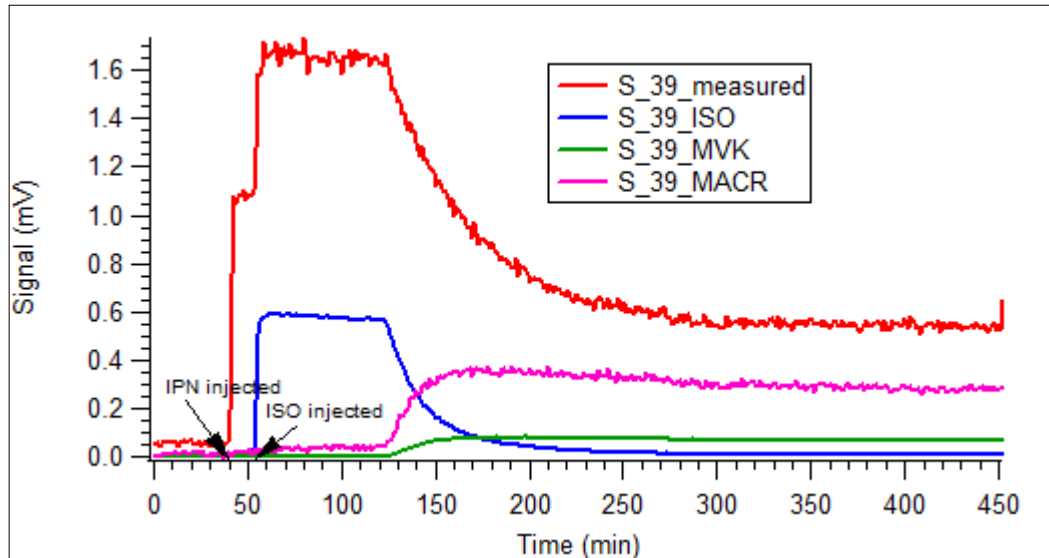


Figure 3.11a De-synthesis of peak 39 signal into known contributors

So we were able to get the sum:

$$S_{39,calculated}(t) = S_{39,ISO}(t) + S_{39,MVK}(t) + S_{39,MACR}(t)$$

And from here we got the remaining signal (Figure 3.11b) as the difference between the measured signal at peak  $m/z=39$  and calculated signal given as the contribution of isoprene plus MVK and MACR:

$$S_{39,difference} = S_{39,measured} - S_{39,calculated}$$

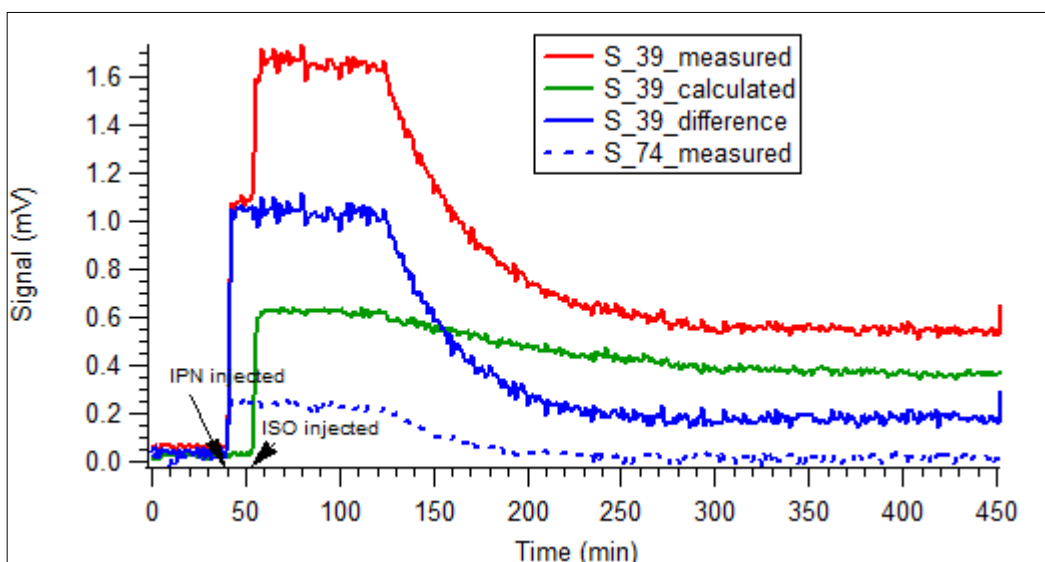


**Figure 3.11b** The signal difference between measured and calculated values for peak 39

The residual signal (Figure 3.11b:  $S_{39,difference}$ ) contains the contribution from IPN (there is a non zero response factor of IPN to peak 39, based on the IPN reference spectra<sup>4</sup>, ) but also may contain the contribution of any first or second generation product as the  $S_{39,difference}$  decays to a constant value after all the isoprene and IPN are consumed ( $m/z=74$  representing IPN is also shown in Figure 3.11b). By plotting the residual signal,  $S_{39,difference}$ , versus signal of  $m/z=74$  (IPN) we notice that there is not a zero intercept, suggesting that contributions from other compounds are possible.

<sup>4</sup> IPN reference spectra are prepared by Aeysha Ahmed

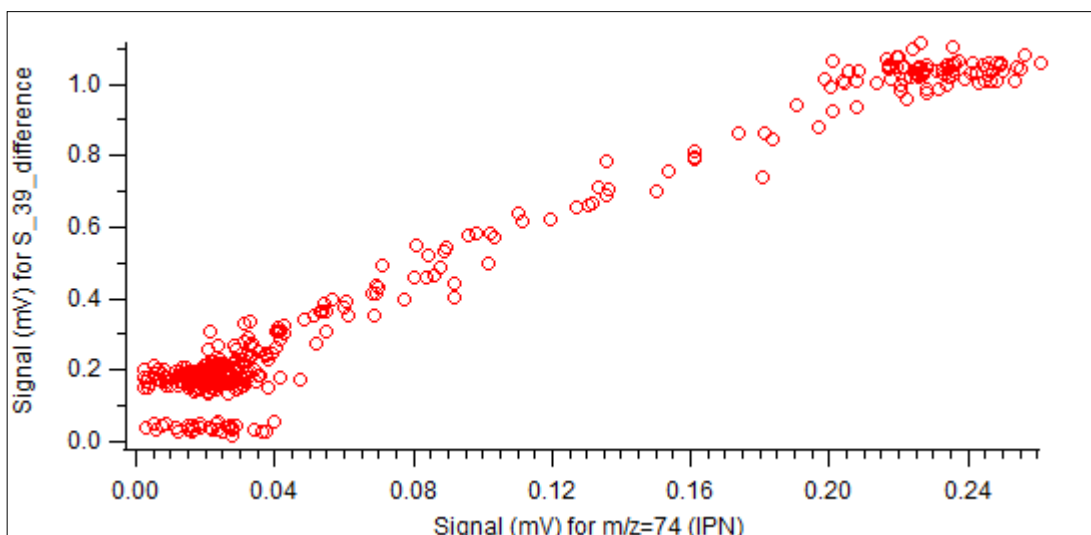


**Figure 3.12 Residual signal  $S_{39,difference}$  versus Signal of  $m/z=74$  (IPN)**

A detailed subtraction procedure for every detected (measured) peak is beyond the scope of my work. I have been focused on those peaks which substantially come from isoprene, MVK and MACR .

### **3.1.2 Product Yield (%) calculation**

By plotting calculated concentration of isoprene, MVK and MACR as a function of time (Figure 3.13) we can calculate yield of formation of MVK and MACR.

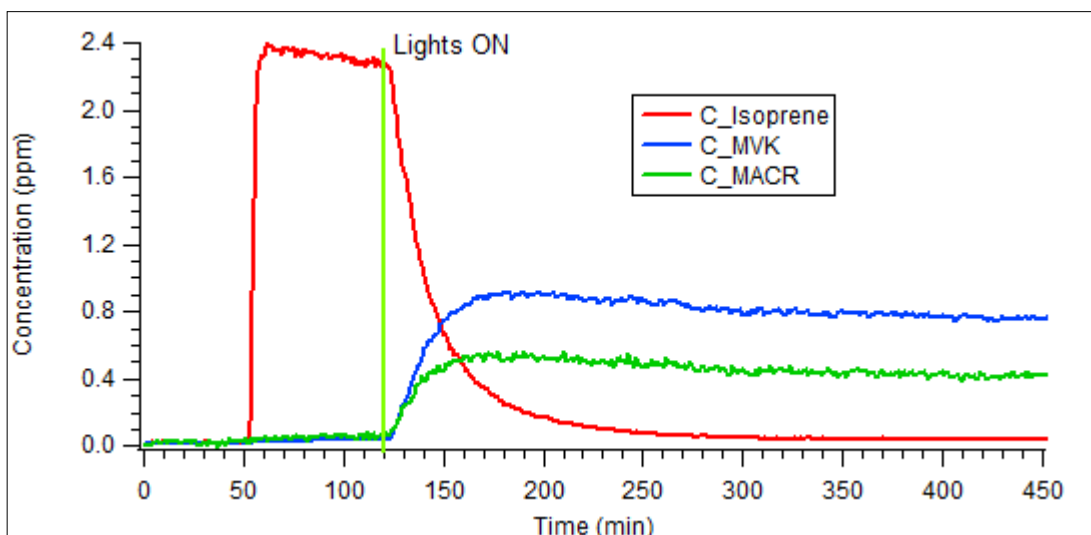


**Figure 3.13 Concentrations (ppm) of isoprene, MACR and MVK as function of time**

The yield of methacrolein (MACR) and methyl vinyl ketone (MVK) is the ratio of the amount of MACR or MVK formed over the amount of isoprene consumed. MACR and MVK are main first generation products of isoprene photo-oxidation, but at the same time they start being consumed (photooxidized) as they are formed, giving birth to second generation products. So the concentration of MACR and MVK that we measure using IT-TOF Mass Spectrometer is the expression of this difference. Below it is described “The first and second generation” procedure<sup>5</sup>, (developed by Prof. Mozurkewich) , used to calculate product yield for MVK and MACR :

Let’s consider the general case by following two reactions:



and write their rate equations :

<sup>5</sup> We have described here the whole procedure which includes also second generation products P2. A detailed elaboration of second generation products is done during discussion about SOA formation from MACR (see pg 66-67)

$$\frac{d[\text{Isoprene}]}{dt} = -k_1[\text{OH}][\text{Isoprene}] \quad (\text{Equation 3.8})$$

$$\frac{d[\text{P1}]}{dt} = \beta k_1[\text{OH}][\text{Isoprene}] - k_2[\text{OH}][\text{P1}] \quad (\text{Equation 3.9})$$

$$\frac{d[\text{P2}]}{dt} = k_2[\text{OH}][\text{P1}] \quad (\text{Equation 3.10})$$

where  $k_1$  and  $k_2$  are rate constant and  $\beta$  is the branching ratio (yield) .There should actually be a separate branching ratio for each of two steps, but since only the product of two will appear in the final result we can, without loss of generality, combine them into a single branching ratio and apply that to either step.

To solve these equations, we introduce the dimensionless variables:

$$x \equiv \frac{[\text{Isoprene}]}{[\text{Isoprene}]_0} ; \quad y \equiv \frac{[\text{P1}]}{[\text{Isoprene}]_0} ; \quad z \equiv \frac{[\text{P2}]}{[\text{isoprene}]_0} ; \quad r \equiv \frac{k_2}{k_1}$$

where  $[\text{Isoprene}]_0$  is initial isoprene concentration. Now if we divide Equation 3.8 by

Equation 3.9, and make these substitutions we obtain:

$$\frac{dy}{dx} = \frac{ry}{x} - \beta \quad (\text{Equation 3.11})$$

Multiplying both sides by  $dx$ , dividing both sides by  $x^r$  and rearranging gives:

$$\frac{dy}{x^r} + \left( \frac{\beta}{x^r} + \frac{ry}{x^{1+r}} \right) dx = 0 \quad (\text{Equation 3.12})$$

which is an exact differential. Integrating it from  $y=0$  when  $x=1$  ( $[\text{Isoprene}]=[\text{Isoprene}]_0$ )

gives:

$$\frac{1}{x^r} \left( y + \frac{\beta x}{1-r} \right) = \frac{\beta}{1-r} \quad (\text{Equation 3.13})$$

or

$$y = \frac{\beta(x^r - x)}{1 - r} \quad (\text{Equation 3.14})$$

If some of the product is already present when the reaction begins ( $y=y_0$  when  $x=1$ ) then

Equation 3.11 becomes:

$$y = y_0 x^r + \frac{\beta(x^r - x)}{1 - r} \quad (\text{Equation 3.15})$$

By applying in our case  $[P1] = [\text{MVK}]$  or  $[P1]=[\text{MACR}]$  we plot  $y \equiv \frac{[\text{MVK}]}{[\text{Isoprene}]_0}$

versus  $x \equiv \frac{[\text{Isoprene}]}{[\text{Isoprene}]_0}$  (Figure 3.14) or  $y \equiv \frac{[\text{MACR}]}{[\text{Isoprene}]_0}$  versus  $x \equiv \frac{[\text{Isoprene}]}{[\text{Isoprene}]_0}$

(Figure 3.15). Note that initial isoprene concentration,  $[\text{Isoprene}]_0$ , is taken as one point in time, at the moment before the lights are turned on and the reaction starts. Then by fitting the Equation 3.15 in these plots<sup>6</sup> we obtained the yield of formation of MVK and MACR:

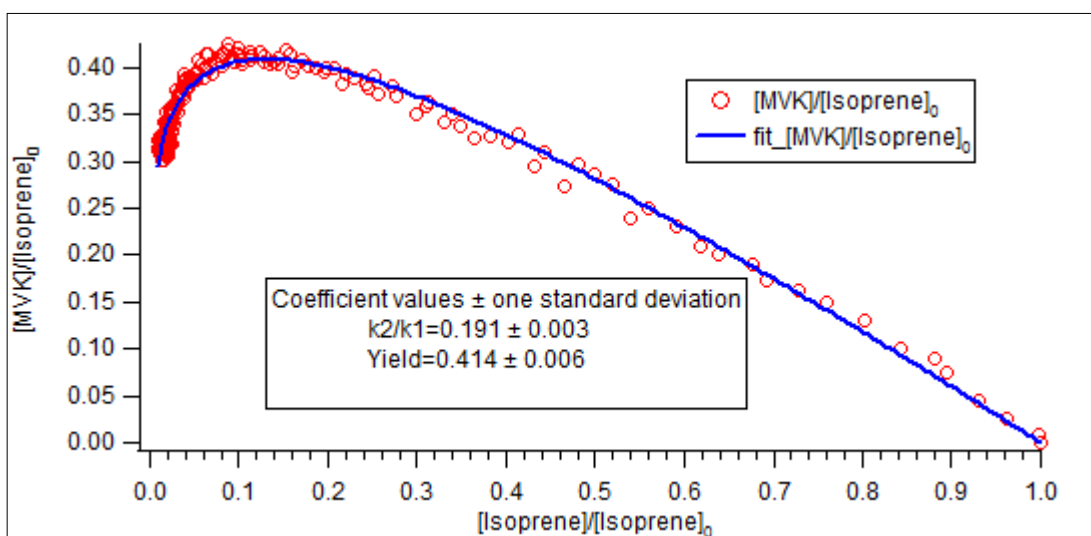


Figure 3.14 “First generation product” procedure used to calculate MVK yield

<sup>6</sup> During fitting procedure (weighted fit) we assumed that initial product values are 0 ( $0 \pm 0$ )

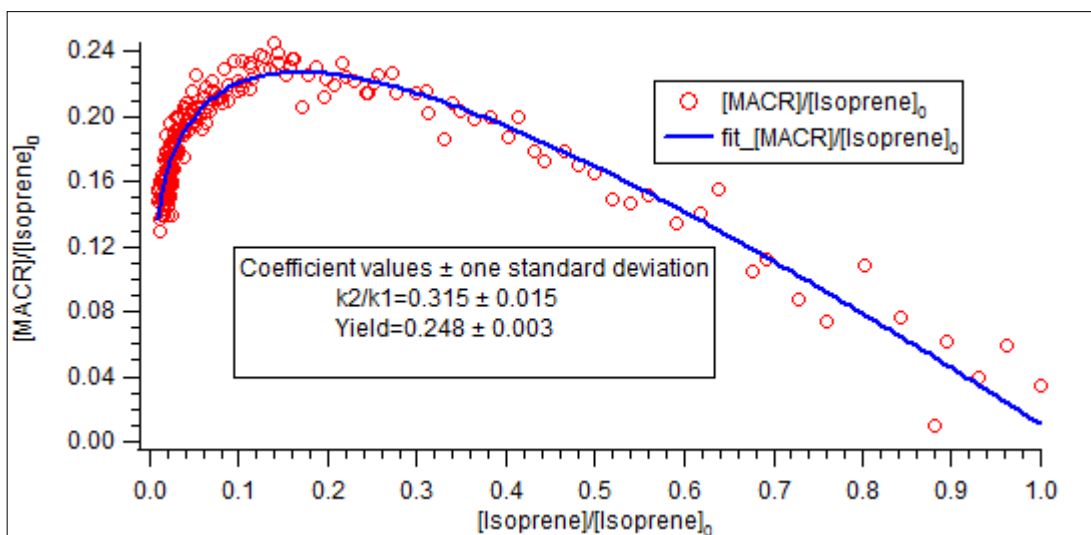


Figure 3.15 “First generation product” procedure used to calculate MACR yield

MVK yield =  $41.4 \pm 0.6^7$  %

MACR yield =  $24.8 \pm 0.3$  %

These values are in good agreement with those reported in other published works (Table 3.2). Further work is required in the future to investigate the effect of NO<sub>x</sub> level, temperature, OH concentration, relative humidity, on the yield results.

**Table 3.2: Product Yields (%) from OH-initiated oxidation of isoprene in the presence of NO**

Product	Previous work	This work
MVK	$29 \pm 7^a$ , $36 \pm 4^b$ , $32 \pm 5^c$ , $44 \pm 6^d$	$41.4 \pm 0.6$
MACR	$21 \pm 5^a$ , $25 \pm 3^b$ , $22 \pm 2^c$ , $28 \pm 4^d$	$24.8 \pm 0.3$

a: [Tuazon et al., 1990a] ; b: [Paulson et al., 1992] ; c: [Miyoshi et al., 1994] ; d: [Sprengnether et al., 2002].

<sup>7</sup> It should be noted that throughout this work whenever error limits are calculated they don't include the effect of systematic errors.

The fitting procedure described above provides us with valuable information related to rate constant of MVK and MACR photo-oxidation reactions initiated by OH radicals. So, from plots in Figure 3.14 and Figure 3.15 we have found that rate constant ratio ( $k_2/k_1$ ) is  $0.191\pm 0.003$  and  $0.315\pm 0.015$  for MVK and MACR, respectively. Assuming that rate constant for photo-oxidation of isoprene is  $k_1=1.02\times 10^{-10}$   $\text{cm}^3\text{molecule}^{-1}\text{s}^{-1}$  [Atkinson, R. and Aschmann, S. M., 1984], we calculate that for MVK,  $k_2=1.95\times 10^{-11}$   $\text{cm}^3\text{molecule}^{-1}\text{s}^{-1}$  and for MACR,  $k_2=3.21\times 10^{-11}$   $\text{cm}^3\text{molecule}^{-1}\text{s}^{-1}$ , which are close to reported values (Table 3.3):

**Table 3.3 Rate constant of photooxidation reactions for MVK and MACR**

Product	Previous work ( $\times 10^{-11}$ ), ( $\text{cm}^3\text{molecule}^{-1}\text{s}^{-1}$ )	This work ( $\times 10^{-11}$ ), ( $\text{cm}^3\text{molecule}^{-1}\text{s}^{-1}$ )
MVK	$1.79\pm 0.28$ , <sup>a</sup> $2.03\pm 0.17$ , <sup>b</sup> $1.73\pm 0.21$ , <sup>c</sup>	$1.95 \pm 0.12$
MACR	$3.14\pm 0.49$ , <sup>a</sup> $2.79\pm 0.12$ , <sup>b</sup> $3.22\pm 0.10$ , <sup>c</sup>	$3.21 \pm 0.29$

a: [Kleindienst et al., 1982]; b: [Gierczak et al., 1997]; c: [Chuong and Stevens, 2003]

### 3.1.3 Some interesting peaks

So far, we have been able to identify, quantify and calculate yield production for the two major products (MVK and MACR) of isoprene photo-oxidation. There were still a number of detected peaks in our mass spectra which drew our attention, as they show up after the oxidation of isoprene has started ( $m/z=82$ ,  $84$ , and  $85$  peaks as it is elaborated in

more details in paragraph 3.1.1) and on the other hand they are not fragments of any of our major products (MVK and MACR) (except  $m/z=85$ : see below)

The work done to investigate about their identity and mechanism of formation is presented here.

First by plotting in one graph (Figure 3.16) signal intensities vs time for peaks at mass to charge ratio : 82, 84, 85, we see their evolution and decay over time.

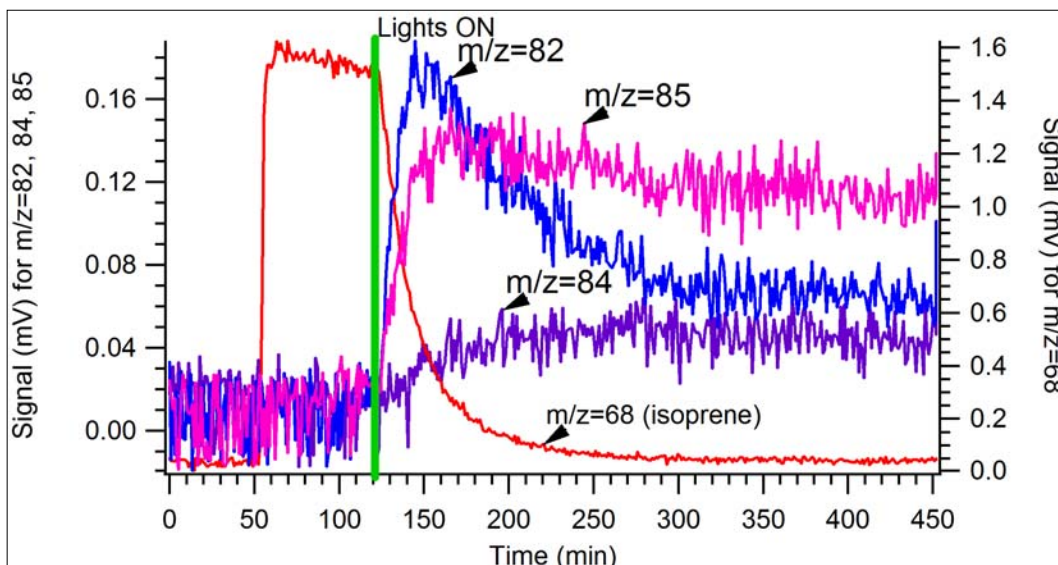


Figure 3.16 Signal (mV) vs time for  $m/z=82, 84, 85$  peaks

We will start our discussion here with  $m/z=82$  peak which shows a more pronounced signal and a rapid decay.

*Some consideration about identity of  $m/z=82$  species .*

First: What is the  $m/z=82$  species : a first or second generation product?

$m/z = 82$  appears at in the same time as isoprene ( $m/z=68$ ) starts to be consumed (oxidized) (In Figure 3.17 we have plotted the signal of  $m/z=82$  vs the signal of  $m/z=68$

(isoprene) consumed, calculated as difference between initial intensity of  $m/z=68$  peak (before lights ON) and intensity signal at a given time ).

$m/z=82$  seems to be a first generation product as it starts to be produced immediately after the isoprene starts to be consumed.

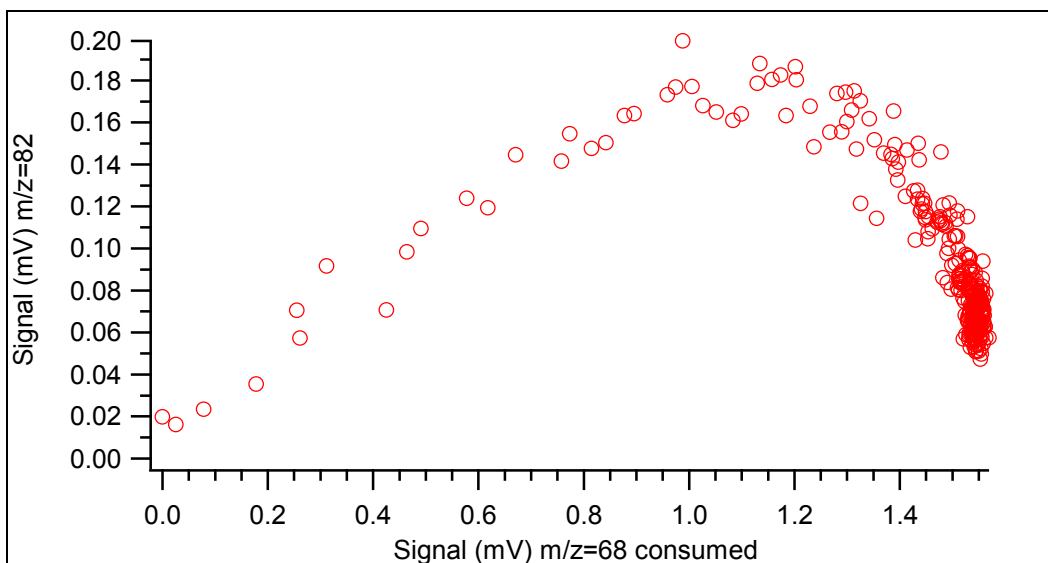


**Figure 3.17** Signal of  $m/z=82$  species vs signal of  $m/z=68$  (isoprene) consumed

The signal of  $m/z=82$  species keeps growing until more than 50% (about 1.2 mV) of isoprene is consumed and then its decay prevails over its formation.

Second: What's its identity?

Here we will discuss two hypotheses about the identity of  $m/z=82$  species:

1.  $m/z=82$  species is a molecular ion of 3-methyl furan (MW=82)
2.  $m/z=82$  species is a fragment of a hydroxycarbonyl compound (MW=100)

1. A number of studies (Tuazon et al, 1990; Paulson et al, 1992; Sprengnether et al, 2002) have reported 3-methyl-furan (MW=82) as a minor product (<2-5%) of isoprene photo-oxidation by OH radicals.

Also Atkinson et al, 1989 have measured the rate constant for reaction of 3-methyl furan with OH radical as  $9.35 \times 10^{-11} \text{ cm}^3 \text{ molecule}^{-1} \text{ s}^{-1}$  (with an estimated overall uncertainty of  $\pm 20\%$ ) at 296 K.

We calculated the rate constant for  $m/z = 82$  (based on “first and second generation products” procedure, described above) developed by Prof. Mozurkewich using IGOR Pro), assuming that during our experiment it is oxidized only by OH radicals.

Recalling Equation 3.8 – Equation 3.15 and by applying in our case we have  $[P1] \equiv [m/z=82 \text{ signal}]$  and  $[Isoprene] \equiv [m/z=68 \text{ signal}]$ , we have:

$$y \equiv \frac{[m/z = 82 \text{ signal}]}{[m/z = 68 \text{ signal}]_0} \quad \text{and} \quad x \equiv \frac{[m/z = 82 \text{ signal}]}{[m/z = 68 \text{ signal}]_0}$$

By plotting  $y$  vs  $x$  and fitting Equation 3.15 to it, (Figure 3.18) we got  $r=k_2/k_1$  to be  $0.75 \pm 0.015$  and by assuming  $k_1=(1.02 \pm 0.04) \times 10^{-10} \text{ cm}^3 \text{ molecule}^{-1} \text{ s}^{-1}$  [Atkinson, R. and Aschmann, S. M., 1984], rate constant of oxidation reaction of  $m/z=82$  species comes out to be  $k_2=(7.65 \pm 0.46) \times 10^{-11} \text{ cm}^3 \text{ molecule}^{-1} \text{ s}^{-1}$ , which is just barely within the error limits of published value. However this is an indication that  $m/z=82$  species could be 3-methyl furan.

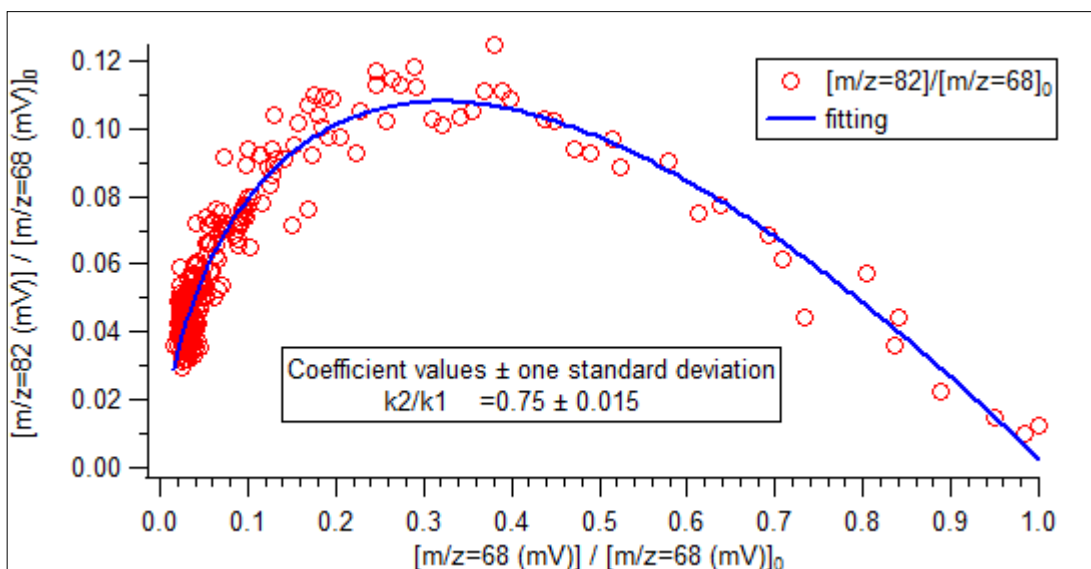


Figure 3.18 “First generation” fitting plot used to calculate relative rate constant

The proposed mechanism of formation of 3-methyl furan from the oxidation of isoprene is given below (Atkinson et al, 1989):

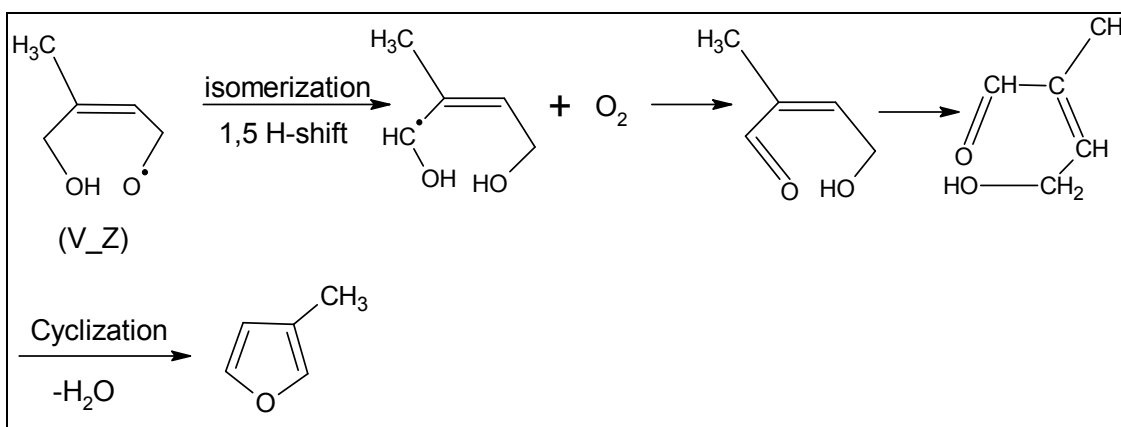


Figure 3.19 The proposed mechanism of formation of 3-methyl furan [Atkinson et al., 1989]

In this proposed pathway we have an  $\delta$ -hydroxy alkoxy radical which via 1,5 H-shift becomes an double hydroxyl radical which by reacting with  $O_2$  produces an C5 hydroxy carbonyl (MW=100) which in turns by cyclization loses one molecule of water giving 3-

methyl furan. Not having presented solid arguments for the last step in this mechanism (cyclization) confronted with reported C5-hydroxycarbonyl as first generation products of photo-oxidation of isoprene with a yield of 19.3%  $\pm$ 6.1 (Zhao et al) suggests investigation of second hypothesis that m/z=82 species detected in TOF instrument could be a fragment of C5-hydroxycarbonyl compound. To further shed light into this relationship we used Atmospheric Pressure Chemical Ionization Mass Spectrometer (APCI MS), run by Zoya Dobrusin<sup>8</sup>, which along with our TOF Mass Spectrometer sampled from the Smog Chamber during another isoprene experiment. It should be briefly noted that H<sub>3</sub>O<sup>+</sup> acts as a chemical ionization agent by adding a proton (H<sup>+</sup>) to analyte molecules or their fragments in the APCI source. Also H<sub>3</sub>O<sup>+</sup> upon collision with other molecules of water forms a series of small clusters H<sub>3</sub>O<sup>+</sup>(H<sub>2</sub>O)<sub>n</sub> (n=0-4). Once a molecule more basic (higher Proton Affinity) than H<sub>2</sub>O enters the APCI source, the proton is transferred to it, and subsequent collisions form clusters of the newly protonated species.

We got very similar time dependence for ions m/z=83 and m/z=101, obtained from APCI MS, as shown below in the Figure 3.20 and Figure 3.21. It seems that they are in a relationship parent/fragment. This hypothesis has found strong support by plotting these ions against each other (Figure 3.22), where we have a nice straight line and zero intercept. Is the m/z=101 species a water cluster of m/z=83 ion or is m/z=83 species a fragment of m/z=101 ion? We see that the signal at m/z=101 is much larger than at m/z=83. That would seem reasonable if m/z=101 ion is the parent and m/z=83 ion is a

---

<sup>8</sup> All graphs related to APCI MS are prepared by Zoya Dobrusin with whom we had very fruitful discussions about the relationship between m/z=83 and m/z=101 species

fragment because typically water clusters are lower in intensity compared to their parent ion.

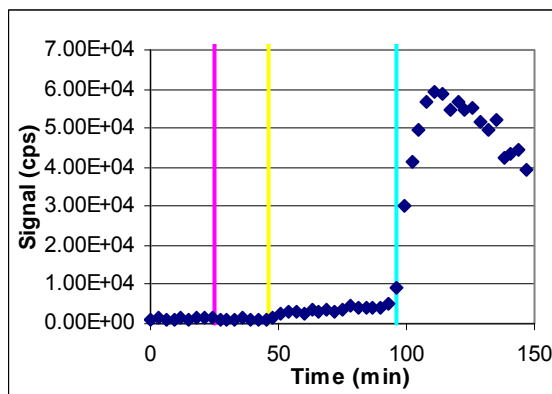


Figure 3.20  $m/z=83$  time profile

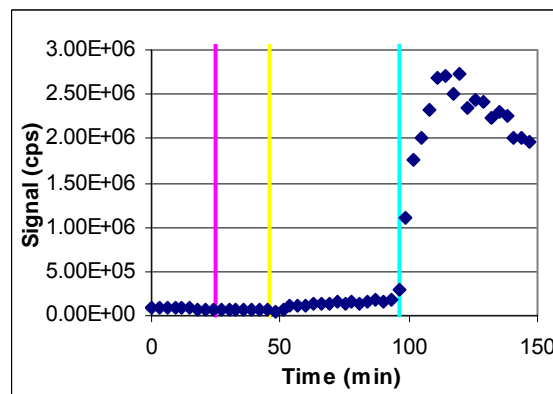


Figure 3.21  $m/z=101$  time profile

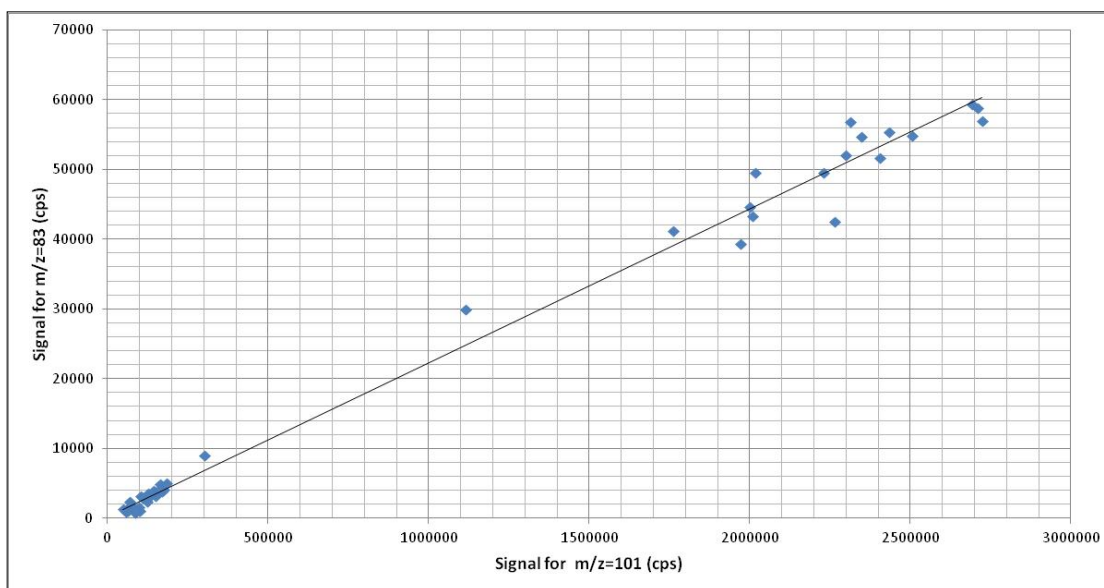


Figure 3.22 Relationship between  $m/z=83$  and  $m/z=101$  species

To further investigate the relationship between ion  $m/z=101$  and any potential fragment of it, we use MS/MS mode of APCI MS, which allow us for any selected ion (in our case  $m/z=101$  ion) to fragment it and monitor the behaviour of fragments over time.

By using Selected Monitoring Scans (SMS) with a Collision Energy (CE) 5 eV for  $m/z=101$  ion, we got the time dependence for the following fragments:  $m/z=83$  (Figure 3.23, 101/83 means that 83 is obtained from the fragmentation of 101),  $m/z=73$  (Figure 3.24, 101/73),  $m/z=59$  (Figure 3.25, 101/59),  $m/z=55$  (Figure 3.26, 101/55).

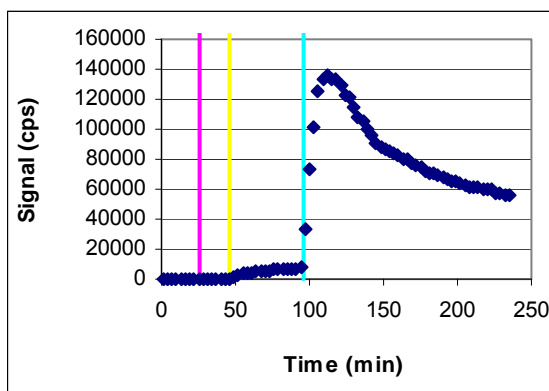


Figure 3.23 101/83, [M+H]<sup>+</sup>, M=100u, -18

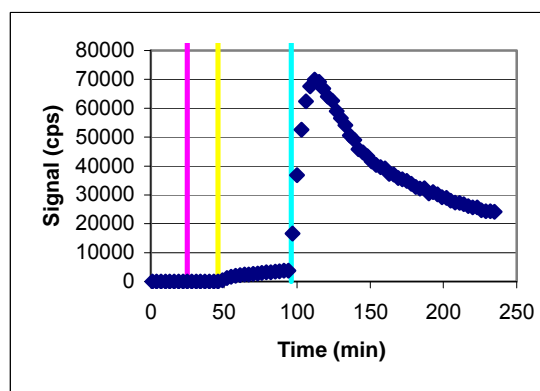


Figure 3.24 101/73, [M+H]<sup>+</sup>, M=100u, -28

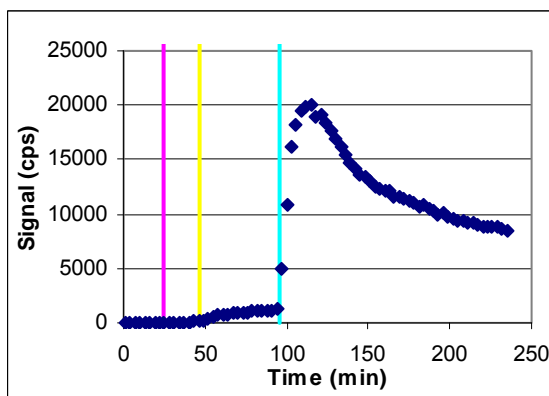


Figure 3.25 101/59, [M+H]<sup>+</sup>, M=100u, -42

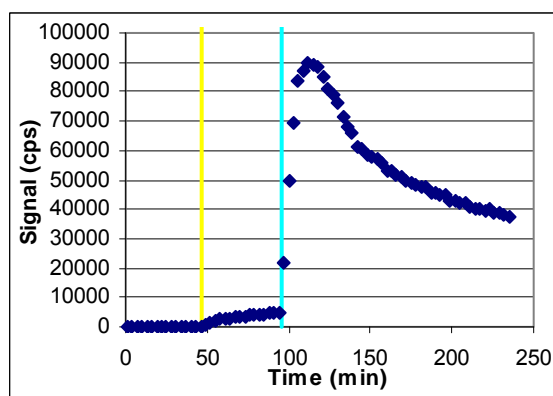


Figure 3.26 101/55, [M+H]<sup>+</sup>, M=100u, -46

By carefully looking at these plots we see that they have very similar pattern which suggests that they all reflect the time dependence of a hydroxycarbonyl species. So, we have here a number of fragments coming from  $m/z=101$  ion during SMS all of which it

seems that make sense: the  $m/z$  83 fragment is the loss of  $H_2O$  (makes sense for an alcohol), 73 is the loss of  $CO$  (makes sense for carbonyl), 59 is protonated acetone or propionaldehyde with the other fragment being ketene ( $H_2C=C=O$ ), and 55 would be loss of both  $H_2O$  and  $CO$ . Furthermore we don't think that makes sense to get  $m/z=73$  ion from a water cluster of  $m/z=83$  since the cluster should lose  $H_2O$  much more readily than  $CO$ .

Based on the analysis of two hypotheses built above we assign the  $m/z=82$  species (mass 100) to a gamma-hydroxycarbonyl, either 4-hydroxy-2-methyl-crotonaldehyde (Figure 3.29: Mechanism of formation of C4- and C5- hydroxycarbonyls : coming from V\_Z and VI\_E alkoxy isomers) or 4-hydroxy-3-methyl-crotonaldehyde (Figure 3.29 : coming from VI\_Z alkoxy isomer).

As described above we calculated rate constant of  $m/z=82$  species (actually a hydroxycarbonyl species) photo-oxidation. To date there is no experimental data for rate constant of OH initiated hydroxycarbonyl oxidation. Based on Structure-Activity Relationship (SAR) [mcm.leeds.ac.uk/MCM] method, it's estimated that rate constant for OH-initiated C5-hydroxycarbonyls oxidation to be  $4.5 \times 10^{-11} \text{ cm}^3 \text{ molecule}^{-1}\text{s}^{-1}$ . Our result ( $7.65 \times 10^{-11} \text{ cm}^3 \text{ molecule}^{-1}\text{s}^{-1}$ ) is within a factor of 2 compared to the reported value. This is in agreement with declared uncertainty of SAR method [Kwok, E. S. C., and Atkinson, R., 1995].

#### *Some consideration about identity of $m/z=84$ species*

The peak at  $m/z=84$  showed up after the light were turned on and oxidation of isoprene started. There are a number of studies that have detected  $m/z = 84$  and suggested it to be a

carbonyl species (C5-carbonyl  $C_5H_8O$  (MW=84) as molecular ion), in presence (Yu et al, 1995) and absence ( Bellkelberg et al, 2000) of NO, but so far there is not any agreement about the mechanism of formation.

Based on the “First generation product” procedure (Figure 3.27) we calculated rate constant ratio ( $k_2/k_1$ ) to be  $0.14 \pm 0.013$  and assuming  $k_1=(1.02\pm 0.04) \times 10^{-10} \text{ cm}^3 \text{ molecule}^{-1} \text{ s}^{-1}$  [Atkinson, R. and Aschmann, S. M., 1984], it comes out that the rate constant of our 84 species is  $(1.43\pm 0.13) \times 10^{-11} \text{ cm}^3 \text{ molecule}^{-1} \text{ s}^{-1}$ .

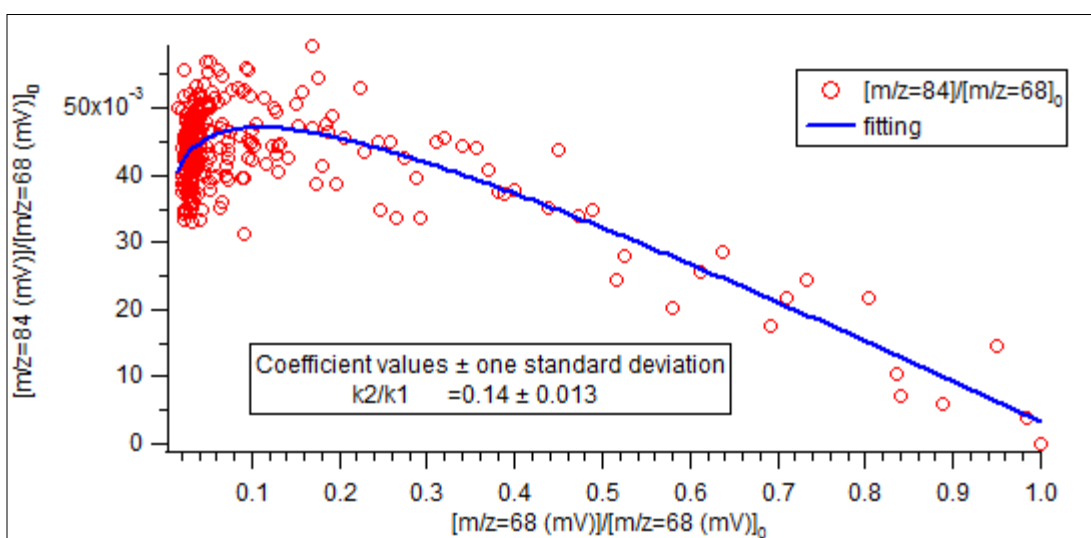


**Figure 3.27** Fitting procedure used to calculate rate constant for  $m/z=84$  species

*Some consideration about identity of  $m/z=85$  species*

Reference spectra of methacrolein shows that peak  $m/z=85$  appeared as a peak originated from methacrolein. On the other hand a number of studies (Zhao, J. at al, 2004) have identified C4-hydroxycarbonyl (MW=86) as one of the products of isoprene photo-oxidation in the presence of NO, which suggest that  $m/z=85$  could be assigned as deprotonated ion of a C4-hydroxycarbonyl. Knowing the concentration of methacrolein formed (calculated previously) we were able to separate the signal attributable to

methacrolein (S\_85\_MACR) and getting the signal of  $m/z=85$  attributable potentially to C4-hydroxycarbonyl (MW=86), (S\_85\_carbonyl). Figure 3.28 represents de-synthesis of peak 85 signal. At this point it is not clear why  $m/z=82$  and  $m/z=85$  species representing C5- and C4- hydroxycarbonyl compounds respectively, show very different decay patterns (very different reactivities).

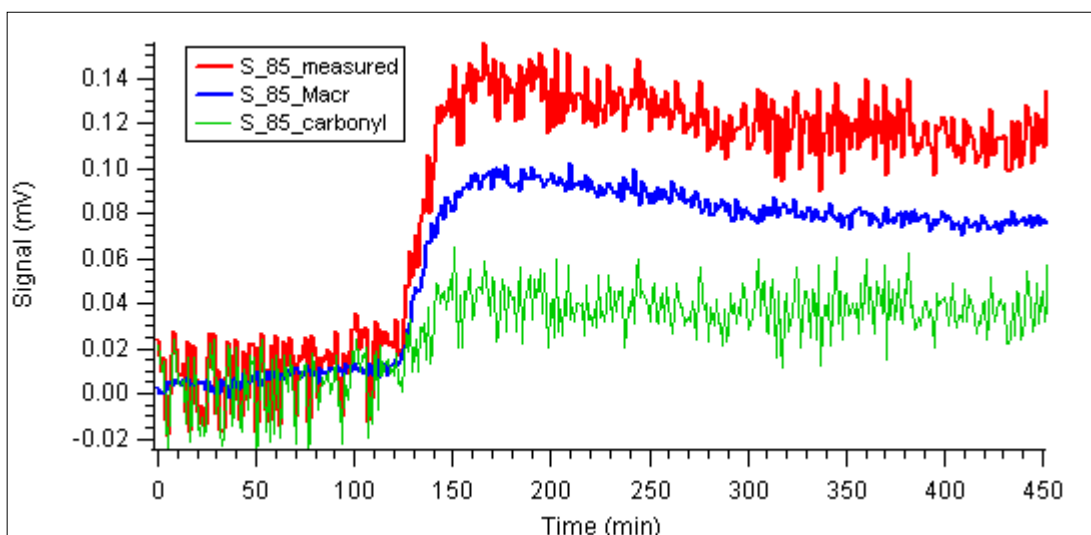


**Figure 3.28 De-synthesis of peak 85 signal**

*Some consideration about the mechanism of formation of hydroxycarbonyl compounds*

The mechanisms proposed for the formation of C4-(MW=86) and C5-(MW=100) hydroxycarbonyls (Zhao et al, 2004) is given below (Figure 3.29):

The alkoxy radicals (see Figure 1.1-1.4 in Chapter 1 for the proposed mechanism of their formation) are key intermediates in isoprene oxidation reactions. They may potentially undergo decomposition, isomerization, or reaction with  $O_2$ . Decomposition of  $\beta$ -hydroxyalkoxy radicals leads to the formation of methyl vinyl ketone (MVK) and methacrolein (MACR) along with formaldehyde.

In contrast, the decomposition barriers of the  $\delta$ -hydroxyalkoxy are significantly higher, rendering this pathway implausible. On the other hand, except for the alkoxy radical (VI,E), H-migration of the  $\delta$ -hydroxyalkoxy radicals occurs readily via a 1,5 H-shift to form double hydroxyl radicals, which then react to form C4 ( $C_4H_6O_2$ , MW=86) or C5 ( $C_5H_8O_2$ , MW=100) hydroxycarbonyls.

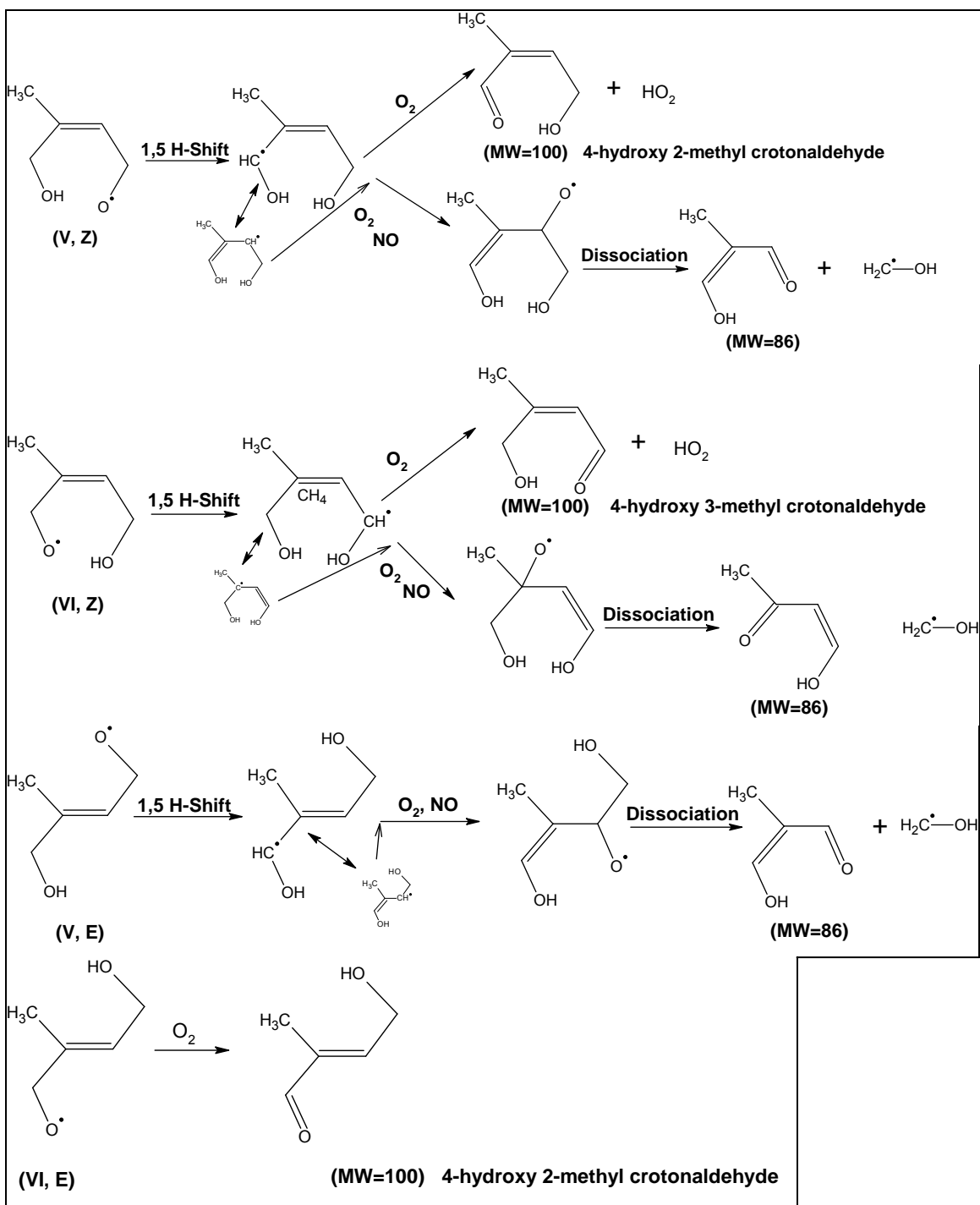


Figure 3.29 Mechanism of formation of C4- and C5- hydroxycarbonyls

## **3.2 Particulate phase products**

In recent years particulate matter formation from the isoprene photo-oxidation has drawn attention of a large number of research groups due to fact that isoprene is the most abundant biogenic VOC emitted in the atmosphere and evidences from field studies (Claeys et al, 2004, Kleindienst et al, 2007, Surrat et al, 2007) and laboratory experiments (Pandis et al, 1991, Miyoshi et al, 1994, Kroll et al, 2005,2006, Surrat et al, 2006, Ng et al, 2006) show that isoprene photo-oxidation indeed contributes to SOA. Those studies have shed light into the mechanism of formation of SOA from isoprene and the chemical composition of SOA, but still great uncertainties remain about the main intermediates and chemical mechanism of particle growth.

### **3.2.1 Secondary Organic Aerosol (SOA) formation and growth**

My work was focused on the investigation of the mechanism of formation and growth of SOA from photo-oxidation of isoprene, during Smog Chamber experiments.

In the previous chapters we have described the conditions in which the isoprene experiments are performed and SOA is investigated.

From the Figure 3.30 we see particulate matter formation as the isoprene is consumed (photooxidized).

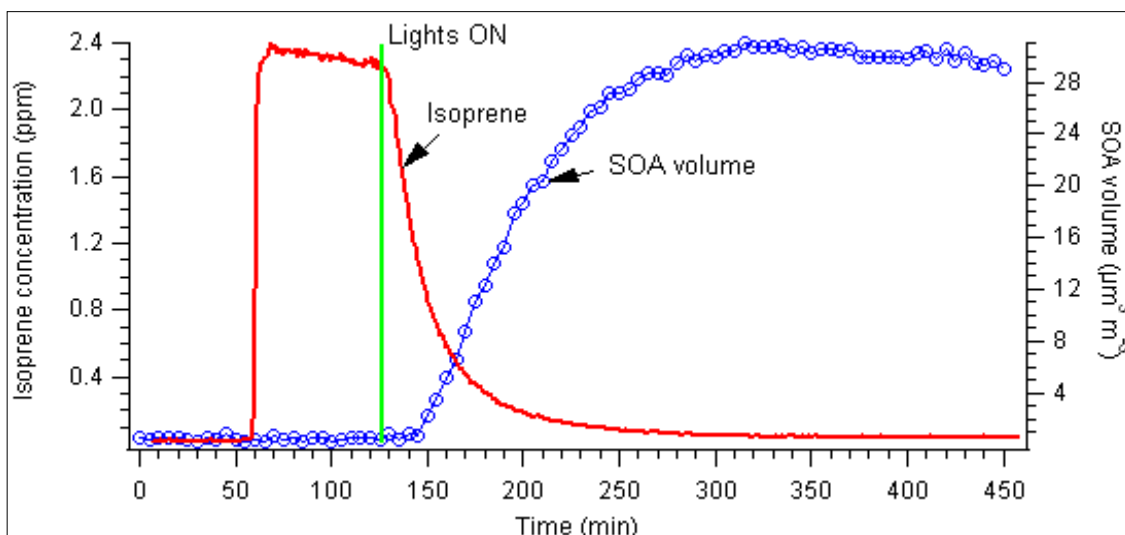


**Figure 3.30 SOA growth and isoprene concentration vs time**

Particulate matter starts to form approximately 20 min after the initiation of isoprene photo-oxidation, which corresponds to more than 50% of isoprene consumed. This implies that SOA formed is not a first generation product. In graph below (Figure 3.31) we see two main first generation products of isoprene photo-oxidation, methyl vinyl ketone and methacrolein, and their relative position to SOA growth.

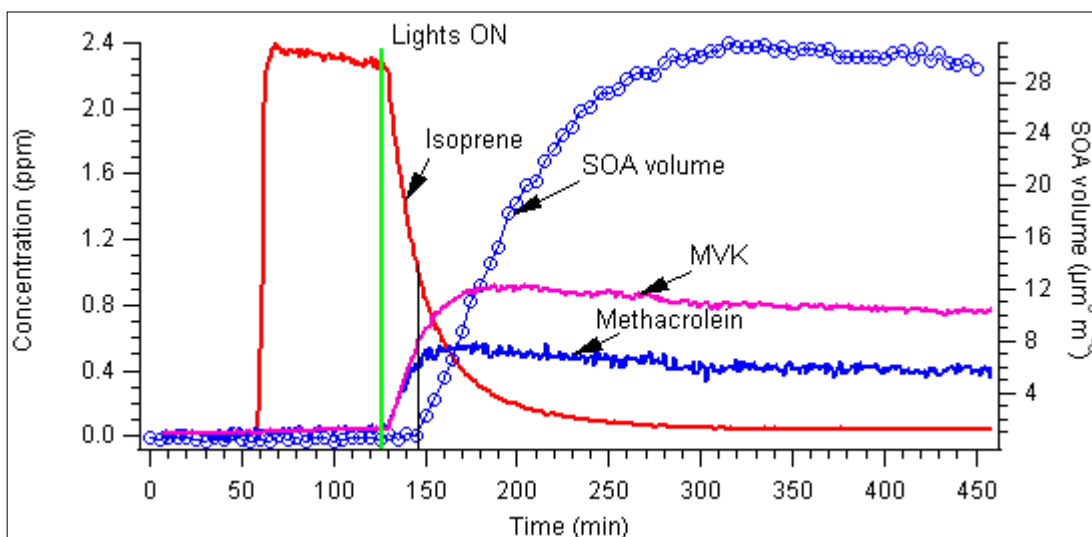


**Figure 3.31 SOA growth and isoprene, MVK, MACR concentration profiles**

### 3.2.2 Contributors to aerosol formation

In order to further understand the implication of MVK and MACR in SOA formation two additional studies are carried out in which methyl vinyl ketone and methacrolein are photooxidized under high NO<sub>x</sub> conditions.

#### *The role of Methyl Vinyl Ketone (MVK) in SOA formation*

We carried out two MVK chamber experiments by injecting into the chamber ~700 ppb MVK and 4ppm NO (Figure 3.32a), and ~1.4 ppm MVK and 8 ppm NO (Figure 3.32b) where SOA formation was investigated. No aerosol formation was observed in those experiments, although more than half of the initial amount of MVK is consumed, concluding that oxidation of MVK does not lead to SOA formation and as a result during isoprene experiment, MVK, a main first generation product, does not contribute to aerosol formation:

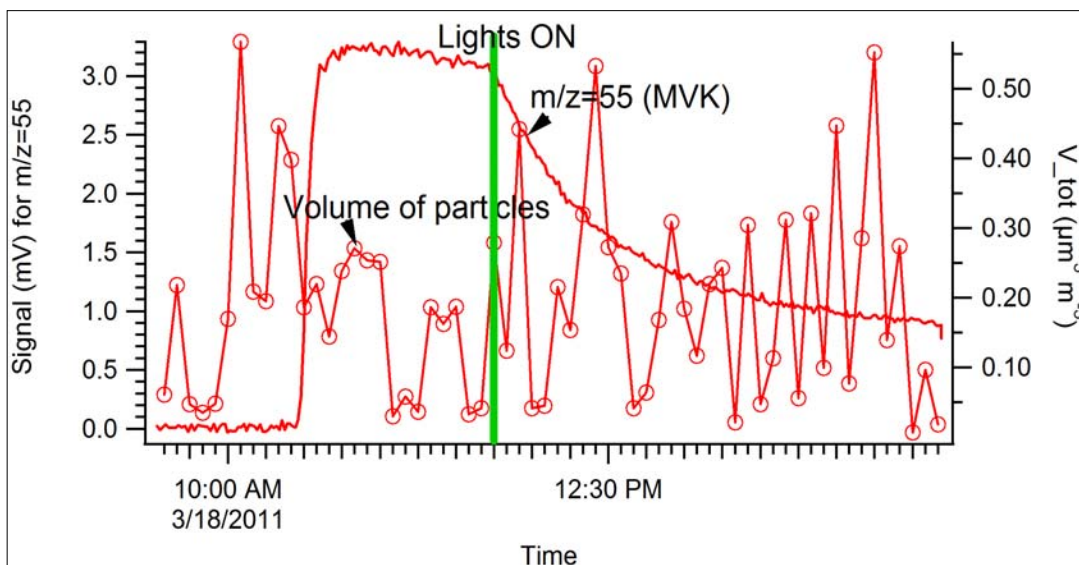


Figure 3.32a SOA growth during MVK chamber experiments (March 18, 2011)

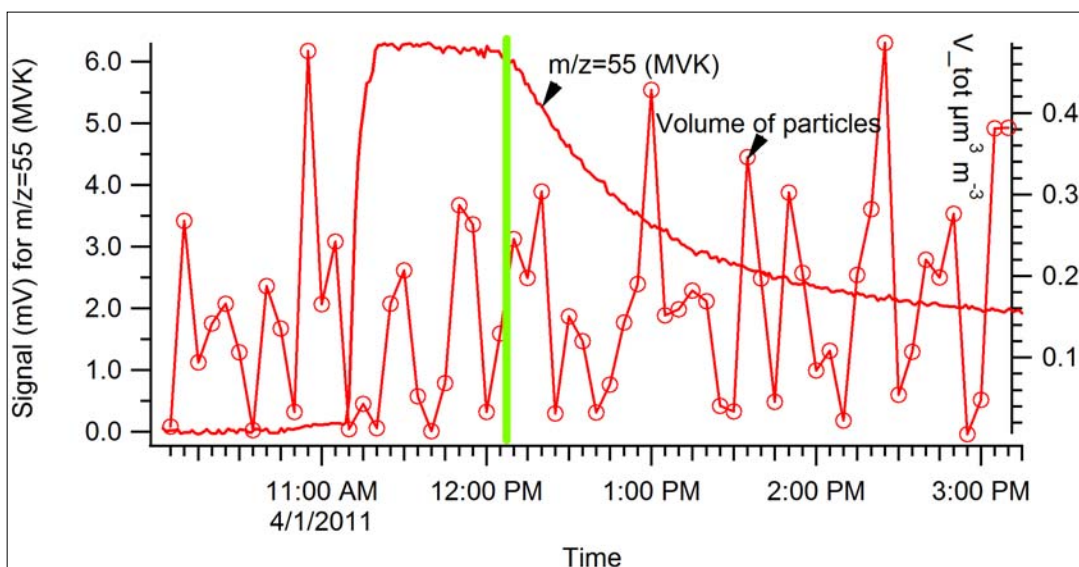
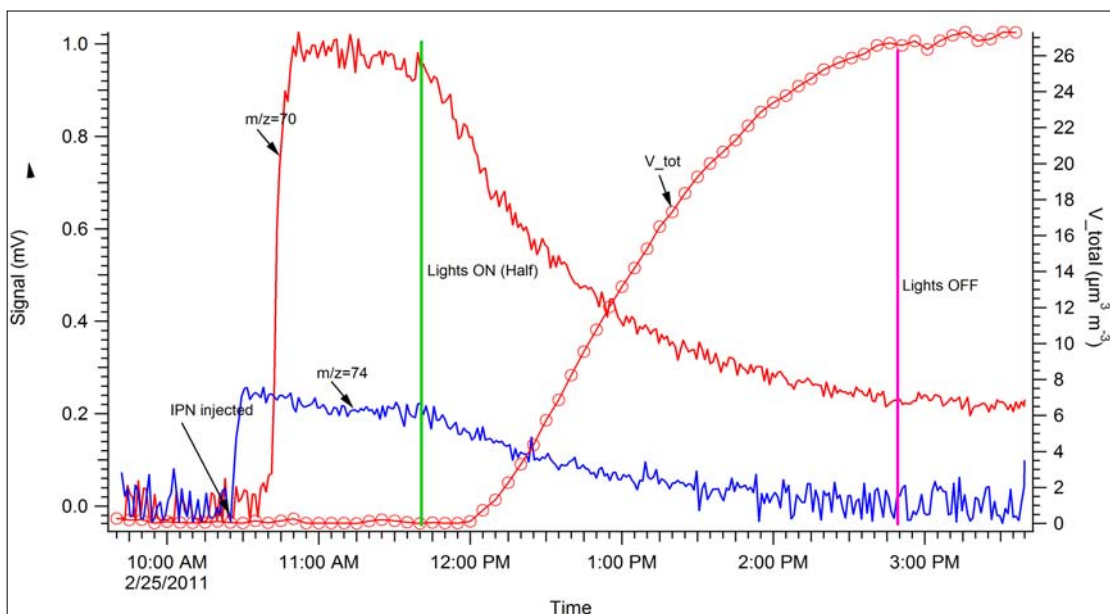


Figure 3.32b SOA growth during MVK chamber experiment (April 01, 2011)

### *The role of Methacrolein in SOA formation*

A number of methacrolein Smog Chamber experiments were carried out in order to investigate the role of methacrolein in SOA formation by injecting 0.6 – 1.4 ppm methacrolein and 2ppm NO<sub>x</sub> for each experiment. By plotting in the same graph the

signal of  $m/z=70$  (the main peak of methacrolein) and total volume of SOA as a function of time we were able to observe the relationship between methacrolein being consumed and particulate matter being formed.



**Figure 3.33 SOA growth during MACR chamber experiment**

From Figure 3.33, it's interesting to see that methacrolein oxidation leads to particulate matter formation. The plot also shows that particulate matter formation started approximately 20 min after the oxidation of MACR started, suggesting that it is first or second generation products of MACR oxidation (second or third generation products of isoprene oxidation) that contribute to the particles formation.

The suggestion that the aerosol is formed in part from second generation product of methacrolein oxidation is also supported by plotting volume of particles formed vs methacrolein consumed, Figure 3.35. We have here upward curved line.

Recalling Equation 3.8 – Equation 3.10, where instead of isoprene now we have methacrolein and going further in our elaboration, we first divide equation (3.10) by (3.8) and substituting the dimensionless variable gives:

$$\frac{dz}{dx} = -\frac{ry}{x} \quad (\text{Equation 3.16})$$

Then using equation 3.14 to substitute for y yields:

$$\frac{dz}{dx} = \frac{r\beta(1-x^{r-1})}{1-r} \quad (\text{Equation 3.17})$$

Integrating this with  $z=0$  when  $x=1$  yields:

$$z = \left(\frac{\beta}{r-1}\right) \left[ (1-f)^r + rf - 1 \right] \quad r \neq 1 \quad (\text{Equation 3.18})$$

where  $f$  is the fraction of methacrolein consumed that is

$$f \equiv 1 - x = 1 - \left( \frac{[\text{MACR}]}{[\text{MACR}]_0} \right)$$

The equation 3.18 describes the dependence of a second generation product (such as aerosol volume/mass) on fraction of hydrocarbon consumed. Since the right hand is directly proportional to the branching ratio  $\beta$ , the shape of the curve depends only on the value of  $r=k_2/k_1$ . This is illustrated in Figure 3.34 (prepared by Prof.Mozurkweich)

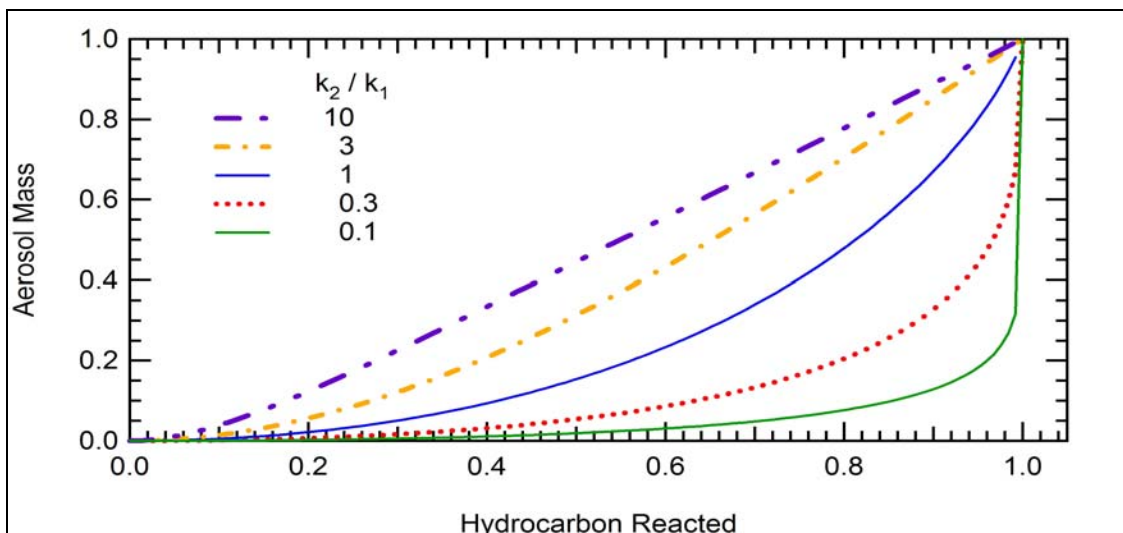


**Figure 3.34** Aerosol mass, expressed as a fraction of the mass when the reaction is complete, versus hydrocarbon reacted, expressed as a fraction of the initial hydrocarbon concentration, for various values of the ratio of rate constants.

A simplified analysis of these curves shows that when  $k_2 \gg k_1$  the shape of the lines approaches a straight line and we can speak of the aerosol as a first generation product. When  $k_2 \leq k_1$ , then we have curved lines and this is the case when parent hydrocarbon is converted to a first generation product which on turn in a rate determining step forms a second generation product. This is illustrated with upward curved lines.

By plotting volume of aerosol, expressed as a fraction of volume when the reaction is complete, versus methacrolein consumed, expressed as a fraction of the initial methacrolein concentration, we are able fit equation 3.18 to the plot. The fitting provides valuable information as the ratio of rate constants and product yield.

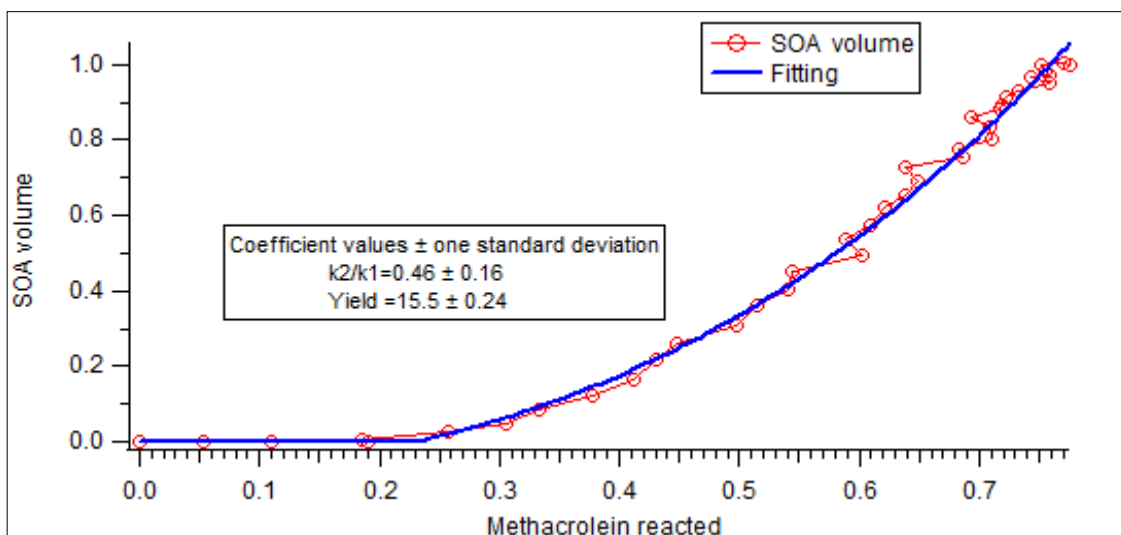


**Figure 3.35 Volume of particles formed, expressed as a fraction of volume when reaction is complete, versus MACR reacted, expressed as a fraction of the initial methacrolein concentration**

By comparing the shape and value of  $r=k_2/k_1$  coefficient (0.46) of the methacrolein curve with those in the Figure 3.34, we can assign particulate matter formed (SOA) to a second generation product.

From the above plot we see that there is a delay in the particle formation: it starts after an amount of methacrolein is consumed. This could be as a result that aerosol formed is a multiple generation product of methacrolein photo-oxidation or because some product must be accumulated to reach the vapor pressure needed for nucleation.

To investigate the reason of that delay on the particle formation we carried out three experiments where we have different amount of methacrolein injected (as illustrated in Figure 3.36 by plotting methacrolein ( $m/z=70$ ) signal intensity (mV) vs time).

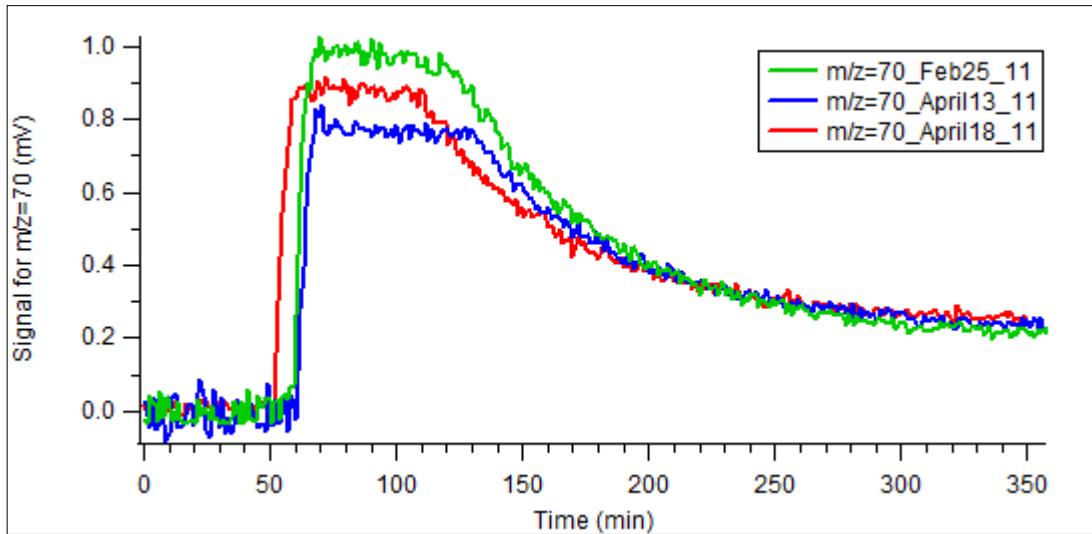


**Figure 3.36** Time profile of methacrolein concentration (as  $m/z=70$  in mV)

By plotting in the same graph total volume of particles vs the amount of methacrolein consumed, Figure 3.37, we investigate if the delay would be related to the amount of methacrolein consumed or not.

A constant delay, in term of the amount of methacrolein consumed, would be an indication that delay is due to vapor pressure built up, or otherwise multiple generation products could be in stake.

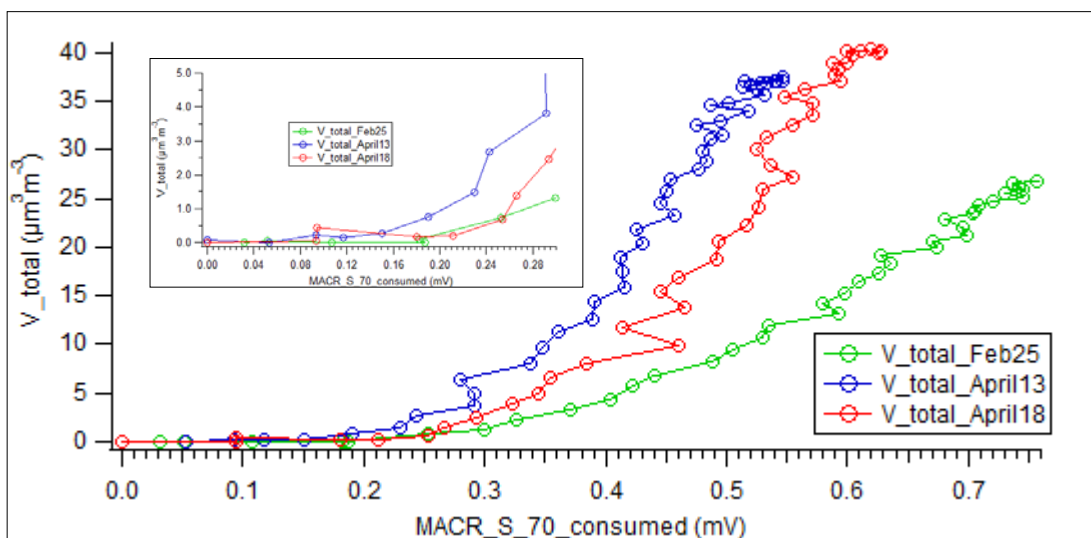


**Figure 3.37 SOA growth versus methacrolein consumed in different experiments (insertion: a zoomed view close to the area where aerosol formation begins)**

The plot shows that we likely have different amount of methacrolein being consumed at the moment of particle growth (different delays). This observation coupled with the fact that we have upward curving lines is an indication that aerosol formed is a second generation product of methacrolein photo-oxidation and the time delay observed (Figure 3.37) is likely due to that. Additional experiments would be needed to better clarify the moment when the aerosol growth starts, related to the amount of methacrolein consumed.

It should also be noted that attempts to fit the equation 3.18 to these lines gave inconsistent results in terms of rate constant ratio and product yield (which was expected to be the same in all experiments), which could be a result of a number of assumptions made when the equation 3.18 is built up, or because inconsistent results were taken from the experiments.

Recent working condition of our mass spectrometer did not allow us to go further in these investigations.

Products from the oxidation of methacrolein (Tuazon and Atkinson, 1990; Orlando et al., 1999), methyl vinyl ketone (Tuazon and Atkinson, 1989) and C5 hydroxycarbonyls (Baker et al., 2005) have been measured. Most of those second generation products (of isoprene) are small water-soluble compounds, such as glyoxal, methylglyoxal, glycolaldehyde, and hydroxyacetone. Additionally, larger (C3-C5) products, likely with several (3 or more) functional groups, can also be formed (Paulot et al., 2009). Both these classes of second- (and later)- generation products may be key components and/or precursors of isoprene SOA.

During our methacrolein photo-oxidation chamber experiments we were not able to see (detect) the new peaks that could correspond to products of photo-oxidation of methacrolein due to low sensitivity of the instrument.

The MACR chamber experiment could be used to calculate the quantitative contribution of MACR in particle formation during isoprene experiment. So the ratio of Volume of particles formed from MACR to Total Volume of particles formed during isoprene experiment gives the required contribution:

$$\text{Ratio} = \frac{(V_{\text{Macr}})_{\text{Iso.exp.}}}{(V_{\text{tot}})_{\text{Iso.exp}}} \quad (\text{Equation 3.19})$$

Volume of particles formed from MACR during isoprene experiment could be estimated by first calculating MACR consumed during isoprene experiment and then going to the graph of total volume vs MACR consumed, during MACR experiment (Figure 3.38) we can estimate the respective value (see below). For comparison, the total volume of aerosol formed during isoprene experiment is  $30 \pm 2 \mu\text{m}^3 \text{ m}^{-3}$ .

So, first we have to find MACR consumed during isoprene experiment:

$$(\Delta C_{MACR})_{Isoprene\_exp}$$

In order to take into consideration the fact that some of methacrolein starts being consumed as soon as is formed, we used “first generation products” procedure .

From the “first generation products” plot (Figure 3.15), we have a "yield" of methacrolein formed from the photo-oxidation of isoprene. Multiplying that by the amount of isoprene consumed at any given time gives the total of methacrolein formed at this time. Then subtracting the concentration of methacrolein at this time gives the amount consumed.

So

$$(\Delta C_{MACR})_{Isoprene\_exp}(t) = [\beta \Delta C_{Isoprene}(t)] - C_{MACR}(t) \quad (\text{Equation 3.20})$$

Where:

$(\Delta C_{MACR})_{Isoprene\_exp}(t)$  is amount of methacrolein consumed at the time  $t$

$\Delta C_{Isoprene}(t)$  is amount of isoprene consumed at the time  $t$

$\beta$  is yield of methacrolein formed

$C_{MACR}(t)$  is the measured concentration of methacrolein at the time  $t$

Earlier in this work we have calculated the yield of methacrolein formed to be 24.8 %

( $\beta = 0.248$ ) (see Figure 3.15)

So using equation 3.20, *at the moment that all isoprene is consumed*, we have:

$$(\Delta C_{MACR})_{Isoprene\_exp} = 0.41 \pm 0.02 \text{ ppm}$$

Going to Figure 3.38 , we estimate that for  $0.41 \pm 0.02$  ppm of methacrolein consumed, there are  $0.62 \pm 0.04 \mu\text{m}^3 \text{m}^{-3}$  volume of SOA formed (Figure 3.38a represents a zoomed picture of Figure 3.38 close to area of interest).

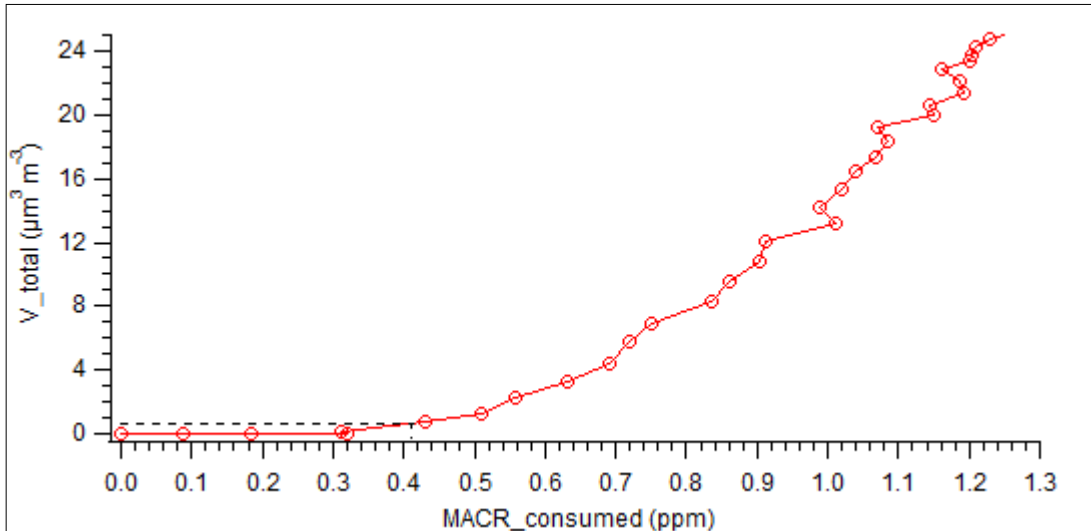


**Figure 3.38 Volume of particles formed vs methacrolein consumed during methacrolein experiment**

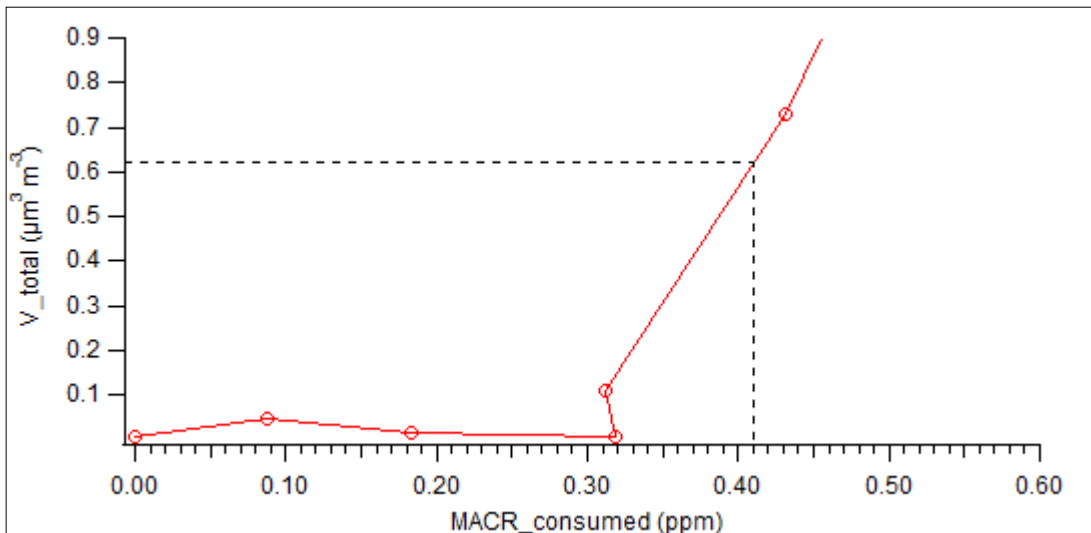


**Figure 3.38a A zoomed picture of Fig. 3.38 close to the origin of the plot**

This is the estimated amount of SOA formed from photo-oxidation of methacrolein during isoprene experiment.

Now from equation 3.4 we have :

$$\frac{(V_{\text{Macr}})_{\text{Isoprene\_exp}}}{(V_{\text{tot}})_{\text{Isoprene\_exp}}} = \frac{0.62 \pm 0.04 \mu\text{m}^3 \text{ m}^{-3}}{30 \pm 2 \mu\text{m}^3 \text{ m}^{-3}} = 2.07 \pm 0.27 \%$$

This result indicates that methacrolein as a contributor to aerosol formation gives a small portion of the total volume of aerosol formed.

We can estimate an upper limit of the yield of aerosol formed, using the slope of the line AB (Figure 3.39).

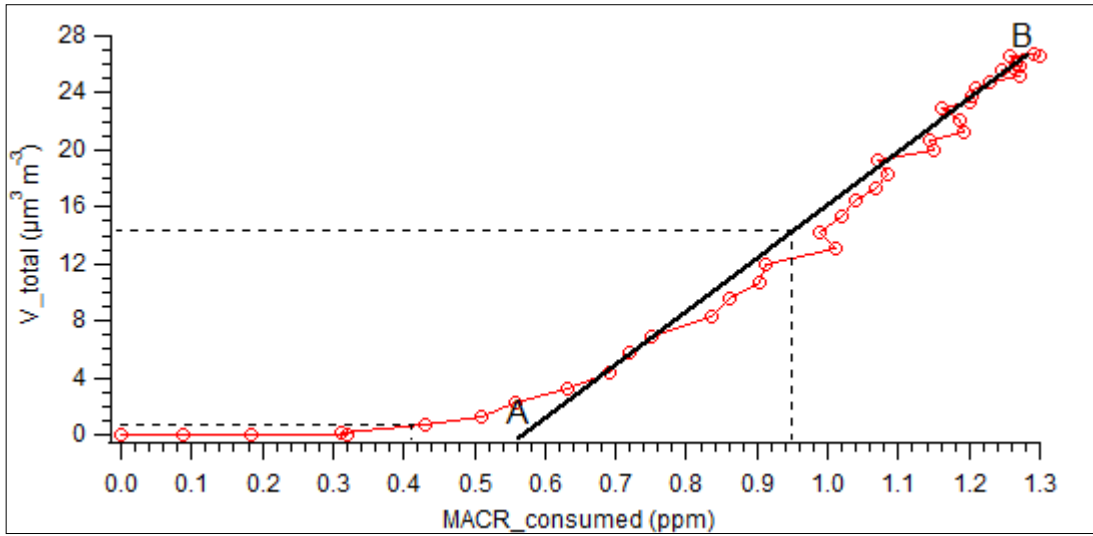


**Figure 3.39 Linear approximation AB used to estimate the yield of MACR**

So, we will have the volume of aerosol formed per every unit (ppm) of methacrolein consumed given as  $\alpha$  (the slope of line AB):

$$\alpha = \frac{14.48 \pm 0.02 \mu\text{m}^3 \text{ m}^{-3}}{0.95 \pm 0.005 \text{ ppm}} = 15.24 \pm 0.26 \frac{\mu\text{m}^3 \text{ m}^{-3}}{\text{ppm}}$$

Then we can calculate the amount of SOA formed from MACR photo-oxidation during isoprene experiment:

$$(V_{\text{Macr}})_{\text{Isoprene\_exp}} = \alpha \times (\Delta C_{\text{MACR}})_{\text{Isoprene\_exp}}$$

$$(V_{Macr})_{Isoprene\_exp} = 15.24 \pm 0.26 \frac{\mu\text{m}^3 \text{ m}^{-3}}{\text{ppm}} \times 0.41 \pm 0.02 \text{ ppm} = 6.25 \pm 0.55 \mu\text{m}^3 \text{ m}^{-3}$$

Hence we calculate the contribution of methacrolein to aerosol formation during isoprene experiment as :

$$Yield = \frac{(V_{Macr})_{Isoprene\_exp}}{(V_{tot})_{Isoprene\_exp}} \times 100 = \frac{6.25 \pm 0.55 \mu\text{m}^3 \text{ m}^{-3}}{30 \pm 2 \mu\text{m}^3 \text{ m}^{-3}} \times 100 = 20.8 \pm 3.1 \%$$

These calculations show that significant part of SOA formed during the photo-oxidation of isoprene still need to be identified in terms of contributors and mechanism of formation.

#### *The role of m/z=82 species in SOA formation*

By plotting in one graph (Figure 3.40) signal of m/z=82 species and total volume of particles formed vs time we see that there is a correlation between particle formation and the moment when 82 species starts to be consumed, which suggest that species 82 might well contribute to aerosol formation.

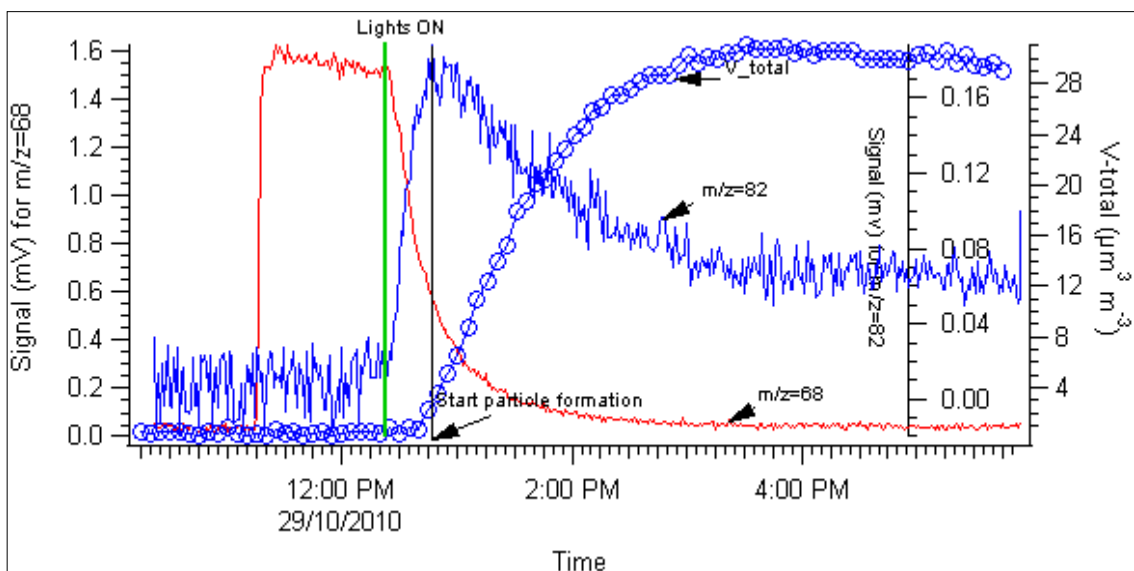


**Figure 3.40** Signal of  $m/z=82$  species and volume of particles formed vs time

In Figure 3.41 we have plotted total volume of particles formed vs 82 species consumed expressed in mV. We see here again that we have an increase of the total volume of particles as the amount of 82 species is consumed.

Here we likely have a linear correlation (straight line) between the SOA growth and  $m/z=82$  consumed which indicate that this species may well contribute to aerosol formation.

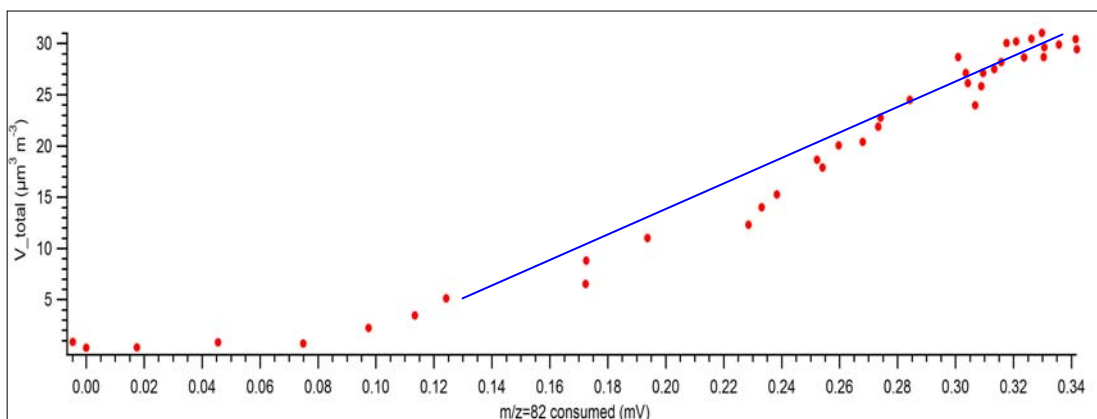


**Figure 3.41** Volume of particles formed vs  $m/z=82$  species consumed

As discussed earlier in this chapter we assigned  $m/z=82$  species to a gamma-hydroxycarbonyl ( $C_5H_8O_2$ , MW=100), either a 4-hydroxy-2-methyl-crotonaldehyde or a 4-hydroxy-3-methyl-crotonaldehyde. Separate OH-initiated photo-oxidation experiments of C5-hydroxycarbonyls compounds (similar to those of MACR and MVK ) would be needed to further investigate and possibly quantify the contribution to aerosol formation.

## Chapter 4: Conclusion and future directions

There were two main objectives of this work: i) to investigate isoprene OH initiated photo-oxidation mechanism, in presence of high NO<sub>x</sub> level, using chemical ionization mass spectrometry exemplified by our Ion Trap Time of Flight Mass Spectrometer (IT-TOF MS) and ii) to investigate SOA formed from isoprene photo-oxidation using a DMA coupled with a CPC, during Smog Chamber experiments.

Using an Ion Trap – Time of Flight Mass Spectrometer which uses chemical ionization in the Source Chamber and a Flight Tube for ion analysis, we were able to identify and quantify the formation of two main known products of isoprene OH initiated photo-oxidation : methyl vinyl ketone and methacrolein. The calculated product yields of MVK and MACR, using “first generation product” procedure were in good agreement with published works.

We presented here the de-synthesis approach applied for analysis of mass spectra, which consisted of successively subtracting the signal of known compounds with the use of response factors, by first getting concentration profiles of them and then their contribution to specific peaks. During this work the application of this approach was confined in those peaks which substantially come from isoprene, MVK and MACR.

Our instrument demonstrated sufficient capabilities to detect some interesting peaks at  $m/z=82$ , 84, and 85, which are likely to represent C5-hydroxycarbonyl (C<sub>5</sub>H<sub>8</sub>O<sub>2</sub> MW=100), C5-carbonyl (C<sub>5</sub>H<sub>8</sub>O MW=84) and C4-hydroxycarbonyl (C<sub>4</sub>H<sub>6</sub>O<sub>2</sub> MW=86)

compounds, respectively, but it fell short in detecting larger mass to charge ratio species. An ongoing work should be performed in order to further optimize the working parameters of our IT-TOF MS, to be able to detect larger mass to charge ratio ions as this would improve significantly our investigation of a larger number of gas-phase products and their possible role to aerosol formation.

A more detailed analysis is done related to identification of  $m/z=82$  species as it showed a more pronounced signal intensity, compared to  $m/z=84$  and  $m/z=85$  species, and because of the intriguing fact that it could represent a molecular ion of 3-methyl furan (MW=82), a compound reported as first generation product of isoprene photo-oxidation, or a fragment of C5-hydroxycarbonyl compound. Using a APCI Mass Spectrometer, as described in details in this work, we were able to conclude that our  $m/z=82$  species represent a C5-hydroxycarbonyl compound. We calculated the rate constant of OH initiated photo-oxidation for  $m/z=82$  species to be  $7.65 \times 10^{-11} \text{ cm}^3 \text{ molecule}^{-1} \text{ s}^{-1}$ .

A substantial part of my work was also investigation of possible formation of Secondary Organic Aerosol (SOA) from the photo-oxidation of isoprene, contributors and mechanism of this process.

Photo-oxidation of isoprene in presence of high level of NO<sub>x</sub>, as our experiments showed, leads to Secondary Organic Aerosol formation but over delayed timescales. These results indicate that a key step in SOA formation is the further gas-phase oxidation of first generation reaction products. Separate chamber experiments with major first generation products (MACR and MVK) are carried out to better understand this role.

Methacrolein Smog Chamber experiments showed that methacrolein is an intermediate in SOA formation, although not the only one. MVK, another important first generation product of isoprene photo-oxidation does not lead to aerosol formation, as our experiments demonstrated.

By plotting the total volume of aerosol formed versus methacrolein consumed we were able to fit the equation which describes the dependence of second generation product (such as aerosol volume) on hydrocarbon consumed (Equation 3.18), and hence calculated the rate constant ratio ( $k_2/k_1$ ). By doing so, and based on a more general discussion about how the values of rate constant ratio is reflected on the shape of the curves, we have an indication that aerosol formed from photo-oxidation of methacrolein is a second generation product. This is further supported from the observation that we likely have different amount of methacrolein being consumed at the moment of particle growth (different delays). On the other hand, during methacrolein photo-oxidation chamber experiments, due to low sensitivity of the instrument, we were not able to see (detect) the new peaks (after the initiation of photo-oxidation) that could correspond to expected products.

Attempts to fit the above mentioned equation to lines of different experiments gave inconsistent results in terms of rate constant ratio and product yield, which were expected to be the same in all experiments. More experiments would be required to get more insight into the relationship between particle growth and methacrolein consumed expressed in a mathematical equation, as soon as the working condition of our Time of Flight Mass Spectrometer will allow.

The contribution of methacrolein to total volume of aerosol formed during photo-oxidation of isoprene is estimated to be in the range of 2% to 21%, which represents a small fraction of total volume formed. This suggests that other contributors and pathways should be considered and elaborated in order to better understand the mechanism of formation and chemical composition of aerosol particles during isoprene photo-oxidation experiments.

While our experiments were carried out within narrow ranges of NO<sub>x</sub>, temperature, OH concentration, relative humidity, it would be very interesting, in future, to elucidate the impact of such parameters in aerosol yields, in an attempt to better encompass and characterize ambient conditions.

We showed here that  $m/z=82$  species (a C<sub>5</sub>-hydroxycarbonyl compound) may well contribute to aerosol formation, but separate OH-initiated photo-oxidation experiments of C<sub>5</sub>-hydroxycarbonyls compounds (similar to those for MACR and MVK ) would be needed to further investigate and possibly quantify the contribution to aerosol formation.

The research on isoprene OH-initiated photo-oxidation, its mechanism, gas and particle phase products still remains a challenging task in the future which would require not only further optimization of our instruments but possibly usage of other techniques (e.g. PTR-MS has shown to be especially promising in quantification of hydroxycarbonyls [Zhao, J., et al., 2004] ), and on the other hand it would have profound impacts on elucidation of the chemistry of atmospheric VOCs.

## Appendix

The plots below (A1 – A6) represent measured and calculated signals for peaks at  $m/z=55, 65, 67, 68, 69, 70$  as a function of time. For each measured value of signal the experimental error is given and expressed as one standard deviation ( $\sigma$ ) based on the propagation through the analysis from estimated noise level. The magnitude of uncertainty is calculated based on the consistency of the baseline, sensitivity setting, baseline noise and the height of the peaks in the spectra. The plots for difference signal between measured and calculated values are also given below (A1.1 – A6.1).

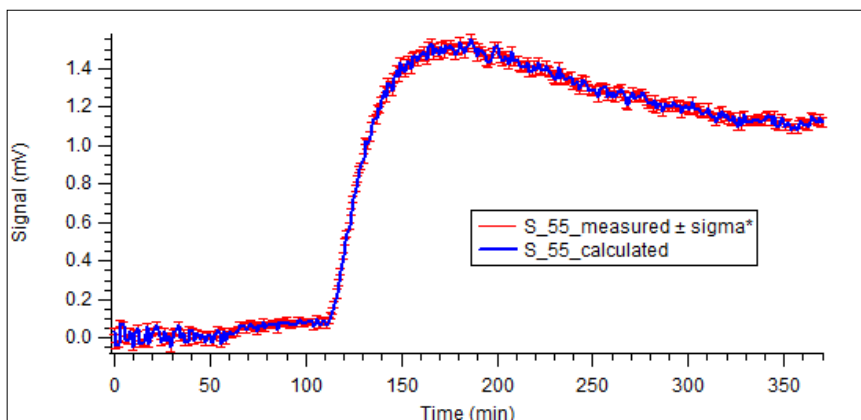


**Figure A1: Measured and calculated signals for peak at  $m/z=55$**

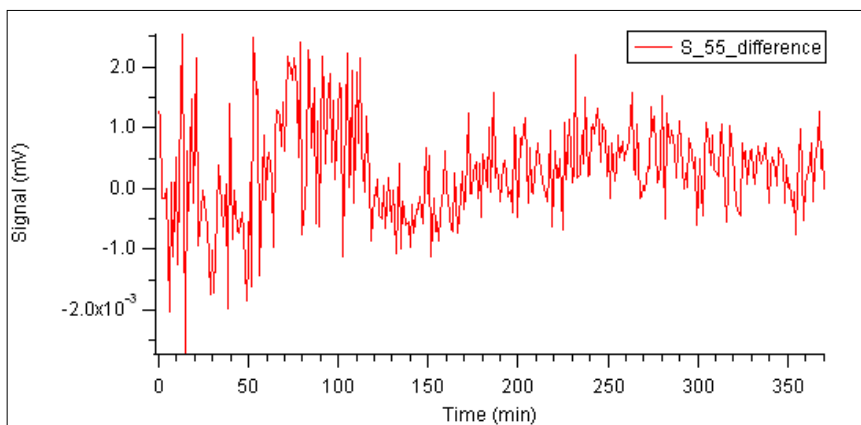


**Figure A1.1 : Difference signal for peak at  $m/z=55$**

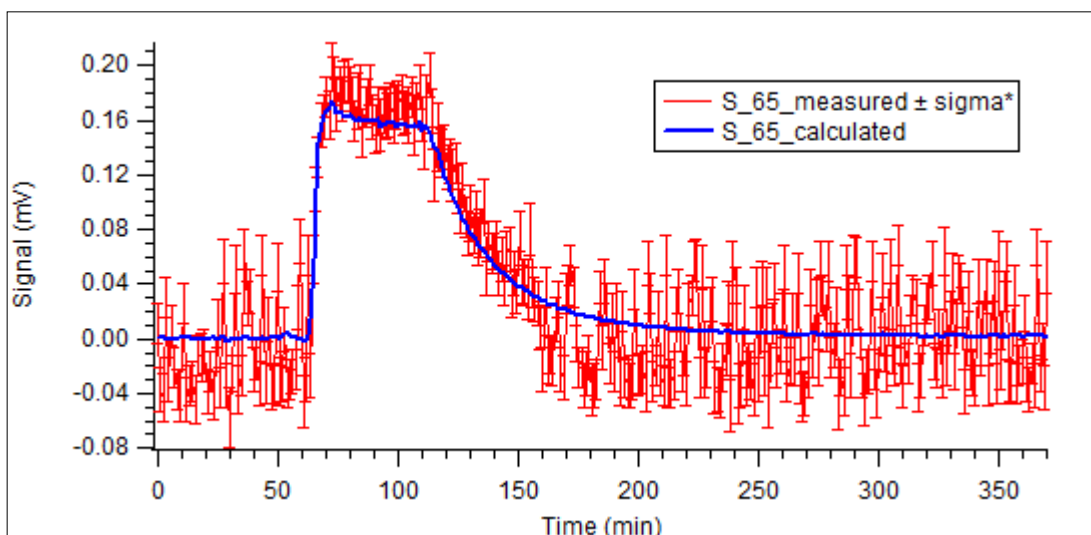


Figure A2: Measured and calculated signals for peak at  $m/z=65$

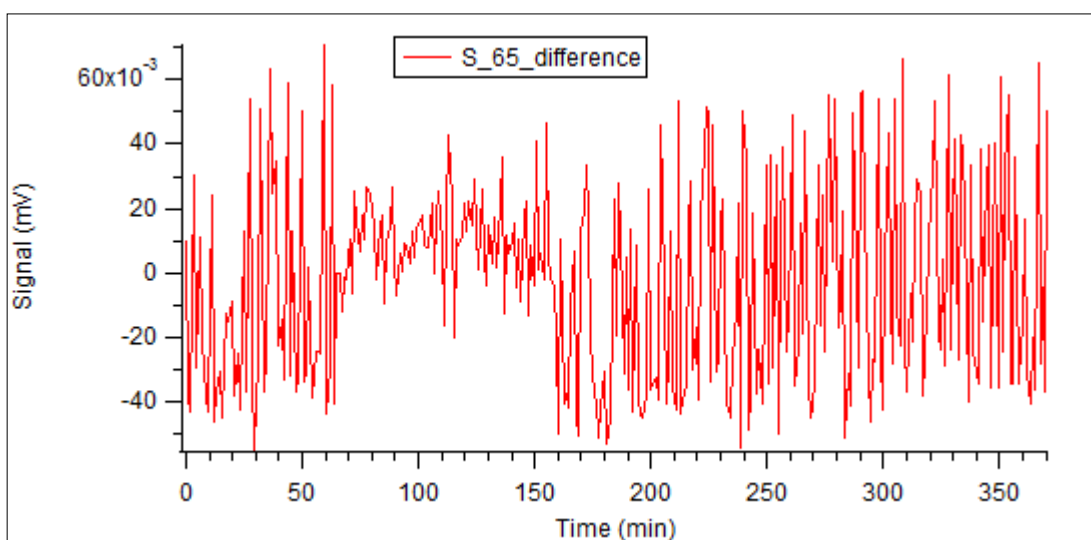


Figure A2.1: Difference signal for peak at  $m/z=65$

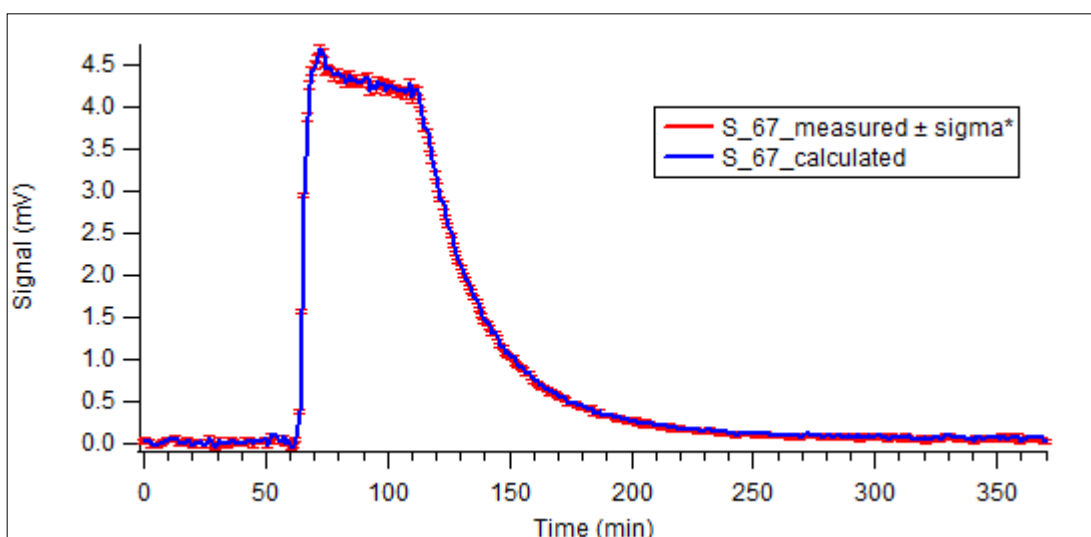


Figure A3 : Measured and calculated signals for peak at  $m/z=55$

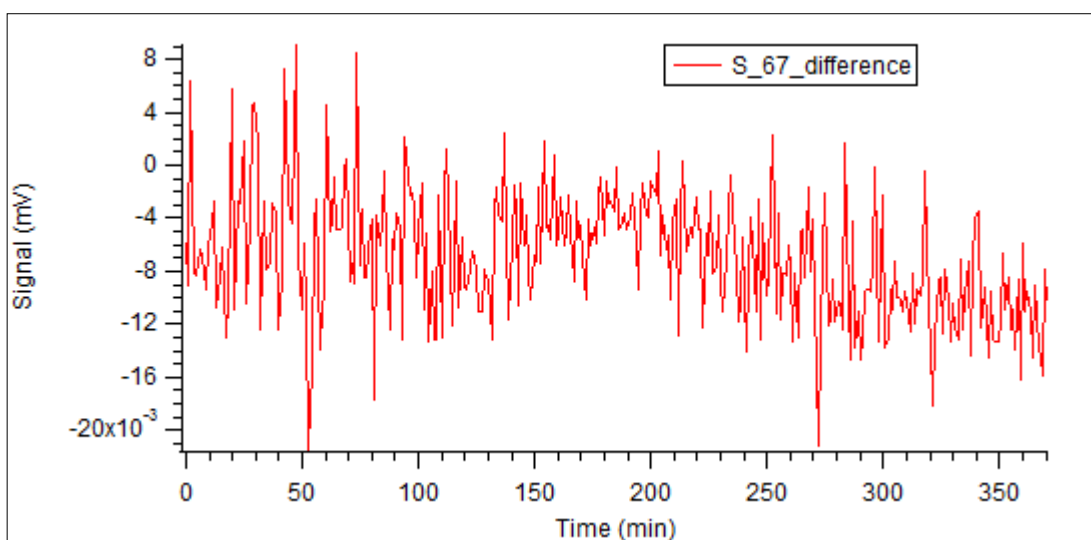


Figure A3.1 : Difference signal for peak at  $m/z=67$

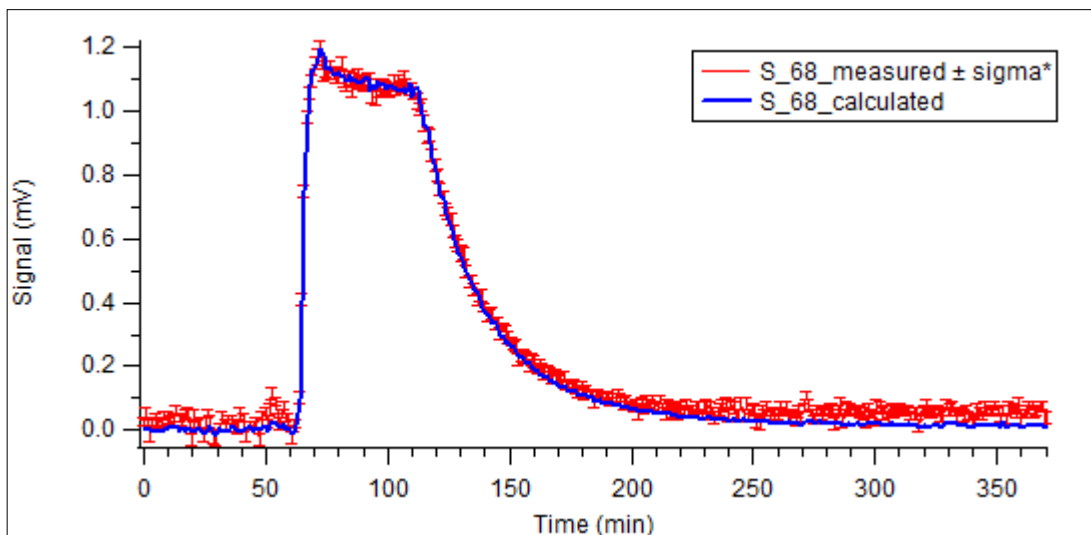


Figure A4 : Measured and calculated signals for peak at  $m/z=68$

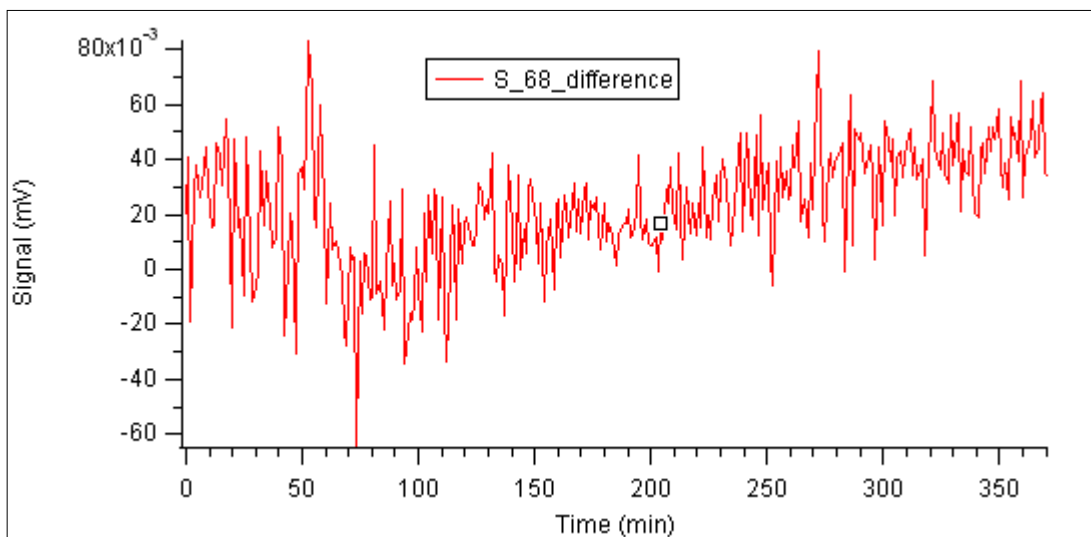


Figure A4.1 : Difference signal for peak at  $m/z=68$

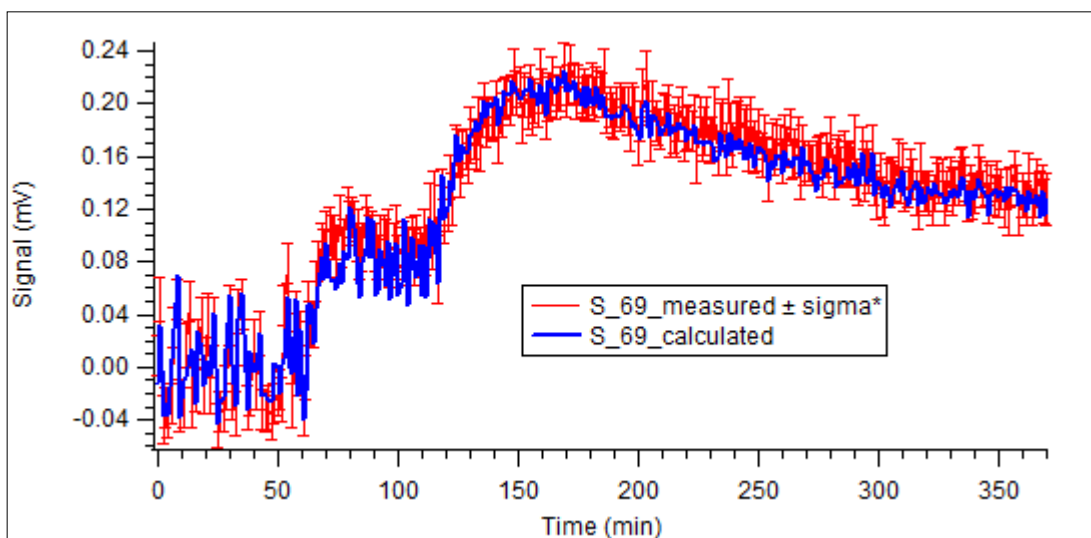


Figure A5 : Measured and calculated signals for peak at  $m/z=69$

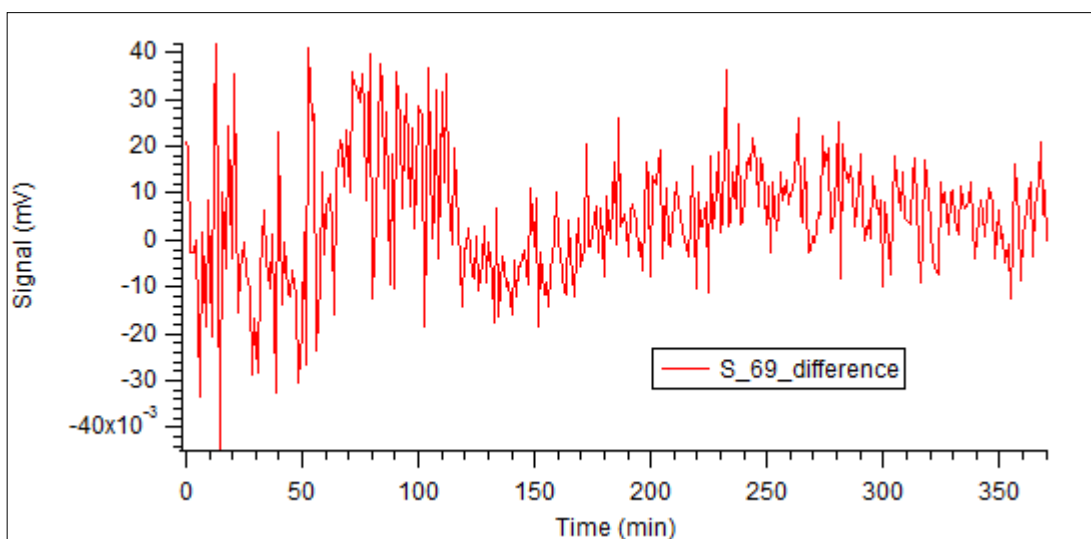


Figure A5.1 : Difference signal for peak at  $m/z=69$

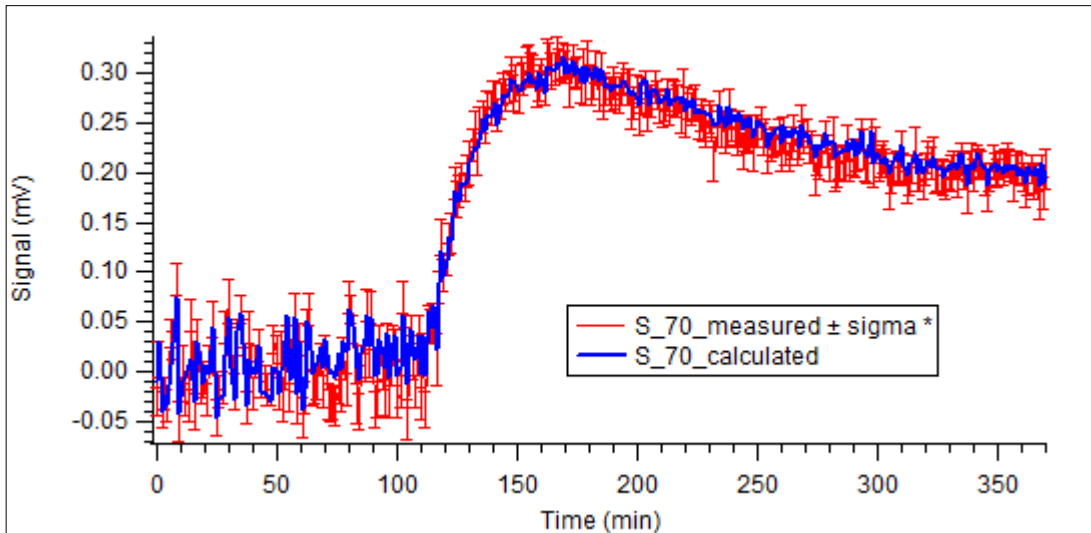


Figure A6 : Measured and calculated signals for peak at  $m/z=70$

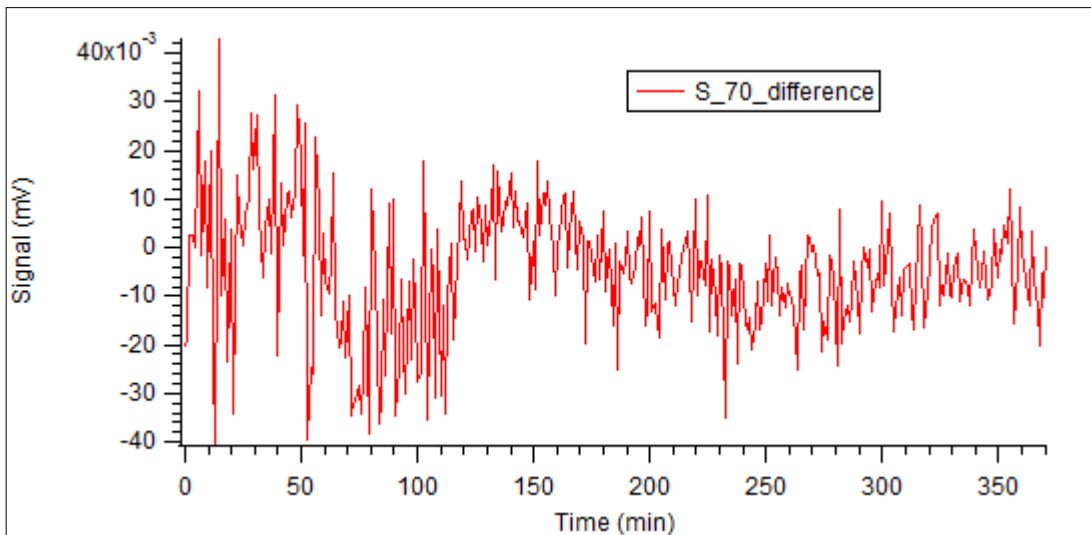


Figure A6.1 : Difference signal for peak at  $m/z=70$

## References

1. Atkinson, R. and Aschmann, S. M. , *Int. J. Chem. Kinet.* , **16** , 1175 , 1984
2. Atkinson, R; Aschmann, S.M; Tuazon E.C; Arey, J; Zielinka, B.: Formation of 3-Methylfuran from the gas-phase reaction of OH radicals with isoprene and the Rate Constant for its reaction with OH radicals. *Int. J. Chem. Kinet.* 21, 593-604, 1989.
3. Atkinson, R.: Gas-phase tropospheric chemistry of organic compounds. *Journal of Physical and Chemical Reference Data*, Monograph 2, 1–216, 1994.
4. Atkinson, R.: *Int. J. Chem. Kinet.*, 29, 99, 1997
5. Atkinson, R., Arey, J.: Gas-phase tropospheric chemistry of biogenic volatile organic compounds: a review. *Atmospheric Environment* 37 Supplement No. 2 S197–S219, 2003.
6. Auld, J.: A smog chamber study of mechanisms for  $\beta$ -pinene oxidation by hydroxyl radicals. PhD Dissertation 2009.
7. Baker, J., Arey, J., and Atkinson, R.: Formation and reaction of hydroxycarbonyls from the reaction of OH radicals with 1,3 butadiene and isoprene, *Environ. Sci. Technol.*, 39, 4091-4099, 2005.
8. Bellkelberg, H.J., Boge, O., Seuwen, R., Warneck P.: *Chem. Phys.*, 2, 4029, 2000
9. Boge, O., Miao, Y., Plewka, A., and Herrmann, H.: Formation of secondary organic particle phase compounds from isoprene gasphase oxidation products: An aerosol chamber and field study, *Atmos. Environ.*, 40, 2501–2509, 2006.

10. Carlton, G. A., Wiedinmyer, C., Kroll H. J.,: A review of Secondary Organic Aerosol (SOA) formation from isoprene, *Atmos. Chem. Phys.*, 9, 4987-5005, 2009
11. Chambers, M. D., Grace, I. L., Andresen, D. B.,: Development of an Ion Store/Time-of-Flight Mass Spectrometer for the Analysis of Volatile Compounds in Air. *Anal. Chem.* , 69, 3780-3790, 1997.
12. Chuong, B. and Stevens, P. S. , *J. Phys. Chem. A.* 107 , 2185.2003.
13. Chien, M. B., Michael, M. S., Lubman M. D.,: The design and performance of an ion trap storage – reflectron time of flight mass spectrometer. *Intern. Journal of Mass Spectrometry and Ion Processes.* 131.1994
14. Claeys, M., Graham, B., Vas, G., Wang, W., Vermeylen, R., Pashynska, V., Cafmeyer, J., Guyon, P., Andreae, M. O., Araxo, P., and Maenhaut, W., : Formation of Secondary organic aerosols through photo-oxidation of isoprene, *Science*, 303, 1173-1176, 2004a.
15. Claeys, M., Wang, W., Ion, A. C., Kourtchev, I., Gelencser, A., and Maenhaut, W.: Formation of secondary organic aerosols from isoprene and its gas-phase oxidation products through reaction with hydrogen peroxide, *Atmos. Environ.*, 38, 4093–4098, 2004b.
16. De Gouw J., Jimenez J. L.,: Organic Aerosols in the Earth’s Atmosphere, *Environ. Sci. Technol.*, 43, 7614–7618, 2009.
17. Dibble, T. S., *J. Phys. Chem.* 103, 8559, 1999 Dommen, J., Metzger, A., Duplissy, J., Kalberer, M., Alfarra, M. R., Gascho, A., Weingartner, E., Prevot, A. S. H., Verheggen, B., and Baltensperger, U.: Laboratory observation of oligomers

18. EDGAR (2005) EDGAR 32FT2000 dataset.  
<http://www.mnp.nl/edgar/model/v32ft2000edgar/>
19. Gierczak, T., Burkholder, J. B., Talukdar, R. K., Mellouki, A., Barone, S. B. and Ravishankara, A. R. , Chem. , **110** , 1 , 1997
20. Edney, E. O., Kleindienst, T. E., Jaoui, M., Lewandowski, M., Offenberg, J. H., Wang, W., and Claeys, M.: Formation of 2-methyl tetrols and 2-methylglyceric acid in secondary organic aerosol from laboratory irradiated isoprene/NO<sub>x</sub>/SO<sub>2</sub>/air mixtures and their detection in ambient PM<sub>2.5</sub> samples collected in the eastern United States, Atmos. Environ., 39, 5281–5289, 2005.
21. Fuentes, J.D., Lerdau, M., Atkinson, R., Baldocchi, D., Bottenheim, J.W., Ciccioli, P., Lamb, B., Geron, C., Gu, L., Guenther, A., Sharkey, T.D., Stockwell, W.: Biogenic hydrocarbons in the atmospheric boundary layer: a review. Bulletin of the American Meteorological Society 81, 1537–1575, 2000.
22. Guenther, A. B., Hewitt, C.N., Ericson, D., et al : A global model of natural volatile organic compound emissions. J. Geophysical Research, 100 (D5): 8873-8892, 1995.
23. Holzinger, R., Millet, D. B., Williams, B., Lee, A., Kreisberg, N., Hering, S. V., Jimenez, J., Allan, J. D., Worsnop, D. R., and Goldstein, A. H.: Emission, oxidation, and secondary organic aerosol formation of volatile organic compounds as observed at Chebogue Point, Nova Scotia, J. Geophys. Res.-Atmos., 112, D10S24, doi:10.1029/2006JD007599, 2007.

24. Ion, A. C., Vermeulen, R., Kourtchev, I., Cafmeyer, J., Chi, X., Gelencser, A., Maenhaut, W., and Claeys, M.: Polar organic compounds in rural PM<sub>2.5</sub> aerosols from K-puszta, Hungary, during a 2003 summer field campaign: Sources and diel variations, *Atmos. Chem. Phys.*, 5, 1805–1814, 2005, <http://www.atmos-chem-phys.net/5/1805/2005/>.
25. Jang, M., Czoschke, N. M., Lee, S., and Kamens, R. M.: Heterogeneous atmospheric aerosol production by acid-catalyzed particlephase reactions, *Science*, 298, 814–817, 2002.
26. Kleindienst, T. E., Harris, G. W. and Pitts Jr., J. N. , *Environ. Sci. Technol.* , **16** , 844 , 1982.
27. Kleindienst, T. E., Jaoui, M., Lewandowski, M., Offenber, J. H., Lewis, C. W., Bhave, P. V., and Edney, E. O.: Estimates of the contributions of biogenic and anthropogenic hydrocarbons to secondary organic aerosol at a south-eastern US location, *Atmos. Environ.*, 41, 8288-8300, 2007a.
28. Kleindienst, T. E., Lewandowski, M., Offenber, J. H., Jaoui, M., and Edney, E. O.: Ozone-isoprene reaction: Re-examination of the formation of secondary organic aerosol, *Geophys. Res. Lett.*, 34, L01805, doi:10.1029/2006GL027485, 2007b.
29. Koppmann R. :Volatile Organic Compounds in the Atmosphere. Blackwell Publishing Ltd.,Singapore.2007
30. Kroll, J. H., Ng, N. L., Murphy, S. M., Flagan R. C., and Seinfeld, J. H.,: SOA formation from isoprene photo-oxidation under high NO<sub>x</sub> conditions , *Geophys. Res. Lett.*, 32, L18808, doi:10.1029/2005GL023637, 2005.

31. Kroll, J. H., Ng, N. L., Murphy, S. M., Flagan R. C., and Seinfeld, J. H.,: SOA formation from isoprene photo-oxidation, *Environ. Sci. Technology.*, 40, 1869-1877, 2006.
32. Kwok, E. S. C., and Atkinson, R.,: Estimation of hydroxyl radical reaction rate constants for gas-phase organic compounds using a structure-activity relationship: an update, *Atmospheric Environment* Vol.29, No.14, 1685-1695, 1995
33. Kroll, J. H., Chan, A. W. H., Ng, N. L., Flagan, R. C., and Seinfeld, J. H.: Reactions of semivolatile organics and their effects on secondary organic aerosol formation, *Environ. Sci. Technol.*, 41, 3545–3550, 2007.
34. Lanz, V. A., Alfarra, M. R., Baltensperger, U., Buchmann, B., Hueglin, C., and Prevot, A. S. H.: Source apportionment of submicron organic aerosols at an urban site by factor analytical modelling of aerosol mass spectra, *Atmos. Chem. Phys.*, 7, 1503–1522, 2007; <http://www.atmos-chem-phys.net/7/1503/2007/>.
35. Lanz, V. A., Alfarra, M. R., Baltensperger, U., Buchmann, B., Hueglin, C., Szidat, S., Wehrli, M. N., Wacker, L., Weimer, S., Casseiro, A., Puxbaum, H., Prevot, A. S. H.: Attribution of submicron organic aerosols during wintertime inversion by advanced factor analysis of aerosol mass spectra, *Environ. Sci. Technol.*, 42, 214–220, 2008.
36. Lei, W.; Zhang, R. *J.Phys. Chem* 105, 3808, A 2001
37. Marcolli, C., Canagaratna, M. R., Worsnop, D. R., Bahreini, R., deGouw, J. A.,Warneke, C., Goldan, P. D., Kuster,W. C.,Williams, E. J., Lerner, B. M., Roberts, J. M., Meagher, J. F., Fehsenfeld, F. C., Marchewka, M., Bertman, S. B., and Middlebrook, A. M.: Cluster Analysis of the Organic Peaks in Bulk Mass

- Spectra Obtained During the 2002 New England Air Quality Study with an Aerodyne Aerosol Mass Spectrometer, *Atmos. Chem. Phys.*, 6, 5649–5666, 2006,
38. Miyoshi, A.; Hatakeyama, S.; Washida, N. : *J. Geophys. Res.*, 99, 18779, 1994
39. Mueller, J.-F., Geographical distribution and seasonal variation of surface emissions and deposition velocities of atmospheric trace gases. *J. Geophysical Research*, 97: 3787-3804, 1992
40. Ng, N. L., Kroll, J. H., Keywood, M. D., Bahreini, R., Varutbangkul, V., Flagan, R. C., Seinfeld, J. H., Lee, A., and Goldstein, A. H.: Contribution of first- versus second-generation products to secondary organic aerosols formed in the oxidation of biogenic hydrocarbons, *Environ. Sci. Technol.*, 40, 2283–2297, 2006.
41. Ng, N. L., Kwan, A. J., Surratt, J. D., Chan, A. W. H., Chhabra, P. S., Sorooshian, A., Pye, H. O. T., Crouse, J. D., Wennberg, P. O., Flagan, R. C., and Seinfeld, J. H.: Secondary organic aerosol (SOA) formation from reaction of isoprene with nitrate radicals (NO<sub>3</sub>), *Atmos. Chem. Phys.*, 8, 4117–4140, 2008, <http://www.atmos-chem-phys.net/8/4117/2008/>.
42. Orlando, J. J., Tyndall, G. S., and Paulson, S. E.: Mechanism of the OH-initiated oxidation of methacrolein, *Geophys. Res. Lett.*, 26, 2191-2194, 1999
43. Pandis, S. N., Paulson, S. E., Seinfeld, J. H., and Flagan, R. C. : Aerosol formation in the photo-oxidation of isoprene and  $\beta$ -pinene., *Atmos. Environ.*, 25, 997-1008, 1991
44. Park, J; Jongma, C. G; Zhang R. North, S. W. *Phys. Chem. Chem. Phys.*, 5, 3638, 2003.

45. Paulson, S. E.; Flagan, R. C.; Seinfeld, J. H. Atmospheric photo-oxidation of isoprene, Part I: The hydroxyl radical and ground-state atomic oxygen reactions. *Int. J. Chem. Kinet.*, 24, 79-101, 1992.
46. Plewka, A., Gnauk, T., Brüggemann, E., and Herrmann, H.: Biogenic contributions to the chemical composition of airborne particles in a coniferous forest in Germany, *Atmos. Environ.*, 40, 103–115, 2006.
47. Sprengnether, M.; Demerjian, K. L.; Donahue, N. M.; Anderson, J. G. Product analysis of the OH oxidation of isoprene and 1,3-butadiene. *J. Geophys. Res.* 2002, 107, D15, 4268, doi: 10.1029/2001JD000716
48. Surratt, J. D., Murphy, S. M., Kroll, J. H., Ng, N. L., Hildebrandt, L., Sorooshian, A., Szmigielski, R., Vermeylen, R., Maenhaut, W., Claeys, M., Flagan, R. C., and Seinfeld, J. H.: Chemical composition of secondary organic aerosol formed from the photo-oxidation of isoprene, *J. Phys. Chem. A*, 110, 9665–9690, 2006.
49. Surratt, J. D., Lewandowski, M., Offenberg, J. H., Jaoui, M., Kleindienst, T. E., Edney, E. O., and Seinfeld, J. H.: Effect of acidity on secondary organic aerosol formation from isoprene, *Environ. Sci. Technol.*, 41, 5363–5369, 2007.
50. Szmigielski, R., Surratt, J. D., Vermeylen, R., Szmigielska, K., Kroll, J. H., Ng, N. L., Murphy, S. M., Sorooshian, A., Seinfeld, J. H., and Claeys, M.: Characterization of 2-methylglyceric acid oligomers in secondary organic aerosol formed from the photo-oxidation of isoprene using trimethylsilylation and gas chromatography/ion trap mass spectrometry, *J. Mass Spectrom.*, 42, 101–116, 2007.

51. Tuazon, E. C. and Atkinson, R.: A Product Study of the Gas-Phase Reaction of methyl vinyl ketone with the OH Radical in the Presence of NO<sub>x</sub>, *Int. J. Chem. Kinet.*, 21, 1141-1152, 1989
52. Tuazon, E. C.; Atkinson, R. Product study of the gas-phase reaction of isoprene with the OH radical in the presence of NO<sub>x</sub>. *Int. J. Chem. Kinet.*, 22, 1221-1236, 1990a
53. Tuazon, E. C. and Atkinson, R.: A Product Study of the Gas-Phase Reaction of methacrolein with the OH Radical in the Presence of NO<sub>x</sub>, *Int. J. Chem. Kinet.*, 22, 591-602, 1990b
54. Wang, W., Kourtchev, I., Graham, B., Cafmeyer, J., Maenhaut, W., and Claeys, M.: Characterization of oxygenated derivatives of isoprene related to 2-methyltetrols in Amazonian aerosols using trimethylsilylation and gas chromatography/ion trap mass spectrometry, *Rapid Commun. Mass Sp.*, 19, 1343–1351, 2005.
55. Yu, J.; Jeffries, H. E; Le Lacheur, R. M. *Environ. Sci. Technol.*, 29, 1923, 1995
56. Yu, S., Bhave, P. V., Dennis, R. L., and Mathur, R.: Seasonal and regional variations of primary and secondary organic aerosols over the Continental United States: Semi-empirical estimates and model evaluation, *Environ. Sci. Technol.*, 41, 4690–4697, doi:10.1021/es061535g, 2007.
57. Zhao, J., Zhang, R., Fortner, E.C., North, S.W. Quantification of hydroxycarbonyls from OH-isoprene reactions. *J. Am.Chem.Soc.* 126,2686-2687, 2004